Maximum Abutment Scour Depth in Cohesive Soils

Seung Jae Oh[1], Jean-Louis Briaud[2], Kuang-An Chang[3], Hamn-Ching Chen[4]

[1] Ph.D., Research Assistant, Texas A&M University, Department of Civil Engineering, College Station, TX 77843-3136, seungjaeo@gmail.com
[2] Professor, Texas A&M University, Department of Civil Engineering, College Station, TX 77843-3136, briaud@tamu.edu
[3] Associate Professor, Texas A&M University, Department of Civil Engineering, College Station, TX 77843-3136, kchang@civil.tamu.edu
[4] Professor, Texas A&M University, Department of Civil Engineering, College Station, TX 77843-3136, hcchen@civil.tamu.edu

ABSTRACT: Most conventional methods to predict the depth of abutment scour were developed with flume test results using cohesionless soils, and those methods have been used to the abutment scour depth prediction in cohesive soils. Generally floodplains where most abutments are located are composed of less erodible soils such as cohesive soils. Therefore those methods usually predict overly conservative scour depths. For the cost effective designs, a series of flume tests were carried out using Porcelain clay. Based on dimensional analysis and the test results, a new method to predict the bridge abutment scour depths is proposed. The new method built on the difference between the local Froude number and the critical Froude number. Because abutment scour occurs only when the local velocity is higher than the critical velocity which is the maximum velocity the channel bed material can withstand.

INTRODUCTION

Floodplains where most bridge abutments exist are typically composed of cohesive soils such as silts and clays. The soil properties of cohesive soils on erosion resistance are much complicated than those of cohesionless soils. Cohesionless soils resist erosion by buoyant weight and the soil particle friction, while cohesive soils do it by electromagnetic and electrostatic interparticle forces (Briaud et al. 1999b). The critical shear stress, which is the maximum shear stress soil particles can resist from the flow, of uniformly distributed cohesionless soils linearly decreases with particle size decrease. On the contrary, the critical shear stress of cohesive soils cannot be defined by the particle size (Briaud et al. 2001). Moreover, the erosion rate of cohesive soils can be 1,000 times slower than that of coehsionless soils, and a few days may generate only a small fraction of the maximum scour depth (Briaud et al. 2004). Hence, both the critical velocity and the scour rate should be considered in the prediction of scour depth in cohesive material for more accurate and economic bridge design and maintenance, and these requirements stimulated to the development of the SRICOS-EFA (Scour Rate In Cohesive Soils – Erosion Function Apparatus) method.

The SRICOS-EFA method was initially developed to predict the depth around single circular pier in cohesive soil (Briaud et al. 1999b). It was further developed to predict complex pier scour and contraction scour (Briaud et al. 2004). Moreover, more complicated but realistic geological and hydrological conditions were considered (Briaud et al. 1999a).

In the present study a method to predict the maximum abutment scour depth in cohesive soils is introduced to extend the use of the SRICOS-EFA method to the scour depth prediction around the toe of abutment. The method was developed using the results of a series of large flume tests for abutment scour in cohesive soils.

PREVIOUS STUDIES ON MAXIMUM ABUTMENT SCOUR DEPTH

Since most prediction methods to predict abutment scour depths are developed flume test results using cohesionless soils, many equations include soil particle sizes to define the critical shear stress or erodibility.

Froehlich's study

Froehlich (1989) collected abutment scour test results taken by other researchers in rectangular channels in different laboratories from 1953 to 1985, and performed data regression using a total of 164 clear-water and 170 live-bed abutment scour measurements in sand. He proposed both the live-bed and the clear-water abutment scour equation as follows:

Clear-water scour:

$$\frac{y_{s(Abut)}}{y_1} = 0.78 \cdot K_1 \cdot K_2 \cdot \left(\frac{L'}{y_1}\right)^{0.63} \left(\frac{y_1}{D_{50}}\right)^{0.43} Fr_1^{1.16} \sigma_g^{-1.87} \quad (1)$$

Live-bed scour:

$$\frac{y_{s(Abut)}}{y_1} = 2.27 \cdot K_1 \cdot K_2 \cdot \left(\frac{L'}{y_1}\right)^{0.43} Fr_1^{0.61} \quad (2)$$

where $\sigma_g = \left(D_{84}/D_{16}\right)^{0.5}$ is the geometric standard deviation of the bed material, and D_{16}, D_{50}, and D_{84} are the particle size for 16, 50 and 84 percentile of weight, respectively, $Fr_1 = \left(V_1 / \sqrt{g \cdot y_1}\right)$ is Froude number based on approach water depth and approach velocity, K_1 is the correction factor for abutment shape that has a value of 1.0, 0.82 and 0.55 for vertical wall, wing-wall, and spill-through abutment, respectively. K_2 is the correction factor for the alignment of the abutment with respect to the flow direction ($K_2 = \left(\theta / 90\right)^{0.13}$) with θ being the angle of abutment alignment (the embankment is skewed downstream if $\theta < 90°$, and skewed upstream if $\theta > 90°$, L' is the average length of abutment ($L' = A_e / y_1$ with A_e being the flow area obstructed by the embankment), y_1 is the water depth in the approach section, and $y_{s(Abut)}$ is the maximum abutment scour depth

Sturm's study

Sturm (2004) conducted a series of flume tests and analyzed test results of bridge abutment scour depths in compound channels. The equation of the maximum abutment scour depth in the compound channel was suggested as:

$$\frac{y_{s(Abut)}}{y_{f0}} = 8.14\left[\frac{q_{f1}}{M \cdot q_{fc0}} - 0.4\right] \tag{3}$$

where M is the discharge contraction ratio defined as $M = (Q - Q_{block})/Q$ with Q being the total discharge and Q_{block} being the discharge blocked by the approach embankment, $q_{f1}(=V_{f1} \cdot y_{f1})$ is the unit flow rate at the approach section with the effect of backwater induced by the abutment, $q_{fc0}(=V_{fc0} \cdot y_{f0})$ is the critical unit flow rate on the floodplain without the effect of backwater, V_{f1} is the approach average velocity on the floodplain, $V_{fc0}\left(= \frac{1}{k_n} \cdot \sqrt{(Gs-1)\tau_{*c}} D_{50}^{1/3} y_{f0}^{1/6}\right)$ is the critical velocity on the floodplain without backwater effect, Gs is the specific gravity of cohesionless soil, k_n is constant in Strickler-type relationship for Manning's n $\left(n = k_n D_{50}^{1/6}\right)$, τ_{*c} is the critical value of Shields' parameter, y_{f0} is water depth on floodplain without backwater effect, and y_{f1} is the approach water depth on the floodplain.

SRICOS-EFA METHOD

The principle of the SRICOS-EFA method is summarized here to provide a necessary background. The SRICOS-EFA method is highly dependent on the maximum scour depth and the shear stress between the flow and soil interface. The methodology of maximum scour depth is developed by flume test results, and the maximum shear stress on the channel bed is developed by three-dimensional numerical simulations. The procedure of SRICOS method is consisted with following steps.

(1) Obtain standard 76.2 mm diameter Shelby tube samples as close to the bridge support as possible.
(2) Conduct EFA test (Briaud et al. 1999a) of the samples to obtain the critical shear stress (τ_c) and the erodibility curve of erosion rate versus shear stress ($\dot{z}$ vs. τ).
(3) Determine the maximum shear stress τ_{max}.
(4) Obtain the initial scour rate $(\dot{z}_i)$ corresponding to τ_{max}.
(5) Develop the complete scour depth y_s vs. t curve.
(6) Predict the depth of scour by reading the y_s vs. t at the time corresponding to the duration of the flood using

$$y_s(t) = \frac{t}{\frac{1}{\dot{z}_i} + \frac{t}{y_s}} \tag{4}$$

where t is time (hour), and y_s is the maximum scour depth.

EXPERIMENTS

A concrete flume with dimension of 45.7 m in length, 3.7 m in width and 3.4 m in depth was used to conduct the abutment scour tests. A sediment pit, which has dimensions of 7.5 m in length, 3.7 m in width and 1.5 m in depth, is located around the middle of the flume. The pit was filled with the Porcelain clay, and the geotechnical properties of the clay are given in Table 1. The Porcelain clay is classified as CL (clay with low plasticity) by ASTM D-2487. The critical shear stress of the Porcelain clay was obtained after 11 EFA (Erosion Function Apparatus) tests as $\tau_c = 0.8$ Pa.

Table 1 – Geotechnical properties of the Porcelain clay.

Property	Average	Property	Average
Liquid Limit	30.7 %	Initial water content	25 %
Plastic Limit	16.6 %	Median grain size (D_{50})	0.0035 mm
Plasticity Index	14.1 %	Undrained shear stress	21.2 kPa

Two types of channel were used for flume tests: one is a rectangular channel, and the other is a compound channel. The channel cross sections are shown in Figure 1. Three types of abutment made of plywood were used in the flume tests: the first one is the wing wall shape, the second one is the spill-through shape with a 2(H):1(V) slope, and the third one is the spill-through shape with a 3(H):1(V) slope.

A point gauge was used to measure the water depth and the maximum scour depth, and a bed profiler was used to scan the channel bottom topography. The velocity was measured at the 60% of water depth from the free surface by two side looking 3-D ADVs (Acoustic Doppler Velocimeters).

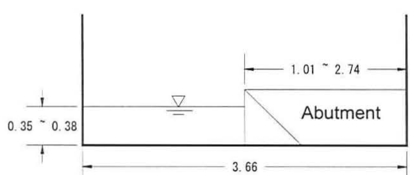

(a) Rectangular channel

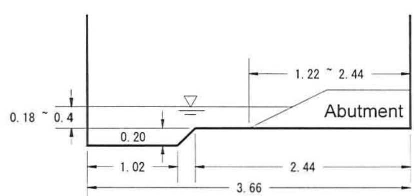

(b) Compound channel

Figure 1 – Cross sectional views of channel configuration. (units: meter)

TEST RESULTS

Eighteen flume tests were conducted by varying the abutment shape, approach embankment length, abutment alignment, channel shape, water depth and flow velocity. During each test the channel bottom was scanned as many times as possible, and the maximum scour depth in each measurement ($y_{s(Abut)}(t)$) was recorded because scour develops very slowly in cohesive soil. This is different with scour development in cohesionless soil. Velocity was measured at the beginning, approximately 100 hours after the test started, and before end of the test.

Figure 2(a) shows the pattern of time average velocity, and Figure 2(b) shows the pattern of the turbulence intensity ($TI = \sqrt{\sigma_x^2 + \sigma_y^2 + \sigma_z^2}$ where σ is the standard deviation of measured velocity and the subscription x, y and z are the direction of flow) at the beginning of the test. The change of channel bottom bathymetry during the test is given in Figure 3. The maximum average velocity was found to be close to the wall which is away from and downstream of the abutment (dashed circle in Figure 2(a)), while the highest turbulence intensity was around the toe of the abutment at slightly downstream (dashed circle in Figure 2(b)). These patterns are coincident with locations at which the deepest contraction scour and the abutment scour were measured during every measurement (Figure 3).

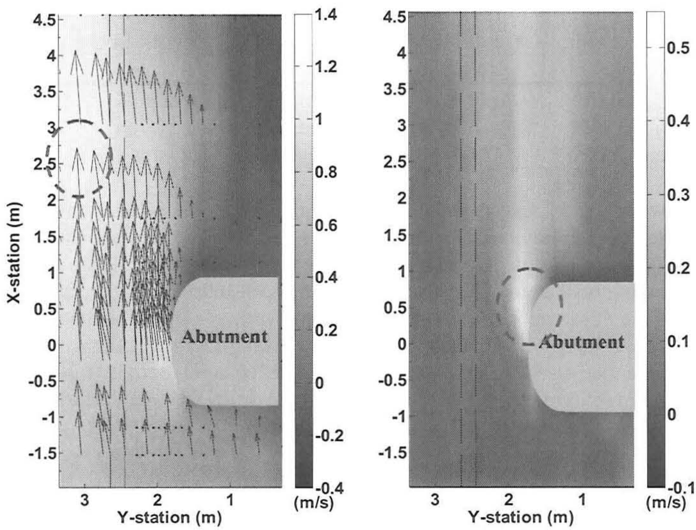

(a) Time averaged velocity (b) Turbulence intensity

Figure 2 – Pattern of velocity in the beginning of test.

The scour depth was recorded as a function of time as $y_{s(Abut)}(t)$. At the end of each test, the scour depth was still developing although the test time is longer than 300 hours (Figure 3 and Figure 4). It is therefore not feasible to obtain the maximum scour depth directly through the test. A hyperbolic model was thus used to obtain the maximum abutment scour depths (Figure 4).

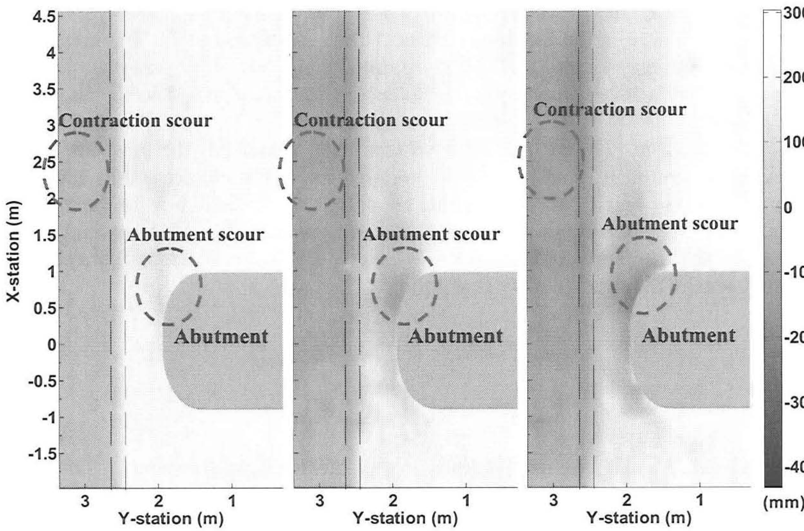

(a) After 60 hours (b) After 189 hours (c) After 320 hours

Figure 3 – Scour development.

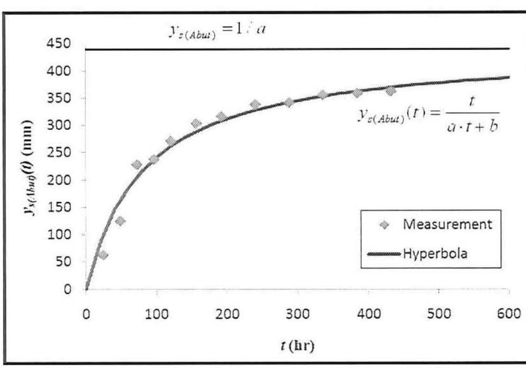

Figure 4 – Measurement and hyperbolic fit.

During experiments, it was found that the maximum scour depth, in the same test conditions except abutment shape, of the 2(H):1(V) spill through abutment is 70% of that of the wing-wall abutment. This ratio is close to the abutment shape correction factor between the spill-through abutment and the wing-wall abutment in Melville (1992). However, contrary results were found in the abutment alignment effect to previous studies (Froehlich 1989; Melville 1992; Richardson and Davis 1995). The maximum scour depth for the abutment skewed upstream is less than that for the abutment normally aligned to the flow. The contrary may be due to the use of different types of abutment. The spill-through abutment which induces a relatively smooth flow around the toe of the abutment was used in this study, whereas vertical abutments were used in the previous studies. This is evidenced in *TI*. The maximum *TI* for the abutment with $\theta = 120°$ was approximately 10% less than that for the abutment with $\theta = 90°$. Note that the turbulence pattern is identical to the abutment scour pattern.

As shown in Figure 2 and Figure 3, the local velocity is the most important parameter on abutment scour. However, it cannot be easily calculated. In addition, flume tests cannot account for all possible conditions in the field. For the calculation of the local velocity around the abutment, the approximation in Maryland SHA Bridge Scour Program (*ABSCOUR*) was adopted. The method to convert the hydraulic data to the local velocity is as follows:

$$V_{f2} = \begin{cases} Q/A_2, \text{ for short setback } \left((L_f - L') \le 5y_{m1}\right) \\ Q_{fp1}/A_{f2}, \text{ for long setback } \left(L' \le 0.25L_f\right) \\ \text{otherwise use a linearly interpolated velocity between} \\ Q/A_2 \text{ for } (L_f - L') = 5y_{m1} \text{ and } Q_{fp1}/A_{f2} \text{ for } L' = 0.25L_f \end{cases} \tag{5}$$

where Q_{fp1} is the discharge on the floodplain at the approach section immediately upstream of the abutment, A_2 is total flow area at the contracted section, A_{f2} is the flow area on the floodplain at the contracted section, and L_f is the width of floodplain at the approach section, and y_{m1} is the water depth of main channel at the approach section.

DIMENSIONAL ANALYSIS

The variables affecting abutment scour can be expressed in equation (6) and rewritten in dimensionless form in equation (7) below.

$$y_{s(Abut)} = f(y_{m1}, y_{f1}, L_f, L', Sh, \theta, g, V_{f2}, \mu, V_{fc}) \tag{6}$$

$$\frac{y_{s(Abut)}}{y_{f1}} = f\left(\frac{L_f - L'}{y_{f1}}, Sh, \theta, Fr_{f2}, Fr_{fc}, \mathrm{Re}_{f2}\right) \tag{7}$$

where Sh is the abutment shape, θ is the alignment angle of abutment, μ is the viscosity of water, $Fr_{f2} = \dfrac{V_{f2}}{\sqrt{gy_{f1}}}$, $Fr_{fc} = \dfrac{V_{fc}}{\sqrt{gy_{f1}}} \dfrac{\sqrt{\tau_c / \rho}}{gny_{f1}^{1/3}}$, and $\mathrm{Re}_{f2} = \dfrac{\rho y_f V_{f2}}{\mu}$

Abutment scour occurs when the local flow velocity is higher than the critical velocity, and continues until the local velocity equals to the critical velocity. Thus the abutment scour equation may be expressed in the form of Froude number difference as follows:

$$\frac{y_{s(Abut)}}{y_{f1}} = K_1 \cdot K_2 \cdot K_L \cdot K_G \cdot K_{\mathrm{Re}} \cdot \alpha_1 \cdot \left(\beta_1 \cdot Fr_{f2} - Fr_{fc}\right)^{\chi_1} \qquad (8)$$

where K_L is the correction factor for the abutment location, K_G is the correction factor for the channel geometry, K_{Re} is the correction factor for the Reynolds number effect, and α_1 , β_1 and χ_1 are constant.

In equation (8), the three constants (α_1, β_1 and χ_1) and four correction factors (K_1, K_2, K_L and K_G) were obtained after data regression using flume test results. They are as follows:

$$\frac{y_{s(Abut)}}{y_{f1}} = K_1 \cdot K_2 \cdot K_L \cdot K_G \cdot 7.94 \cdot \left(1.65 \cdot Fr_{f2} - Fr_{fc}\right) \qquad (9)$$

$$K_1 = \begin{cases} 1.22 & \text{for vertical-wall abutment} \\ 1.0 & \text{for wing-wall abutment} \\ 0.73 & \text{for spill-through abutment with 2:1 Slope} \\ 0.59 & \text{for spill-through abutment with 3:1 Slope} \end{cases}$$

$$K_2 = \begin{cases} 1.0 - 0.005\left|\theta - 90°\right| & \text{for } 60° \le \theta \le 120° \\ 0.85 & \text{otherwise} \end{cases}$$

$$K_G = \begin{cases} 1.0 & \text{for compound channel} \\ 0.42 & \text{for rectangular channel} \end{cases}$$

$$K_L = \begin{cases} -0.23\dfrac{L_f - L'}{y_{f1}} + 1.35 & \text{for } \dfrac{L_f - L'}{y_{f1}} < 1.5 \\ 1.0 & \text{otherwise} \end{cases}$$

In equation (9), the correction factors for the Reynolds number effect was not obtained using the 18 flume test results because the range of Reynolds numbers in the tests are too narrow. As expected, equation (9) fits well to the flume test results of the present study while mostly under estimates when compared with smaller scale laboratory test and over estimates when compared with field data. The main cause of the discrepancy is the Reynolds number effect. The range of Reynolds number in several studies, including the present study, is given in Table 2.

Table 2 – Range of Reynolds numbers (Re_{f2}) in studies

	Froehlich (1989)	Sturm (2004)	Present study	Benedict et al. (2006)
Min. Re_{f2}	7,425	8,433	102,511	143,500
Max. Re_{f2}	71,133	55,451	322,681	11,436,281
Avg. Re_{f2}	50,073	28,248	219,837	2,782,622

Figure 5 shows the effect of Reynolds number on the maximum abutment scour depth. In order to quantify the effect, laboratory data in Table 2 from Froehlich (1989) and Strum (2004) were plotted. Note that the database from Benedict et al. (2006) was not used because the accuracy of the field data is likely to be much lower than that of the laboratory test. According to the curve fitting shown in Figure 5, the effect of Reynolds number can be expressed as

$$K_{\mathrm{Re}} = \frac{1}{0.033 \cdot \mathrm{Re}_{f2}^{0.28}} \tag{10}$$

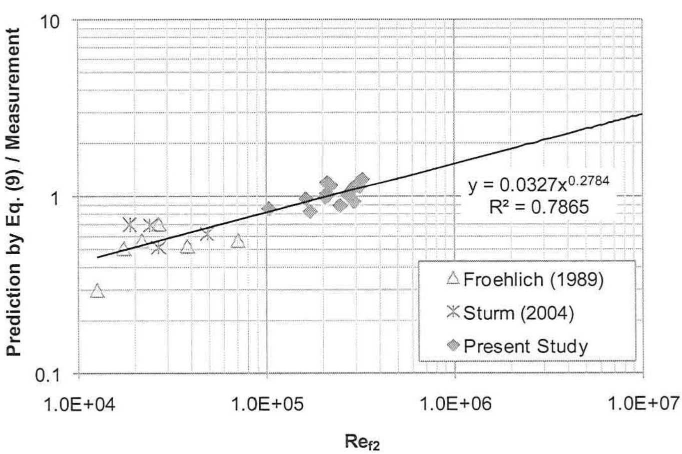

Figure 5 – The effect of Reynolds number in maximum abutment scour depth.

Accordingly, the equation for the maximum abutment scour prediction becomes:

$$\begin{aligned}\frac{y_{s(Abut)}}{y_{f1}} &= K_1 \cdot K_2 \cdot K_L \cdot K_G \cdot K_{\mathrm{Re}} \cdot 7.94 \cdot \left(1.65 \cdot Fr_{f2} - Fr_{fc}\right) \\ &= K_1 \cdot K_2 \cdot K_L \cdot K_G \cdot 243 \cdot \mathrm{Re}_{f2}^{-0.28} \cdot \left(1.65 \cdot Fr_{f2} - Fr_{fc}\right)\end{aligned} \tag{8}$$

CONCLUSION

A series of flume test were conducted for the abutment scour in cohesive soils. A method to predict the maximum abutment scour depth is proposed using the flume test results. The method is based on the difference between the local Froude number and the critical Froude number. Four correction factors, abutment shape, alignment, channel geometry, and abutment location, were included. The scale effect is also considered.

ACKNOWLEDGEMENT

This work was supported by NCHRP (Project No. 24-15(2)). Mr. Stanley R. Davis and Mr. David Reynaud are the technical contacts. Their help are specially thanked.

REFERENCES

ABSCOUR. (Maryland SHA Bridge Scour Computer Program), Maryland State Highway Administration, Version 8, build 1.02, compiled August 14, 2006.

ASTM D2487, American Society for Testing and Materials, Philadelphia, USA

Benedict, S. T., Deshpande, N., Aziz, N.M., and Conrads, P.A. (2006). "Trends of Abutment-Scour Prediction Equation Applied to 144 Field Sites in Scour Carolina." *Open-File Report 03-295*, U.S. Geological Survey, http://pubs.water.usgs.gov/ofr2003-295/ [retrieved 10 January 2009]

Briaud, J.-L., Chen, H. C., Li, Y., Nurtjahyo, P., and Wang, J. (2004). "Pier and Contraction Scour in Cohesive Soils." *NCHRP Report 516*, Transportation Research Board, Washington, D.C.

Briaud, J.-L., Ting, F., Chen, H. C., Cao, Y., Han, S.-W., and Kwak, K. (2001). "Erosion Function Apparatus for Scour Rate Predictions." *J. Geotech. Geoenviron. Eng.*, 127(2), 105-113.

Briaud, J.-L., Ting, F., Chen, H. C., Gudavalli, S. R., Kwak, K., Philogene, B., Han, S.-W., Perugu, S., Wei, G., Nurtjahyo, P., Cao, Y., and Li, Y. (1999a). "SRICOS: Prediction of scour rate at bridge piers." *TTI Report No. 2937-1 to the Texas DOT*, Texas A&M University, College Station, TX, USA.

Briaud, J.-L., Ting, F., Chen, H. C., Gudavalli, S. R., Perugu, S., and Wei, G. (1999b). "SRICOS: Prediction of scour rate in cohesive soils at bridge piers." *J. Geotech. Geoenviron. Eng.*, 125(4), 237-246.

Froehlich, D. C. "Local Scour at Bridge Abutment." *Proceedings of National Conference on Hydraulic Engineering*, 1989, New York, NJ, USA, 13-18.

Melville, B. W. (1992). "Local Scour at Bridge Abutment." *J. Hydraulic Eng.*, 118(4), 615-631.

Richardson, E. V., and Davis, S. M. (1995). "Evaluating Scour at Bridges." *FHWA-IP-90-017, HEC No. 18*, US Department of Transportation, Washington, D.C.

Strum, T. W. (2004). "Enhanced Abutment Scour Studies for Compound Channels." *FHWA-RD-99-156*, Georgia Institute of Technology, School of Civil and Environmental Engineering, Atlanta, GA 30332.

On the Behaviour of Open Filters Under Wave Loading

G. Wolters[1], D. Rudolph[2], B. Hofland[3] and H. Verheij[4]

[1]Deltares | Delft Hydraulics, P.O. Box 177, 2600 MH Delft, The Netherlands, PH +31(0)883358318, email: guido.wolters@deltares.nl
[2]Deltares | Delft Hydraulics, P.O. Box 177, 2600 MH Delft, The Netherlands, PH +31(0)883358362, email: daniel.rudolph@deltares.nl
[3]Deltares | Delft Hydraulics, P.O. Box 177, 2600 MH Delft, The Netherlands, PH +31(0)883358196, email: bas.hofland@deltares.nl
[4]Delft University of Technology and Deltares | Delft Hydraulics, P.O. Box 177, 2600 MH Delft, The Netherlands, PH +31(0)883358137, email: henk.verheij@deltares.nl

ABSTRACT

The design of granular open filters under wave and current loading has raised increasing interest in recent years, especially under marine contractors and consultants. Proper guidelines on the design of open filters, which allow an acceptable and predictable loss of base material under wave and current loading, could lead to significant cost and material savings, and to a more practical application of filters in the field.

In order to improve the knowledge on the behaviour of granular open filters under wave loading, laboratory experiments have been conducted in the Scheldt flume of Deltares | Delft Hydraulics. This paper summarizes the model set-up, test programme and test results. The results include erosion (transport) rates and filter settling for open filter materials on sand.

LITERATURE REVIEW

Granular filters typically employed in coastal engineering fulfill several functions. They prevent e.g. the erosion (washing out) of finer base material or sub-layers due to waves and currents, contribute to the energy dissipation by turbulent flow through void spaces and provide drainage. Granular filters can be designed as geometrically tight filters or geometrically open filters.

The design of geometrically tight filters (no material washout) is relatively simple, but often an unnecessary high number of filter layers and material volume is required. Furthermore, geometrically tight filters are often difficult to realize in the field because of quarry material limitations and when the structure is constructed underwater.

An alternative is a geometrically open filter. In this case the filter is designed in such a manner that the hydraulic loading is too low to initiate significant erosion of the base material. Limited settlement is often permitted in the field. Typical applications of open filters include e.g. offshore bed protections and toe & slope configurations of coastal structures.

The allowed settlement depends on the structure type. For breakwaters and revetments even small amounts of toe settlement can endanger the stability of the armour layer by loosening the bonds between interlocked armour units or placed stone revetments. This can lead to the failure of the structure as a whole (see e.g. CIRIA | CUR | CETMEF 2007).

Since 1980 a lot of research has been conducted on interface stability and initiation of transport in filters which have resulted in varying formulae and design diagrams (see e.g. Bakker et al. 1994, Klein Breteler 1992, Verheij et al 2008, Sumer et al. 2001, Dixen et al. 2008). These research studies have mainly focused on stationary, non-cyclic flow at the point of transport initiation. There is only very limited data on base material transport or induced filter settlement and the data which exist focus on non-cyclic flow conditions. Only Dixen et al (2008) report some findings on transport initiation as function of wave characteristics for a single and multiple layers of rock.

For base material transport through filters only two transport models are known to the authors; other available transport models (see e.g. Van Rijn, 2005) are not applicable to sand transport within filters. These are the transport models of Klein Breteler et al. (1989, 1992) and Den Adel et al. (1992, 1994).

Both models describe the macroscopic transport of base materials through filters. Each has its own restrictions. Both are applicable only for stationary and (fully) turbulent currents and macroscopic transport processes. Microscopic processes (description of the individual particle behaviour) are not included. Den Adel's model is only applicable for bedload transport (and can thus not be used in the suspended transport regime). Both models provide a transport estimate which is accurate to an order of magnitude.

The fundamental applicability of the models for cyclic flows (waves) and larger wave periods T>2-5s is assumed (see also Dixen et al., 2008) but has not been verified. Basis for this assumption is that the initiation of transport occurs under similar conditions for both cyclic and stationary conditions.

The transport model of Den Adel includes, because of its many parameters (e.g. densities ρ and μ, particle velocity, pick-up- and catchfrequency, several proportionality constants), several uncertainties and imponderabilia. Not all of these uncertainties can be quantified in the model. Furthermore, some fundamental problems were found which will be discussed later in this paper.

The model of Klein Breteler is comparatively simplified but has the advantage of less parameters and proportionality constants. The latter model has been used in the present study. While the transport model of Klein Breteler et al. will be described shortly in the following, it is referred to the literature for the model of Den Adel et al. The model is too elaborate to be captured within the constraints of this paper.

Macroscopic transport model

Klein Breteler (1992) introduced the following empirical transport formulae for macroscopic transport within filters (stationary current, homogeneous base material):

$$T_1 = \rho_s \cdot p_1 \cdot \left(i / i_{cr} - 1\right)^{1.25} \quad \text{or} \quad T_2 = \rho_s \cdot p_2 \cdot \left(\left(u_f / u_{f,cr}\right)^2 - 1\right)^{1.5} \qquad (1+2)$$

where

T_i = transport rate in (kg/m/s)
ρ_s = density of transported material (kg/m^3)
$u_{f,cr}$ = critical filter velocity (m/s)
i_{cr} = critical hydraulic gradient (-)
p_i= transport intensity (m^3/m/s)

These formulae are based on the assumption of a turbulent current, i.e. the hydraulic gradient is proportional to the square of the filter velocity. Formula (2), based on $u_{f,cr}$, is derived from the classical formula of Meyer-Peter and Mueller for bedload transport in free surface flows.

The value of the transport intensity p_i seems to be independent of the diameter of the transported material and was found by Klein Breteler (dependent on the formula used) to be in the range of

$p_i = 0.6 - 9.0 \times 10^{-6}\ m^2/s$ with a best fit for $p_i = 1.5 \times 10^{-6}\ m^2/s$

The critical filter velocities were found to be in the range of $u_{f,crit} = 0.037 - 0.102$ m/s. Tested base materials had a median sieve diameter of $D_{50,b}$= 0.16mm and $D_{50,b}$= 0.82mm and filter material diameters between $D_{15,f}$ = 4.2 – 83.8mm (15% values of filter sieve curve).

Further results of the study by Klein Breteler (1992) include:

- Influence of filter material diameter ($D_{f,50}$): The critical transport velocities for fine base material seem to be dependent on the diameter of the filter material. However, this does not seem to be the case for coarser base material (e.g. $D_{50,b}$=0.82mm).
- Influence of material distribution: The amount of transported material is strongly dependent on the size distribution of the material (sieve curve).
- It is assumed that the base material is relatively homogeneous. If this is not the case, the transport per class of diameters becomes relevant (for each material class a different $u_{f,cr}$ is found). Total transport can then be described as the sum of transport over all classes. For this case a stochastic model was proposed, see e.g. Klein Breteler (1992).

Critical filter velocities and gradients

Theoretically the critical filter velocity $u_{f,cr}$ for the initiation of base particle motion (stationary current) is given by Den Adel (1992) and Klein Breteler (1989) as:

$$u_{f,cr} = \left[\frac{n_f}{c_{10}} \left[\frac{D_{15,f}}{\nu_w} \right]^{c_9} \sqrt{\psi_s \cdot \Delta \cdot g \cdot D_{50,b}} \right]^{1/(1-c_9)} \tag{3}$$

with

ν_w = kinematic viscosity of water (m^2/s)
n_f= filter porosity (-)
g = acceleration of gravity (m/s^2)
$\Delta = \rho_s/\rho_w - 1$ = relative submerged density of base material (-)
ρ_s= density of base material, ρ_w= density of water (kg/m^3)
Ψ_S = Shields parameter (-). For $D_{50,b}$=0.15mm: Ψ_S=0.073
c_9, c_{10} = constants dependent on $D_{50,b}$ (-). For $D_{50,b}$=0.15mm: c_9 = 0.2 and c_{10}= 0.78

The critical hydraulic gradient for initiation of transport can be calculated from De Graauw (1983, stationary current):

$$i_{cr} = \left[\frac{0.06}{n_f^3 D_{15,f}^{4/3}} + \frac{n_f^{5/3} D_{15,f}^{1/3}}{1000 D_{50,b}^{5/3}} \right] v_{*cr}^2 \tag{4}$$

using:

$$v_{*cr} = 1.3 D_{50,b}^{0.57} + 8.3 \cdot 10^{-8} D_{50,b}^{-1.2} \tag{5}$$

Please note that relations (4) and (5) are dimension-dependent. For cyclic flows (waves) it is generally assumed that the critical value of the hydraulic gradient (and of the filter velocity) is of the same order of magnitude as for stationary currents.

MODEL SET-UP

The following boundary conditions have been chosen for the initial set-up of the model:

- Fully turbulent conditions ($Re^* = u_{2\%} D_{n50,f} / \nu_w >> 1000$, $u_{2\%}$ = velocity directly above the filter exceeded by 2% of waves)
- Low transport regime (bedload transport): Since transport by suspension is likely to cause a fast damage progression in open filters under prototype conditions (e.g. for breakwater toes) which can result in ultimate structure failure, the focus was initially laid on bedload transport.
- Uni-directional measurement of sand transport: To create sand transport under cyclic conditions irregular (non-sinusoidal) waves need to be employed. Under pure sinusoidal waves effective transport will be minimal since the base material moves back and forth around its original location without any significant displacement (advection). Using 2nd order Stokes waves of varying steepness a net-transport in wave direction was achieved.
- To prevent boundary effects due to seabed lowering (induced by filter settlement) it was decided to stop the test if sea bed lowering of more than 2cm was measured. Otherwise the seabed was not rebuilt between tests.

The set-up of the model is shown in Figures 1 and 2. It consists of a submerged filter construction on a sand bed which is subjected to irregular wave loading with a JONSWAP wave spectrum. Second order (Stokes) waves have been employed to allow the simulation of the correct wave form and wave steepness. Measured were base material (sand) transport, filter settlement using a mechanical profiler, pore pressures and pressure gradients in filter and sand bottom and the x-z velocities directly above the filter.

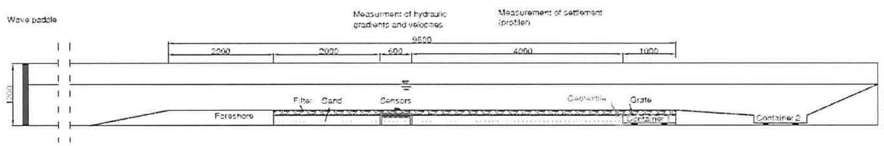

Figure 1. Model set-up in the Scheldt flume of Deltares | Delft Hydraulics

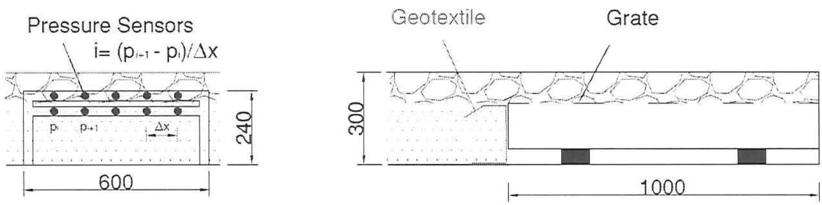

Figure 2. Frame for pressure measurements

A concrete foreshore of 0.3m height was used in which the filter layer of d=5.5 or 10cm thickness and the sand layer of d_s=24.5 or 20cm thickness were embedded. The horizontal concrete section and the first part of the filter section in front of the measurement area (length L=10h, h=water depth) allowed the turbulent flow conditions within the filter layer to become fully developed before any measurement was conducted. Behind the test section a free space of also 10h was left in front of the wave damper. The chosen thickness of the sand layer was sufficiently deep so that the flume bottom did not significantly affect the pore pressure distribution within the sand bed. The chosen filter thickness varied between 3.5 and 2 $D_{n50,f}$ ($D_{n50,f}$ is the nominal median diameter of the filter material) to allow for filter velocities above critical at the filter-sand interface.

The sand layer was carefully installed in a wet state within the wave flume and smoothed. Before testing the flume was filled with water and left for a day to allow all remaining air bubbles to leave the sand. Prior to actual testing the sand bed was exposed to 2 hours of low wave energy. Between tests a minimum layer of water was always kept above the sand bed.

The employed water within the wave flume was stored in a second tank between reconstructions / tests. This way it was ensured that the same water, that was saturated with fine sand particles after the first test, was used for all tests and that no model effects were introduced by using (clean) fresh water in each test.

The transported sand is collected in two containers behind the filter section: The first container collects the transported sand through the filter and along the bed (bedload) and the second any suspended material (> 20-30μm). Finer material (> 20-30μm) could not be accurately measured since it mainly remained suspended in the water after testing. After each test the suspended sand which settled on the wave damper (behind the second container) was flushed back into the 2nd container. Sand transport in opposite direction to the waves was measured by collecting it from the foreshore.

Between filter layer and the first sand container a geotextile was placed. A geotextile was also placed on the first part of the sand container. The geotextile ensured that the sand particles at the boundary between sand bed and container would not simply drop into the container during the oscillatory wave motion but were actually displaced (transported). The horizontal length of the geotextile was 6 or 10 $D_{n50,f}$. Secondly, the geotextile was used to prevent significant boundary affects due to possible scouring in front of the sand container.

The collected sand samples (> 20-30μm) were dried, weighed and analyzed (sieving curve) to verify which particle size ranges were transported.

Measurements were performed of the incident waves, the filter settlement (mechanical profiler, using 3 separate rows), pressures (2 rows of 5 pressure sensors each, 2.5cm above and below the filter-sand interface), x-z-particle velocities (EMS, 2.5cm (~1$D_{n50,f}$) above the seabed), base material transport (collected in sand containers, see above), ripple length, heights and sand movements along the seabed. Videos and photo recordings of all tests were made.

Materials

The following materials have been used in the tests:

- $D_{n50,sand}$= 0.13mm, $D_{n50,filter}$= 20mm and 30mm, $D_{n50,f}$ / $D_{n50,b}$ = 150-230
- A wide grading of the filter material was chosen (M_{85}/M_{15}=3.37) since these are often used in toe and offshore structures.

The porosity of sand and filter material was estimated from the sieving curves to n_s=0.35 and n_f=0.44 respectively. This results in an installed dry, bulk mass density of about 1700 kg/m^3 (sand) respectively 1500 kg/m^3 (filter).

Based on the previously introduced formula for the critical filter velocity and the critical hydraulic gradient the following critical values can be calculated for $D_{f,15}$ = 20-30mm (stationary current): $u_{f,cr}\approx$ 0.02-0.03 m/s and i_{cr}=0.06-0.07.

TEST PROGRAMME

The test programme, see Table 1, included tests with varying wave steepness (s_{op}=0.004-0.027), varying filter thickness (d=2$D_{n50,f}$ and 3.5$D_{n50,f}$) and varying filter material ($D_{n50,f}$=20mm and 30mm). The base material (sand) and the water depth above the open filter (h=0.4m) were kept constant during all tests. This corresponds to values of d/$D_{n50,f}$=1.8, 2.8, 3.3 and d/h=0.14 and 0.25. Tests were conducted for turbulent conditions (Re*>4000, based on $u_{2\%}$), KC=$u_{2\%}T_m/n_fD_{n50,f}$>>40 and mobility numbers of $\theta = u_{2\%}^2/g/\Delta/D_{50,b} > 26.5$. Testing was conducted for wave loading only. The test duration (t) varied between tests based on the observed base material transport. Since the initial tests did not show much sand transport the test duration was continuously increased up to 6 hours. The total test length varied between 1000 waves and 6 hours (>10000 waves).

Tests T01-T04 (see observation section) are not presented here since they proved to be below the threshold for transportation.

Table 1. Testing programme

	Test programme										
	$D_{15,f}$ (mm)	$D_{n50,f}$ (mm)	d (m)	h (m)	H_S (m)	T_p (s)	s_{op} (-)	t (hrs)	Re^* (-)	KC (-)	θ (-)
T05	28	30	0,1	0,4	0,10	2,09	0,015	6	4913	35	27
T06	28	30	0,1	0,4	0,14	2,52	0,014	6	7181	61	57
T07	28	30	0,1	0,4	0,17	5,41	0,004	2	16444	300	297
T08	28	30	0,055	0,4	0,14	2,52	0,014	6	8006	68	70
T09	28	30	0,055	0,4	0,14	1,80	0,027	6	5925	36	39
T10	28	30	0,055	0,4	0,16	5,10	0,004	2	16069	276	284
T11	19	20	0,055	0,4	0,14	2,52	0,014	6	5088	97	64
T12	19	20	0,055	0,4	0,14	1,81	0,027	6	4000	55	40
T13	19	20	0,055	0,4	0,16	5,10	0,004	2	10963	424	297

OBSERVATIONS AND ANALYSIS

The following observations were made during testing:

- The tests were originally set-up to investigate bedload and suspended load transport separately (focusing in first instance on bedload transport), based on the u_{cr} - criteria developed by Den Adel (1992). However, it became apparent during testing that these two regimes could not be separated, since significant base material transport could only be realized once the filter velocities were far above the critical velocity and once base material was also suspended in the water column.
- The observed base material transport for wave loading alone was very low (and appears insignificant compared to transport by current) even for large near-bed velocities and hydraulic gradients ($i_{2\%}/i_{cr}$ = 1-7, $u_{2\%}/u_{f,cr}$=10-40), see Figures 3 & 4. It was observed that while the hydraulic gradients (horizontally measured in the filter between pressure sensors) were sufficiently high to produce initiation of motion around its rest position and suspension of materials, most of the bed material remained in its original vicinity.
- The largest transport rates were observed for waves of low steepness (s_{op}=0.004). These waves caused the largest forces on the seabed (θ~300).
- As expected a decrease in sand material transport was found for smaller filter stone diameters (for D_{n50}=20mm only about half of the volume was transported as for D_{n50}=30mm), see Figure 3 & 4. A reduction of the filter thickness of 3.5 D_{n50} to 2 D_{n50} resulted however in a 20-60% reduction in material transport in all tests. This finding seems somewhat counterintuitive (and should be verified in further tests). A possible explanation is given later in the paper. Furthermore, a steady increase in transport was found for increasing KC values (KC =40-450, KC is proportional to the stroke of the motion at the seabed).
- The tests showed that the base material distribution (sieving curve) changed during transport. Whereas the original sand had a median particle size of $D_{50,b}$=152 μm, the particle size of the transported bedload material was $D_{50,b}$=142

μm and that of the suspended load $D_{50,b}$= 104 μm. The heaviest sand particles were left behind during bedload transport and only the lighter particles were transported in suspended mode.

It was observed that finer sand particles were entrained into the water column (particles <20-30 μm) very quickly, clouding the water. Most of this material was so fine that it remained suspended in the water column even days after testing.

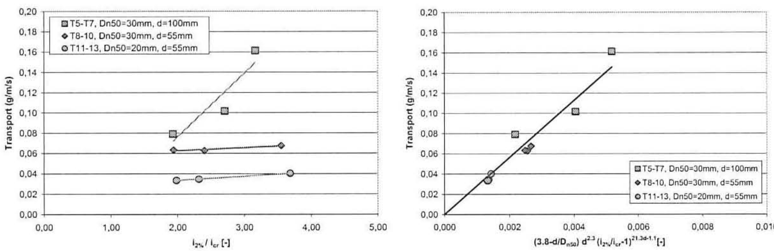

Figure 3. Transport vs. hydraulic gradient

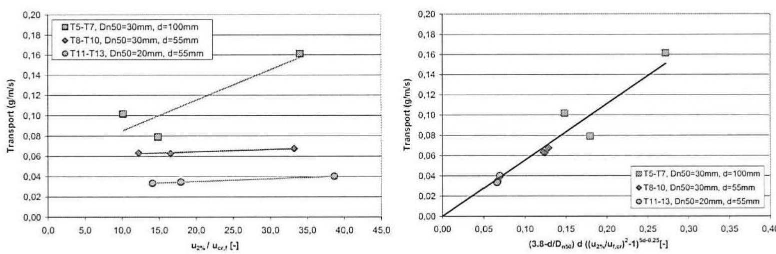

Figure 4. Transport vs. velocity

- Initiation of motion was first observed for H_s=0.06m, $i_{2\%}$=0.1, $u_{2\%}$= 0.12m/s, KC=15). Measurable material transport was first observed for wave heights of H_s=0.1m (test T5, $i_{2\%}$=0.15, $u_{2\%}$= 0.25m/s, KC=35). Dense base material clouds were observed within the filter. At this stage bed ripples became fully formed with heights of 1-2cm and 7-17cm length. The water within the flume appeared completely saturated with fine particles.
- Practically no transport along the bed surface was observed. The measured transport was due to the suspended material clouds within the filter layer, which moved through the filter. This transport process is in conflict with the bedload transport model of Den Adel (1992), which describes horizontal base material movement (particle by particle) along the sand-filter interface (no entrainment in the water column). Observed was however collective (cloud) material movement in wave direction. It appears therefore that den Adel's model (for stationary currents) cannot be employed for base material transport under waves.

Filter settlement

The measured deviations in filter profile are mainly caused by ripple formation and ripple displacement at the sand-filter interface , actual settling effects were very small due to the low amount of base material transport. Based on the measured filter displacement a cumulative filter settlement of 3mm, 1.3mm and 1.1mm was determined over the measurement area of 4.6m x 1m (after tests T7, T10 and T13).

Unfortunately the filter settlement was too small for further analysis and is therefore not considered here any further.

Base material transport

It appears that both filter thickness and filter stone diameter have a significant influence on base material transport. In the conducted experiments the thickness of the filter layer determined the rate of transport increase with hydraulic gradient i (steepness of curve, exponent in formula (1) and (2)) whereas the filter stone diameter determined the minimum amount of transport (factor p_i in formula):

- The influence of the hydraulic gradient (and the filter velocity) is small for small (minimal) filter thicknesses, independent of filter stone diameter. The influence grows rapidly with larger filter thicknesses.
- The same influence can also be detected for the wave steepness: Wave steepness has only minor influence for small filter layers (independent of filter stone diameter). The influence grows rapidly with larger filter thicknesses. The maximum transport is found for low wave steepness.

The given formulae for transport (under stationary current, (1) and (2)) result in transport rates which are consistently larger than the values found for oscillatory flow, by a factor of 30-100. Also, the influences of both filter thickness and stone diameter are not included in these formulae so far. Thus, by taking into account the described linear trends for filter thickness and stone diameter, a new tentative relationship has been developed (valid in the experimental range: $D_{n50,f}/D_{n50,b}$ = 150-230, d/D_{n50}=1.8-3.3, d/h=0.14-0.25, KC=40-450), where D_{n50}= median nominal filter stone diameter (m), d= filter thickness (m), h= water depth (m) and T= transport (kg/m/s); see also Figures 3 and 4:

$$T_1 = \rho_s \cdot p_1 \cdot (i_{2\%} / i_{cr} - 1)^x \quad \text{with } p_1 = 1.5 \cdot 10^{-5} \cdot d^{2.3} \cdot (3.8 - d / D_{n50}), \text{ and } x = 21.3 \cdot \text{d} - 1.1 \text{ with } x \geq 0.05 \tag{6}$$

Similar trends were observed for the velocities (where u_f is replaced here by the near-bed characteristic velocity $u_{2\%}$ measured 1 D_{n50} above the filter layer):

$$T_2 = \rho_s \cdot p_2 \cdot \left(\left(u_{2\%} / u_{f,cr} \right)^2 - 1 \right)^x \quad \text{with } p_2 = 3.4 \cdot 10^{-7} \cdot d \cdot (3.8 - d / D_{n50}), \text{ and } x = 5 \cdot \text{d} - 0.25 \text{ with } x \geq 0.05 \tag{7}$$

These transport relationships describe the total load transport of bed load and suspended load. Most of the material is transported in suspended load, the fraction transported by bed load transport appears negligible under waves.

A preference is given to the relationship for i/i_{cr} since the filter velocities u_f inside the filter were not actually measured in this study (the relationship is based on the velocities measured just above the filter), whereas i and i_{cr} have been directly measured at the sand-filter interface.

The above presented (tentative) relationships still need verification and extension to a larger range of applicability, since they are based on only a few tests so far. Further testing is needed.

CONCLUSIONS

The presented hydraulic model study of a submerged filter structure on a horizontal sand bed shows that under wave influence large amounts of base material are set into motion within the filter and suspended in the water column, but not much is actually transported (factor of 30-100 less than the formulae predict for stationary currents). It is expected that under combined current + wave influence much of this stirred up material will be transported, resulting in possibly much larger transport rates than under waves or currents alone.

REFERENCES

Bakker K.J., Verheij H.J., and de Groot M.B. (1994). "Design relationship for filters in bed protection". *J. Hydraulic Eng.*, 120(9), 1082-1088.

CIRIA | CUR | CETMEF. (2007). "The Rock Manual: The use of rock in hydraulic engineering". 2nd edition, C683, CIRIA, London.

De Graauw A., Van der Meulen T., Van der Does de Bye M. (1983). "Design criteria for granular filters", *Publication 287*, Delft Hydraulics.

Den Adel H., Koenders M.A., Bakker K.J. (1994). "The analysis of relaxed criteria for erosion-control filters." *Canadian Geotechnical Journal*, Vol. 31, Nr. 6, pp. 829-840.

Den Adel H. (1992). "Transportmodel voor filters", Deel 1-3, *report C0-325970/6*, Delft Hydraulics.

Dixen, F.H., Sumer, B.M. and Fredsoe, J. (2008). "Suction removal of sediment from between armor blocks. II: waves", *J. of Hydraulic Engineering*, Vol 134, no 10, October 2008, ASCE.

Klein Breteler M. (1989). "Zandtransport in granulaire filters, horizontale stationaire stroming", *report H869*, Delft Hydraulics.

Klein Breteler M., Den Adel H., Koenders M.A. (1992). "Taludbekledingen van gezette steen, Ontwerpregels voor het filter", *report M1795/H195, XXI*, Delft Hydraulics & Geo Delft.

Sumer, B. M., Cokgor, S., and Fredsøe, J. (2001). "Suction removal of sediment from between armor blocks." *J. Hydraul. Eng.*, 127(4), 293–306.

Van Rijn L.C. (2005). "Principles of sedimentation and erosion engineering in rivers, estuaries and coastal seas", AQUA publications.

Verheij H.J. , Hoffmans G.J.C.M., Den Adel H., Akkerman. G.J. (2009). "Interface stability of granular filterstructures", CUR *(in preparation)*.

Two Complementary Tests for Characterizing the Soil Erosion

C. Chevalier[1], I. Haghighi[2], T.L. Pham[2], Ph. Reiffsteck[3]

Université Paris-Est, LCPC, GER, 58 boulevard Lefebvre, 75015 Paris, France;
[1]PH +33 1 40 43 52 16; email: christophe.chevalier@lcpc.fr
[2]PH +33 1 40 43 52 76; email: iman.haghighi@lcpc.fr
[3]PH +33 1 40 43 52 73; email: philippe.reiffsteck@lcpc.fr

ABSTRACT

For estimating sensitivity of soils to erosion, the Hole Erosion Test (HET) has proved to be an efficient and convenient laboratory apparatus. Measuring sensitivity to erosion in situ with dedicated tests like the Mobile Jets Erosion Test (MoJET) is also of great interest since it allows testing the soil in its real state. However, results are generally not easily linked between laboratory and in situ tests and this is a great shortcoming of theses methods. The presented study is based on comparative tests with Hole Erosion Test and Mobile Jets Erosion Test apparatus, and tries to address this need. In this purpose, different remolded textures of soil were tested in order to cover a wide variety of situations. Thus, erosion parameters obtained from HET (erosion coefficient and critical shear stress) can be qualitatively linked to MoJET data (initial erosion rate and final eroded mass).
Keywords: Soil erosion, Piping, Surface erosion, Laboratory tests, Parametric study

INTRODUCTION

Recent catastrophic floods occurred among others in France (French county Aude in November 1999 or Gard in September 2002) clearly show the great vulnerability of embankments and dikes to internal erosion and overtopping. The surface and internal erosion do not always lead directly to failure of the structures, but may do so by reducing its overall stability under the working load and water flow. Combinations of these phenomena, if they last long enough may lead to breaching the embankment. It should also be recognized that unlike modern dams, the internal structure of these road and rail embankments and some old dikes dating from the French renaissance were not designed with filters and surface erosion protection (Guiton 1998).

This paper presents the study of reproducible erosive tests using two different apparatus: the recently proposed "Hole Erosion Test" (HET) (ASTM 2005a, Perry 1979, Pham 2008, Pham et al. 2010, Wan and Fell 2002, 2004) and the LCPC "Mobile Jets Erosion Test" (MoJET) (Henensal and Duchatel 1990, Pham 2008) that can be used either in laboratory or in the field. Tests have been carried out with soils prepared with various ground textures and the results have been compared. The results can so be used to establish directives supplementing the actual design guides for road or landscape management (CFG 2004, LCPC and SETRA 1992).

This paper is organized as follow. In a first part (section 2), basic features of the Hole Erosion Test (section 2.1) and the Mobile Jets Erosion Test (section 2.2) are given such as the description of the ground texture used for conducting the both tests (section 2.3). In a second part (section 3), results are presented for the both tests (HET section 3.1 and MoJET section 3.2) and comparisons are finally made (section 4). Conclusion and perspectives are drawn in a last part (section 5).

TESTING METHODS AND MATERIALS

Laboratory erosion tests are a convenient way to understand how various factors affect the complicated process of soil erosion. It is easy in the laboratory to collect runoff water in a measuring tank and to measure the quantity of eroded soil. Many apparatus able to produce an artificial erosion of a soil surface have been thus developed in the past decades (Arulanandan et al. 1980, Bendahmane et al. 2006, Sanchez et al. 1983, Wan and Fell 2002, 2004).

However, tests that can be done in the field are of great interest because they allow testing of the soil in its real initial state with the ability to repeat the test on the structure close to a breach. This is the case of the jet erosion test developed by Hanson (2004) and the MoJET developed at LCPC by Hénensal and Duchatel (1990).

We used in this study a modified version of the HET and the LCPC MoJET to compare results on soils prepared with various ground textures.

Hole Erosion Test (HET)

In order to quantitatively characterize the piping erosion, the Hole Erosion Test recently developed by Wan and Fell (2002,2004) was a great understanding step forward.

We recently design and develop our own HET device (Pham 2008, Pham et al. 2010, Reiffsteck et al. 2006). Similar to the one developed by Wan and Fell, it presents a number of improvements designed to make it easier to use and more comprehensive for measuring parameters of erosion.

Apparatus

The HET device has three parts: an upstream water tank, an eroding unit where the sample is located (Fig. 1) and a downstream water exit.

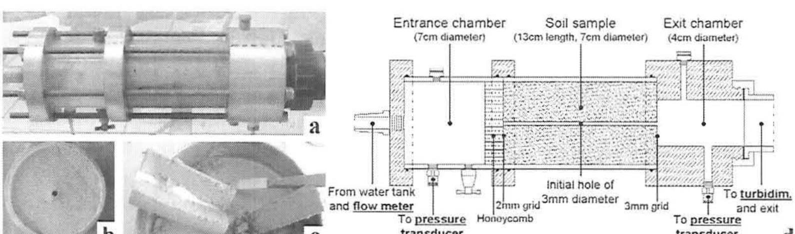

Figure 1. Hole erosion test set-up. (a) Image of eroding unit. (b) Sample before test with 3mm diameter hole. (c) Cut sample after test with molded wax. (d) Drawing of eroding unit. Sensors are indicated in bold and underlined characters.

The upstream tank is a PVC cylinder of 80 liters volume. It can be pressurized by air and recharged with water during the test. A turbine flow meter is placed in the vicinity of the eroding unit.

The column of water downstream is constant at 20cm.

The eroding unit is depicted on figures 1(a-d). It includes three parts. The first part is the entrance chamber of water. In addition to a first miniature pressure transducer, this part includes a honeycomb in order to reduce swirl in entry hole as well as a grid of 2mm. The second part consists of the soil sample itself with a hole of 3mm in diameter. The Plexiglas transparent mold allows checking that no unexpected erosion occurs between the sample and the mold. The third part is the exit room. This section includes a second miniature pressure transducer. A turbidimeter is placed right after this part in order to measure the turbidity of the fluid out of the specimen.

Procedure

Soil samples are prepared into a cylindrical Plexiglas mold. The dimensions are 7cm in diameter and 13cm in length (volume: 500 cm3). The soil is prepared in advance at given water content. Water content and final density are generally defined using a standard Proctor test (ASTM 2005b) for comparison with practical conditions in embankments. The initial hole of 3 mm diameter in the middle of the sample is finally achieved with a vertical drill (Fig. 1b).

After bringing water in all the system and especially in the sample, the air pressure in the upstream water reservoir is raised gradually until the desired pressure drop at the sample is reached. As erosion occurs, the sample hole grows during the test and the water flow increases. This increasing flow induces that head loss in the upstream hydraulic system increases then the pressure in the water reservoir is also increased and the pressure drop ΔP at the sample boundaries is maintained constant. When the total head loss of the hydraulic system is too large, increasing pressure in the reservoir is no longer sufficient to maintain a constant pressure drop in the sample. This happens when the diameter of the hole is nearly the same as the pipes diameter supplying the circuit. The pressure in the tank is slowly reduced and then reduced to zero.

The sample of eroded soil is then taken out of the device and molten wax is poured into the eroded hole. The sample is cut out and the "candle" is prudently extracted (Fig. 1c). This "candle" represents the shape of the hole of the sample after erosion. The volume allows calculating the final average radius of the eroded hole.

During the entire test, from the increase of head charge to the decrease, the data collected by flow meter (flow rate Q), pressure transducers (pressure drop ΔP) and turbidimeter (turbidity T) are stored on a computer using a datalogger. The frequency of acquisition is generally used 1Hz. These measurements and data on initial and final radii allow calculating erosion curves [interpretation method detailed in (Pham 2008, Pham et al. 2010)] i.e. the relationship between the two following physical quantities:

- the shear stress τ, that the flowing liquid applies on the interface (SI unit: Pa),

- the erosion rate $\dot{\varepsilon}$, that represents the mass of soil eroded per unit area and time (SI unit: kg.m^{-2}.s^{-1}).

Mobile Jets Erosion Test (MoJET)

The development of a specific testing apparatus of rotary type called "Mobile Jets Erosion Test" (Fig. 2) was the consequence of research undertaken by LCPC in the 1990's. This work was aimed partly to correlate the soil sensitivity to erosion with laboratory parameters such as plasticity index, methylene blue value, activity, texture and friction angle (Henensal 1993, Henensal and Duchatel, 1990). This apparatus can be implemented on site or used in laboratory and is thus well adapted for comparison with laboratory tests such as previously described Hole Erosion Test.

Apparatus

The mobile water jets test apparatus consists of an active mechanical part, called the "eroding unit", a water tank under controlled air pressure, and various additional units. The eroding unit projects water jets with 0.5 mm diameter nozzles (Fig. 2a) perpendicular to the soil surface which one wants to measure the sensitivity to erosion. Six water jets of similar and well defined characteristics are used. The geometry of this apparatus is quite similar to the submerged jet device developed by Hanson (1993, 2004). However in the LCPC apparatus, the soil is not fully submerged and the arm of the eroding unit, providing a mount for the six jet nozzles, rotates during the test.

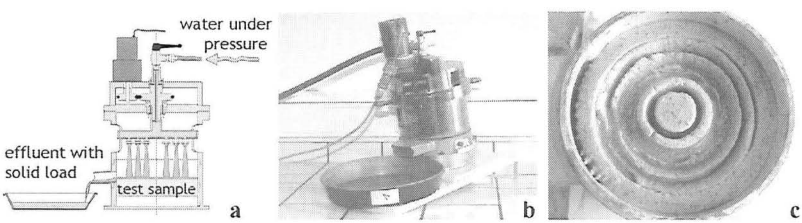

Figure 2. Mobile jets erosion test set-up. (a) Drawing of eroding unit. (b) Image of eroding unit. (c) Sample after test.

Procedure

The first stage of the test procedure is to bring the sample to a given density by static compaction. The sample in its mould is then inserted in the apparatus, which is connected with the pressurized water source. The mould is placed on a 10% slope (6 degree) used for the test (Fig. 2b). The outfall ring is inserted on the mould while directing the outfall towards the downstream of the slope into the top of the measurement container (Fig. 2b). The ground is then subjected to the action of the water jets with the following test parameters:

- air pressure in the water tank: 20 ±2 kPa, imposing flow rate,
- duration of the experiment: 12 minutes with sampling of the whole effluent at 1, 2, 4, 8 and 12 minutes.

After the test, the soil sample shows gullies located where the water jets impact its surface (Fig. 2c).

The quantity of effluent collected for the different times is passed to the drying oven and measured to determine the mass of dry material eroded (Pham 2008). This solid load (i.e. eroded mass as a function of time) can be used to perform qualitative evaluations of erosion, to establish correlations between the amount of soil erosion and the geotechnical properties or to compare the various soil behaviors.

Tested Materials

Different reconstituted textures of soil were tested in order to cover a wide variety of situations.

The textures are made from a mixture of sand, silt and kaolinite clay, to which is added a water content corresponding to 95% of Normal Proctor Optimum (ASTM 2005b). Kaolinite was used as it is a common type of clay in France. These soil textures are positioned on the ternary diagram of USCS classifications (Fig. 3a). The physical characteristics are reported in table 1 and the particle size distribution is shown on Fig. 3b. These textures cover a wide range from the clayey to the sandy soils.

It should be noted that samples are unsaturated and compacted as prepared at 95% of Normal Proctor Optimum (ASTM 2005b). This choice was made in this study as this is the typical state of materials for road or railway embankments. Anyway, the purpose of the present work is to focus on the comparison of two tests, HET and MoJET, using different soil textures and not to report a detailed study on the relative sensitivity of soils to erosion phenomena.

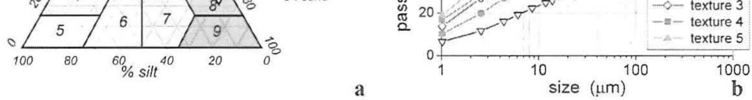

Figure 3. Tested textures. (a) ternary diagram and (b) particle size distribution.

Table 1. Tested textures: components and physical characteristics.

texture	dry mass fraction (%)			water	dry	liq/plastic limits		
	clay	silt	sand	(%)	density	w_L (%)	w_P (%)	IP (%)
1	25	5	70	11	2.1	13.5	-	-
2	35	25	40	11	1.95	19.6	13.9	5.7
3	45	40	15	14	1.9	26.9	20.4	6.5
4	65	5	30	19	1.8	26.1	21.7	4.4
5	70	20	10	26	1.85	35.2	30.0	5.2

RESULTS

Hole Erosion Test (HET)

The results of Hole Erosion Test on the specified textures are represented on figure 4. It represents the erosion rate $\dot{\varepsilon}$ as a function of the shear stress τ at the interface. It should be noted that, for each soil textures, experimental data points were obtained from repeatable tests and also for different pressure drops (Pham 2008, Pham et al. 2010).

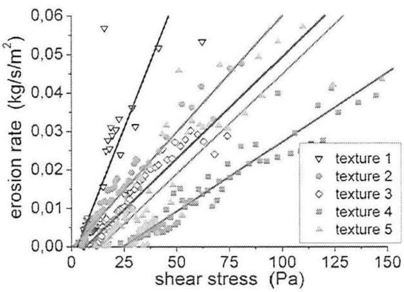

Figure 4. Experimental data and fit of Hole Erosion Test for the different textures.

As underlined in previous experimental and theoretical work (Bonelli et al. 2006, Wan and Fell 2002, 2004), data can be fitted with empirical linear laws with threshold:

$$\dot{\varepsilon} = k_{er}\left(\tau - \tau_c\right),$$

where τ_c is the critical shear stress and k_{er} the erosion coefficient. These coefficients thereafter characterize the erosion process occurring in the HET.

Experimental data for the different soil samples can be easily separated and HET allows well separating the behavior of the different textures. In particular, the texture 1 on one side and the texture 4 on the other are very well distinct from the textures 2, 3 or 5: the texture 1 presents clearly the higher sensitivity to erosion and the texture 4 is the most resistant. It could be noted that whereas the textures 4 and 5 have comparable characteristics (especially for the clay content), they present a really different sensitivity to erosion.

Mobile Jets Erosion Test (MoJET)

The results of Mobile Jets Erosion Test on the specified textures are represented on the figures 5(a,b). Figure 5(a) shows the cumulated eroded mass as a function of time whereas figure 5(b) represent the erosion rate, i.e. the eroded mass by unit of time. Experimental data show a rather good repeatability even if the test is relatively simple.

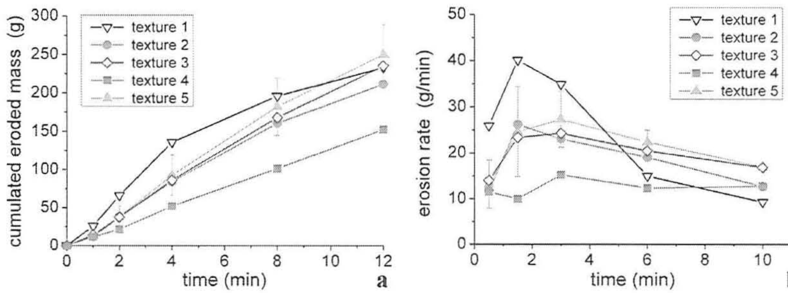

Figure 5. Experimental data of Mobile Jets Erosion Test for the different textures: (a) cumulated eroded mass and (b) erosion rate as functions of time.

Curves on figure 5(b) present two phases. In the first time of the test, there is an increase of the erosion rate corresponding at the initiation and the set-up of the erosion processes. Thereafter, erosion rate decreases as the gullies (see Fig. 2c) are deeper and so the stress applied on their surface decreases.

Experimental data for some soil samples show distinct characteristics even if the MoJET does not allow separating the behavior of all the different textures. In particular, the texture 1 on one side and the texture 4 on the other are very well distinct from the textures 2, 3 or 5 like as already shown with HET: the texture 1 presents clearly the higher sensitivity to erosion and the texture 4 is the most resistant.

COMPARISON OF HET AND MoJET

The characteristics of erosion curves obtained with HET are well defined. In particular, the sensitivity to erosion can be evaluated thanks to the critical shear stress and the erosion coefficient. Concerning the MoJET, even if the test is convenient and the erosion curves are relatively easy to explain, the deduction from theses curves to simple erosion parameters is far from trivial. We thus seek to link both tests by a simple approach of the mechanisms occurring in the MoJET.

Erosion Coefficient (HET) and Initial Erosion Rate (MoJET)

One of the two parameters characterizing HET is the erosion coefficient k_{er}. It is the only parameter that characterizes the erosion for shear stresses far from the threshold. Figure 6(a) represents the erosion coefficient obtained from HET for the different textures.

For the MoJET, the erosion is the more efficient at the early stage of the test since the gullies are relatively small at this time. To characterize the erosion "far from the critical shear stress", we thus choose to consider the erosion rate at the beginning of the test (or "initial erosion rate"). This erosion rate is simply the average one between 1 and 4 minutes. As remarked before, we do not consider the really first stage of erosion (i.e. the first minute) since it is certainly not representative of the erosion process. Figure 6(b) represents the initial erosion rate obtained from MoJET for the different textures.

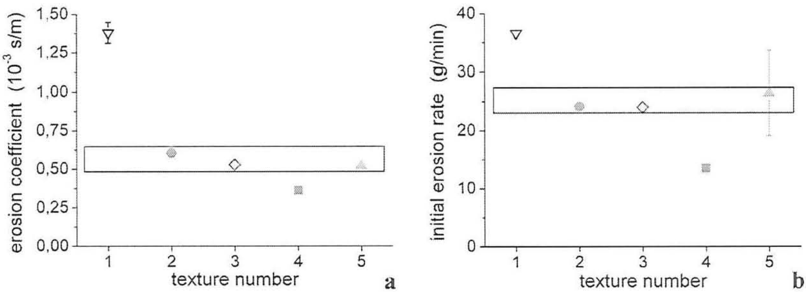

Figure 6. Tests comparison. (a) Erosion coefficient from HET. (b) Initial erosion rate from MoJET for the different textures.

Comparing figures 6(a) and 6(b), we find linkable results from the considered parameters issued from both tests. It could be expected that higher erosion coefficient from HET corresponds to higher initial erosion rate from MoJET. It is indeed what is observed. Texture 1 presents the highest erosion rate and the highest initial erosion rate where as texture 4 presents the lowest ones. The parameters from textures 2, 3 and 5 are not distinct.

Critical Shear Stress (HET) and Final Eroded Mass (MoJET)

The second parameter characterizing HET is the critical shear stress τ_c . It represents the shear stress that it is necessary to overcome in order to erode the soil. Figure 7(a) represents the critical shear stress obtained from HET for the different textures.

For the MoJET, the erosion efficiency decreases with time since the gullies that are full of water are deeper and the action of the water jets is thus less important. If the test lasts enough, one could expect that there is no more eroded mass (as the stress on the walls of the gullies is no more sufficient) and that the final cumulated eroded mass (at 12 min in the MoJET protocol) can so be linked to the critical shear stress. Figure 7(b) represents the final eroded mass (at 12 min) obtained from MoJET for the different textures.

Comparing figures 7(a) and 7(b), we find quite linkable results from the considered parameters issued from both tests. It could be expected that higher critical shear stress from HET corresponds to lower final eroded mass from MoJET. It is indeed what is observed for most of the textures. In particular, it should be noted that in contrary to the previous comparison (Fig. 6a-b), results for texture 1 aren't distinct from ones for textures 2 and 3 for both tests. This observation tends to prove that our differentiation of erosion coefficient and critical shear stress for HET on one side and initial erosion rate and final eroded mass for MoJET on the other has valid aspects. Results on texture 5 are more difficult to interpret and probably point out some of the limits to link the both tests.

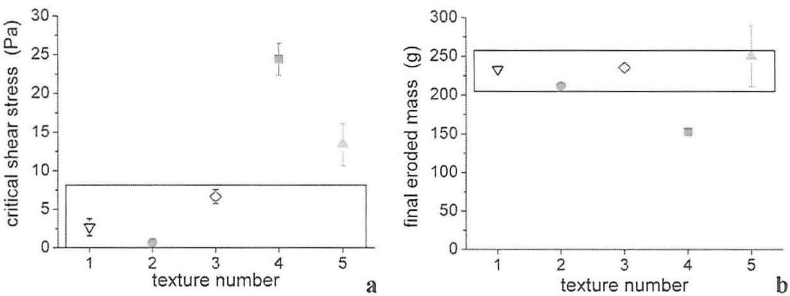

Figure 7. Tests comparison. (a) Critical shear stress from HET. (b) Final eroded mass from MoJET for the different textures.

CONCLUSION AND PERSPECTIVES

We present in this paper two methods to characterize erosion of soil: the Hole Erosion Test and the Mobile Jets Erosion Test, the latter allowing in situ test.

After using HET and MoJET on reference materials and reporting results, we sought to compare erosion characteristics issued from both test.

We thus qualitatively linked on one side the erosion coefficient obtained from HET and the initial erosion rate obtained from MoJET and on the other side the critical shear stress from HET and the final eroded mass from MoJET.

For a better comparison of the tests and understanding of the erosion process in the MoJET, a step forward would probably be to physically model the MoJET in order to obtain erosion parameters quantitatively comparable as the ones from HET. It would be of great interest since MoJET allows testing the soil in its real state and is most convenient and easy to use than HET.

ACKNOWLEDGMENTS

We thank Jean-Louis Tacita for valuable help with the test set-ups.

I. Haghighi benefits and T.L. Pham benefited from a student financial support delivered by the LCPC and the French public work ministry.

This work was partly financially supported by the French research program “ANR ERINOH”.

REFERENCES

Arulanandan, K., Gillogley, E. and Tully, R. (1980). "Development of a quantitative method to predict critical shear stress and rate of erosion of natural undisturbed cohesive soils." Tech Rep. GL-80-5 , U.S. Army Engineers, Waterways Experiment station, Viksburg, MS EU.

ASTM (2005a). "Standard test method for identification and classification of dispersive clay soils by the pinhole test." *Annual book of ASTM standards*, Vol. 04.08, D4647-93(Reapp98).

ASTM (2005b). "Standard test methods for laboratory compaction characteristics of soil using standard effort." *Annual book of ASTM standards*, Vol. 04.08, D698-00.

Bonelli, S., Brivois, O., Borghi, R. and Benahmed, N. (2006). "On modelling of piping erosion." *Comptes Rendus de Mécanique*, 334(8-9): 555-559.

Bendahmane, F., Marot, D. and Alexis, A. (2006). "Experimental parametric study of suffusion and backward erosion." *Journal of Geotech. and Geoenv. Eng.*, 134(1): 57-67.

CFG (2004). "Recommandations pour l'utilisation des géosynthétiques dans la lutte contre l'érosion." www.cfg.asso.fr .

Guiton, M. (1998). "Ruissellement et risque majeur, Phénomènes, exemples et gestion spatiale des crues." *Études et recherches des LPC*, Série Environnement et Génie Urbain EG13.

Hanson, G.J. (1993). "Soil erodibility testing." US Patent N° 5,243,850.

Hanson, G.J. (2004). "Apparatus, test procedures, and analytical methods to measure soil erodibility in situ." *Applied Engineering in Agriculture*, 20(4): 455-462.

Henensal, P. and Duchatel, F. (1990). "L'érodimètre à jets mobiles." *Bulletin des Laboratoires des Ponts et Chaussées*, 167, 47-53.

Henensal, P. (1993). "Lutte contre l'érosion avant, pendant et après les travaux: Les protections végétales et structurelles des surfaces et des pentes." *Études et recherches des LPC*, Série Géotechnique GT54.

LCPC and SETRA (1992). "Guide pour les Terrassements Routiers." Vol. 1 & 2.

Perry, E. B. (1979). "Susceptibility of dispersive clay at Grenada dam, Mississippi, to piping and rainfall erosion." Tech Rep. GL-79-14 , U.S. Army Engineers, Waterways Experiment station, Viksburg, MS EU.

Pham, T.L. (2008). "Erosion et dispersion des sols argileux par un fluide." *PhD Thesis*, Ecole Nationale des Ponts et Chaussées, Paris, France.

Pham, T.L., Chevalier, C., Reiffsteck, P.; Duc, M. and Guédon, S. (2010). "Improvement of hole erosion test and results on reference soils." *in preparation*.

Reiffsteck, P., Pham, T.L., Vargas, R. and Paihua, S. (2006). "Comparative study of superficial and internal erosion tests." *3rd International Conference on Scour and Erosion*, Amsterdam.

Sanchez, R.L., Strutynsky, A.I. and Silver M.L. (1983). "Evaluation of the erosion potential of embankment core materials using the laboratory triaxial erosion test procedure." Tech Rep. GL-83-4, U.S. Army Engineers, Waterways Experiment station, Viksburg, MS EU.

Wan, C.F. and Fell, R. (2002). "Investigation of internal erosion and piping of soils in embankment dams by the slot erosion test and the hole erosion test." UNICIV Report, no. R-412.

Wan, C.F. and Fell, R. (2004). "Investigation of rate of erosion of soils in embankment dams." *Journal of Geotech. and Geoenv. Eng.*, 30(4): 373-380.

The Effects of Exopolymers on the Erosional Resistance of Cohesive Sediments

R. A. Nugent[1], S.M. ASCE, G. Zhang[2], M. ASCE, Ph.D., P.E, and R. P. Gambrell[3], Ph.D.

[1]Department of Civil and Environmental Engineering, Louisiana State University, 1401J Patrick F. Taylor Hall, Baton Rouge, LA 70803; PH (225) 288-6824; email: rnugen2@lsu.edu
[2]Department of Civil and Environmental Engineering, Louisiana State University, 3509 Patrick F. Taylor Hall, Baton Rouge, LA 70803; PH (225) 578-6047; email: gzhang@lsu.edu
[3]Department of Oceanography and Coastal Sciences, Louisiana State University, 3173 Energy, Coast, and Environment Bldg., Baton Rouge, LA 70803; PH (225) 578-6426; email: gambrell@lsu.edu

ABSTRACT

Sediment erosion threatens coastal infrastructure and natural habitats throughout the coastal United States. Conventional soil amendments, such as lime, Portland cement, and polyacrylamide, are effective for improving soil strength and resistance to erosion, but exopolymers have the potential to improve sediment stability without the environmental risks of caustic or toxic compounds. This paper describes how the erosional resistance of a pure kaolinite clay is enhanced using two exopolymer analogues, guar gum, a neutral polysaccharide, and xanthan gum, an anionic polysaccharide. A cohesive strength meter was used to measure the critical shear stress τ_{oCr} of high water content muds, representative of newly placed, hydraulically pumped sediment fill. Guar gum produces a nine-fold increase in τ_{oCr} due to increases in pore fluid viscosity and hydrogen bonding between biopolymer strands and clay particles. Xanthan gum provides much less improvement because of electrostatic repulsion. Practical applications of exopolymers for erosion control are discussed.

INTRODUCTION

Currents or flows gradually remove soil particles on sediment surfaces, and this erosion causes much infrastructure and natural habitat damage, especially along the United States coastline. Louisiana is severely afflicted by this problem, losing one acre of land every 24 minutes because of soft wetland sediment (Fischetti 2001) and subsidence. Of bridge failures between 1989 and 2000, 15.51% were caused by scouring of bridge foundations (Wardhana and Hadipriono 2003), and both external and internal erosion can cause failures of river banks, levees, and dams. One common method for rapidly rebuilding wetlands lost through erosion is hydraulic pumping of dredged sediment to recreate the wetlands. However, the high water content muddy fill deposited by hydraulic pumping has low shear strength, and this poor stability makes freshly deposited fill susceptible to erosion, especially before plants become established.

Care must also be used in amending the soil to improve shear strength because of the toxic or caustic nature of many soil stabilizers. Specifically, ASTM standard D 6276 (ASTM 2006) states that calcium hydroxide or calcium oxide must be added to a soil at a concentration that raises soil pH to 12.4, and this pH is far too alkaline for a healthy marsh ecosystem. Many grouts, such as polyacrylamide, are also toxic, and human exposure must be minimized. Given the large scale and environmentally sensitive nature of wetland restoration projects, traditional amendments are too risky to use. Further, any compound used for improving slurry stability must not inhibit or slow vegetation growth, since plants are also effective for increasing sediment stability. Tengbeh (1993) demonstrated that grass roots can provide a five-fold increase in shear strength over a wide range of water contents, and de Baets et al. (2007) showed that plant roots can increase surface erosion resistance as well. This information provides a strong argument for the use of exopolymers to temporally improve sediment stability because they do not put the environment at risk, like other typical soil stabilizers, while plants become established.

Soil environments have large populations of microorganisms. An important product formed by micro-communities of bacteria, or biofilms, is exopolymers, or extracellular polymeric substances (EPS). Microorganisms produce exopolymers to regulate the microenvironment and to protect themselves against predation and drying. Numerous studies have been performed demonstrating the usefulness of exopolymers in the environment. Typically, exopolymers serve to increase the erosional resistance of sediments when present on sediment surfaces (Widdows et al. 2006; Yallop et al. 2000). For example, in intertidal mudflats, a newly-placed sediment's stability was directly correspondent to that sediment's production and quantity of EPS (Widdows et al. 2006). In sand, *Alteromonas atlantica* built a biofilm that immensely increased the critical shear velocity necessary for the start of sand erosion (Dade et al. 1990). Further, sediment EPS has been found to positively correlate with erosional resistance, while humic acids negatively correlate with erosional resistance (Gerbersdorf et al. 2007).

In addition to erosional stability, a few pilot studies have explored the application of exopolymers to soil treatment and improvement. For instance, artificially added EPS dramatically increased the tensile strength of air-dried strips of the common clay minerals kaolinite and montmorillonite (Chenu and Guérif 1991). Also, the addition of xanthan gum significantly increased the shear strength of Leighton Buzzard sand (Çabalar and Çanakci 2005). Another preliminary study by Nugent et al. (2009) demonstrated how the nanoscale interactions between kaolinite and two EPS analogues, guar gum and xanthan gum, changed the kaolinite's liquid limit.

Louisiana State University (LSU) is studying bioengineered sediment stabilization through the use of exopolymer amendments in an effort to find a solution for wetland erosion that will have minimal environmental impact. Because the Lower Mississippi River Basin and the Northern Gulf Coast mostly have cohesive sediments, this is the type of sediment used in this investigation. This paper describes how the erosional resistance of a pure kaolinite clay is enhanced using two exopolymer analogues, guar gum, a neutral polysaccharide derived from plants, and xanthan gum, a microbially produced anionic polysaccharide. A cohesive strength meter (CSM) is used to measure the critical shear stress τ_{oCr} of high water content muds, representative of newly placed hydraulically pumped dredge fill. Changes in τ_{oCr} are explained in terms of nanoscale chemical and physical interactions between exopolymer strands and clay particles. Methods for practical application of exopolymers for erosion control are then discussed.

MATERIALS AND METHODS

A relatively pure, untreated, kaolinite clay sample purchased from Theile Kaolin Company was used for this study. Particles smaller than 2 μm made up 98 wt.% of the sample. The specific gravity is 2.63, while the average specific surface area measured 20-26 m^2/g (Flick 1989). Kaolinite was chosen to minimize variance caused by the sediment. Although pure mineral kaolinite is not representative of the composition of Louisiana wetland sediment, it provides a good starting point for determining mechanisms of biopolymer and clay interaction. Specifically, pure mineral kaolinite eliminates interference from foreign organic material, and the low cation exchange capacity of kaolinite reduces variance from cations that can significantly change biopolymer and clay interaction (Nugent et al. 2009). However, the interaction mechanisms developed will not be exclusive to kaolinite, which will allow extrapolation to other cohesive soils. Laboratory Grade guar gum was purchased from Fisher Scientific, and NF Grade xanthan gum was purchased from Spectrum Chemical Manufacturing Corporation. These EPS analogs are described below.

Guar Gum

This neutral polysaccharide comes from *Cyamopsis tetragonoloba* seeds (Risica et al. 2005). Guar gum is capable of hydrogen bonding because it possesses many hydroxyl (-OH) groups. Also, it has a neutral charge because it lacks readily ionizable functional groups, such as carboxylic acid (-COOH) groups. It can produce viscous, pseudoplastic aqueous solutions representative of neutral microbial EPS, even though it is derived from plants. Guar gum has a commercial significance because it is readily available and inexpensive. It also has the ability to increase the viscosity of aqueous systems (Whitcomb et al. 1980).

Xanthan Gum

Xanthan gum is an anionic polysaccharide produced by the bacteria *Xanthomonas campestris* (Sutherland 1994). Its anionic charge comes from hydrogen atoms dissociating from carboxylic acid (-COOH) groups to form carboxylate ($-COO^-$) anions. Xanthan gum's hydroxyl (-OH) groups also allow for hydrogen bonding. Xanthan gum is used commercially because just a small amount of it will greatly increase the viscosity of an aqueous system (Hassler and Doherty 1990). An increased shear rate, however, decreases its viscosity because it is pseudoplastic (Milas et al. 1985).

Preparation of Biopolymer and Clay Specimens

The CSM apparatus uses a water jet contained inside a sensor head, and this sensor head is designed to be pressed into sediment surfaces. Thus, the biopolymer and clay muds prepared for the CSM tests had to be prepared in a fashion that provides a consistent, accessible surface for the 63.5 mm (2.5 in.) wide sensor head. Glass beakers (400 ml) filled with 125 ml of mud provided a surface with enough clearance and sufficient sediment depth to prevent the water jet from eroding enough mud to reach the bottom of the beaker. A starting water content of 180% was used for each mud because this amount of water, when mixed with the kaolinite chosen for this test, produces a fluid mud similar in texture to high water content wetland mud.

It is not useful to describe biopolymer concentration in terms of its pore solution concentration because a saturated clay's water content decreases during consolidation and varies in nature. Therefore, the biopolymer mass ratio, or R_{bm}, is used to measure concentration, which is the ratio of dry biopolymer mass to the sediment dry mass. To produce the specimens used for the CSM tests, a 1.5 wt.% guar gum solution and a 1.5 wt.% xanthan gum solution were first made. Although chemical means can be used to produce homogenous biopolymer solutions, physical mixing would be more practical for field purposes. Dry biopolymer powder was slowly added into distilled/deionized (DDI) water that was stirred by a stir bar over several minutes to reduce clumping. An immersion blender was then used to break down biopolymer powder clumps in the solutions to completely homogenize the solutions. Next, predetermined masses of biopolymer solution, dry kaolinite powder, and DDI water were mixed to produce 125 ml specimens with 180% water contents and appropriate R_{bm} values. Nine specimens were made, which included kaolinite without biopolymer, guar gum and kaolinite mixtures with concentrations of 0.005, 0.010, 0.015, and 0.020 R_{bm}, and xanthan gum and kaolinite mixtures with concentrations of 0.005, 0.010, 0.015, and 0.020 R_{bm}. After adding the materials for each specimen, the materials were lightly stirred with a spatula to prevent driving kaolinite powder into the air and to partially mix the mud. Again, the immersion blender was used to make sure the mud was homogenized.

With the specimens fully mixed, each mud was loaded into a beaker by using a spatula to place portions of mud into the center of the beaker, while being careful not to trap any bubbles of air. As the muds were relatively fluid, they flowed outward and formed a reasonably smooth upper surface. Since dredging is normally done during calm weather and wave conditions, freshly deposited slurry will typically have a few days before being exposed to significant erosional events. Thus, the beakers of mud were placed in a refrigerator at 4 °C for 72 hours to let the mud briefly consolidate under its own weight while minimizing the effect of biological degradation. After 72 hours, those refrigerated muds were allowed to warm to room temperature, and any water present on the mud surface was carefully removed with a paper towel. Then, the CSM sensor head was inserted into the mud surface and was used to measure τ_{oCr}, as described in the next section. Figure 1 provides a picture of the sensor head and a schematic of the sensor head inserted into a sediment surface.

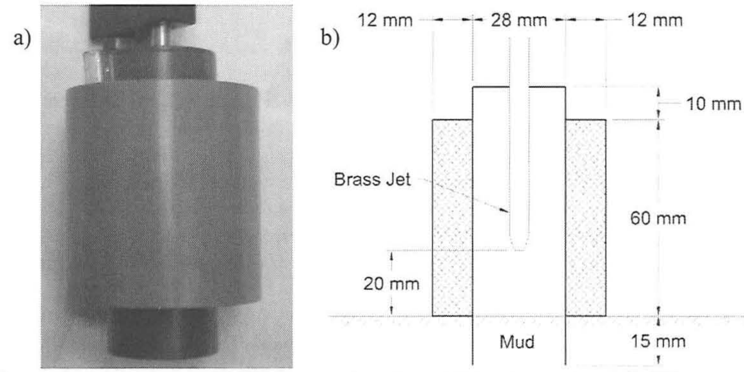

Figure 1. (a) Picture of CSM sensor head and (b) schematic of CSM sensor head cross section inserted into a sediment surface.

Cohesive Strength Meter Methodology and Data Analysis

The apparatus employed was a MKIV 60psi CSM acquired from Partrac Ltd., and it was used based on the guidelines proposed by Tolhurst et al. (1999). With the CSM sensor head in the sediment surface, the sensor head was carefully filled with DDI water, and test program MUD 3 was activated. This test program involves activating the water jet for 0.3 seconds, and then measuring the infrared transmissivity of the water in the sensor head for 30 seconds before activating the jet again. As more sediment is eroded, the transmissivity of the suspension decreases. The jet was initially fired using a driving air pressure of 3.45 kPa (0.5 psi) with the pressure increased by 3.45 kPa (0.5 psi) until a pressure of 34.47 kPa (5 psi) was reached. Afterwards, the pressure was incremented by 6.89 kPa (1 psi) until either a pressure of 413.69 kPa (60 psi) was reached or the operator ended the test early due to the transmissivity approaching 0%. Once the program was complete, some mud around the outside of the sensor head was removed to measure the water content according to ASTM standard D 2216 (ASTM 2006). The sensor head was then removed and cleaned. Because guar gum and xanthan gum are polysaccharides with a high molecular weight, they do not volatilize in the drying oven at 110 ± 5 °C, which means the biopolymer adds to the solid fraction of the water contents and void ratios.

Critical values of shear stress τ_{oCr} for each specimen were determined from the raw CSM data by plotting the transmissivity against time, as shown in Figure 2. Two lines were drawn with the first line going through the linear points before the sediment significantly eroded, and the second line was drawn through the linear points where the sediment is appreciably eroded by the water jet. The intercept is the time where τ_{oCr} is applied to the sediment. As this time is often between jet firings with discrete driving pressures, linear interpolation was used to calculate the intercept jet driving pressure. This driving pressure was then substituted into the equation developed by Tolhurst et al. (1999) to get τ_{oCr}. This equation is used to plot the shear stress curve in Figure 2.

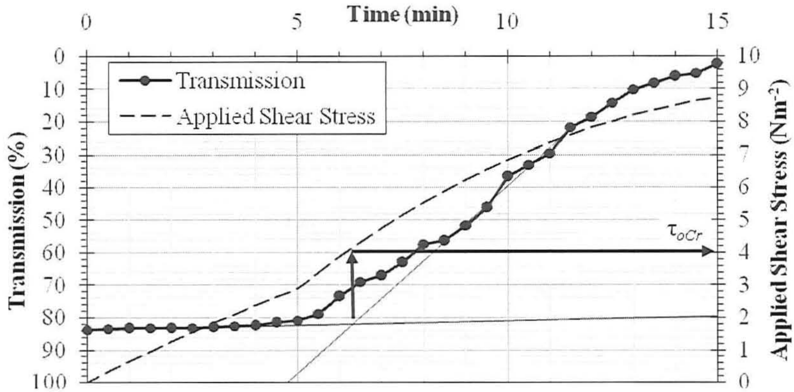

Figure 2. Representative raw CSM data and data analysis.

RESULTS AND DISCUSSION

The results of the guar gum and kaolinite mixture, as well as the results of the xanthan gum and kaolinite mixture are provided in Figure 3. For this figure, the liquid limit values are adapted from Nugent et al. (2009). Except for the 0.015 and 0.020 R_{bm} xanthan gum mixtures, the specimens were able to support the weight of the water filled sensor head needed to successfully complete the CSM tests. The two high concentration xanthan gum mixtures were too fluid to support the water filled sensor head, so valid τ_{oCr} or water content data could not be collected. Erosional resistance for 0.015 and 0.020 R_{bm} guar gum mixtures is increased by a factor of nine over kaolinite on its own, while 0.005 and 0.010 R_{bm} xanthan gum mixtures increase erosional resistance by 1.5 times. Water contents for the tested specimens all fell within 178% ± 4%, which reveals that little consolidation occurred and that the specimens all have approximately the same void ratio.

Figure 3 shows a clear relationship between τ_{oCr} and the liquid limit for guar gum. Nugent et al. (2009) demonstrated that the liquid limit of a guar gum and clay mixture increases as the biopolymer concentration increases because the guar gum boosts the pore fluid viscosity. Since viscosity is a measure of the shear resistance of a fluid, increased pore fluid viscosity leads to greater shear resistance of the overall mixture. In addition, most soils have an undrained shear strength of 1.7-2.0 kPa at the liquid limit (Sharma and Bora 2003), and undrained shear strength is a function of water content (Zentar et al. 2009). Thus, a sediment with a higher liquid limit will generally have a higher undrained shear strength for a given water content. Watts et al. (2003) illustrated a positive correlation between fall cone measured sediment shear strength and τ_{oCr}. As a result, the relationship between τ_{oCr} and the liquid limit is the result of both Casagrande cup and CSM tests indirectly measuring sediment shear strength.

Figure 3 also shows a correlation between τ_{oCr} and the liquid limit for the 0.005 and 0.010 R_{bm} xanthan gum mixtures, although this correlation is muted

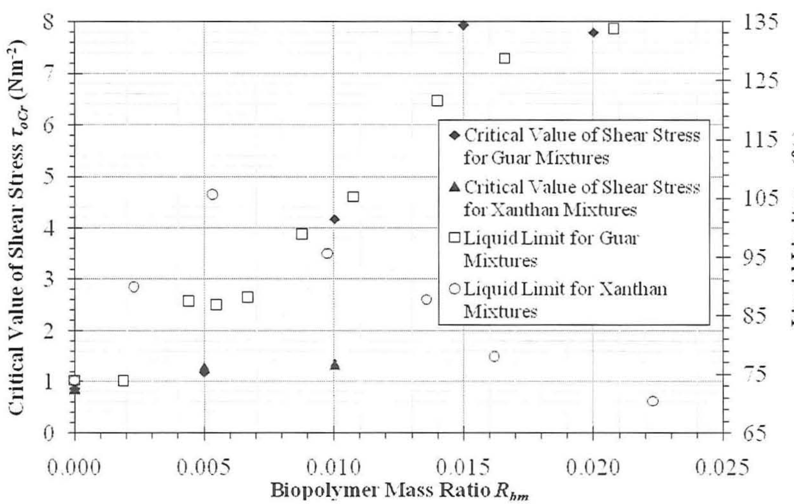

Figure 3. Erosional resistance as a function of biopolymer concentration. Liquid limit values are adapted from Nugent et al. (2009).

compared to the guar gum mixtures. Xanthan gum was also demonstrated by Nugent et al. (2009) to increase the liquid limit by increasing the pore fluid viscosity. However, Nugent et al. (2009) revealed that aggregation caused by xanthan gum at intermediate concentrations reduces the liquid limit to below that of the clay with no biopolymer added. For these intermediate concentrations, the aggregation effect overpowers the pore fluid viscosity effect, while viscosity effects overpower aggregation effects at low and high concentrations. Further, Garrels (1951) demonstrated that the water velocity needed to remove particles from sediment surfaces dramatically decreases as particle size increases for particles smaller than 0.5 mm. The fact that the 0.015 and 0.020 R_{bm} xanthan gum mixtures were too fluid and weak to measure their erosional resistance along with the sediment shear strength and τ_{oCr} correlation provided by Watts et al. (2003) shows that these higher concentration xanthan gum mixtures have a significantly reduced erosional resistance. All together, this suggests that biopolymer induced aggregation negatively affects erosional resistance in xanthan gum mixtures with concentrations greater than 0.010 R_{bm}.

Nugent et al. (2009) also noted that nanoscale interaction between biopolymer strands and clay particles serves to change the liquid limit. Specifically, they found that at biopolymer concentrations with similar pore fluid viscosities, guar gum raises the liquid limit much higher than xanthan gum. This was explained as a result of the guar gum and kaolinite forming an extensive hydrogen bonding network. Xanthan gum and kaolinite interacted little since xanthan gum's negative charge and the overall negative charge kaolinite particles possess at solution pH greater than 2.35 (Alkan et al. 2005) caused electrostatic repulsion that minimized any bonding. A similar effect is demonstrated by the CSM results. Both the 0.020 R_{bm} guar gum mixture and the 0.005 R_{bm} xanthan gum mixture have zero shear rate pore fluid viscosities of about 30 Pa·s (Whitcomb et al. 1980; Milas et al. 1985). However, the 0.020 R_{bm} guar gum mixture has a τ_{oCr} six times greater than the 0.005 R_{bm} xanthan gum mixture. This disparity is the result of the guar gum and kaolinite forming a hydrogen bonding network, while the xanthan gum and kaolinite electrostatically repel each other.

PRACTICAL APPLICATION

Guar gum and xanthan gum that are added to hydraulically pumped dredged sediment can improve resistance to erosion in wetlands, while minimizing environmental damage. Their non-toxicity also allows plant growth that greatly stabilizes the soil. The biopolymer can easily be added to the sediment through a hydraulic dredge's slurry pump, where it can be completely mixed with the sediment by the slurry output pipe's turbulence. This study demonstrates that the addition of guar gum to newly placed slurry can substantially reduce wetland erosion because guar gum can raise erosional resistance by almost one order of magnitude.

Although xanthan gum provides improvement to the soil, the results of this study showed it to be much less than what was provided by guar gum because of its electrostatic repulsion. This may be misleading. In this study, xanthan gum's negative charge could not be balanced by other cations because DDI water is basically cation free and kaolinite has a low cation exchange capacity. However, calcium ions can form cross-links between xanthan gum strands, greatly increasing the mixture's liquid limit (Nugent et al. 2009). Since there is a relationship between liquid limits and erosional resistance, divalent cations could form ionic bridges and improve erosional resistance through cross-linking. Further, monovalent cations in natural sediment should balance xanthan gum's negative charges, allowing it to form hydrogen bonds. Also note that the pore fluid viscosity, aggregation, hydrogen bonding, and electrostatic repulsion mechanisms described are not interactions exclusive to kaolinite. For example, Ma and Pawlik (2007) found that guar gum forms hydrogen bonds with many minerals, including kaolinite. Therefore, it is possible to extrapolate the results for kaolinite to other clays. However, more study is needed to fully characterize these interactions across a broad range of biopolymers and sediments.

CONCLUSIONS

This study involved performing CSM tests on a kaolinite clay mixed with differing amounts of biopolymer to see how the interaction of these materials would affect its resistance to erosion. Two polysaccharides, similar to natural soil EPS, were used. The polysaccharides included the neutral, plant derived guar gum and the anionic bacterial exopolymer xanthan gum. The following conclusions can be made from the results of the tests:

- As Casagrande cup and CSM tests both indirectly measure shear strength, the results of both tests are linked.
- Increasing biopolymer concentration increases the pore fluid viscosity, and this leads to increased erosional resistance.

- Biopolymer induced aggregation negatively effects erosional resistance.
- For a given pore fluid viscosity, guar gum produces substantially more erosional resistance than xanthan gum since guar gum establishes a hydrogen bonding network between guar gum strands and kaolinite particles.

ACKNOWLEDGEMENTS

This study was supported initially by the NOAA/CREST grant and then by the LABoR's RCS grant. R.A. Nugent also received the Donald Clayton Graduate Scholarship award from LSU College of Engineering to partially support his graduate study.

REFERENCES

Alkan, M., Demirbas, O., and Dogan, M. (2005). "Electrokinetic properties of kaolinite in mono- and multivalent electrolyte solutions." *Microporous and Mesoporous Materials*, 83(1-3), 51-59.

ASTM – American Society for Testing and Materials (2006). *Annual Book of ASTM Standards*, 04.08.

de Baets, S., Poesen, J., Knapen, A., and Galinda, P. (2007). "Impact of Root Architecture on the Erosion-Reducing Potential of Roots during Concentrated Flow." *Earth Surface Processes and Landforms*, 32(9), 1323-1345.

Çabalar, A. F., and Çanakci, H. (2005). "Ground Improvement by Bacteria." *Poromechanics - Biot Centennial (1905-2005)*. Abousleiman, Cheng, and Ulm, eds., Taylor and Francis Group, London, England, 707-712.

Chenu, C., and Guérif, J. (1991). "Mechanical Strength of Clay Minerals as Influenced by an Adsorbed Polysaccharide." *Soil Science Society of America Journal*, 55(4), 1076-1080.

Dade, W., Davis, J. D., Nichols, P. D., Nowell, A. R. M., Thistle, D., Trexler, M. B., and White, D. C. (1990). "Effects of Bacterial Exopolymer Adhesion on the Entrainment of Sand." *Geomicrobiology Journal*, 8(1), 1-16.

Fischetti, M. (2001). "Drowning New Orleans." *Scientific American*, 285(4), 76-85.

Flick, E. W. (1989). *Handbook of Adhesives Raw Materials*. 2nd ed., Noyes Publ., Park Ridge, NJ.

Garrels, R. M. (1951). *A Textbook of Geology*, Harper, New York.

Gerbersdorf, S. U., Jancke, T., and Westrich, B. (2007). "Sediment properties for assessing the erosion risk of contaminated riverine sites." *Journal of Soils and Sediments*, 7(1), 25-35.

Hassler, R. A., and Doherty, D. H. (1990). "Genetic Engineering of Polysaccharide Structure: Production of Variants of Xanthan Gum in *Xanthomonas campestris*." *Biotechnology Program*, 6(3), 182-187.

Ma, X., and Pawlik, M. (2007). "Role of Background Ions in Guar Gum Adsorption on Oxide Minerals and Kaolinite." *Journal of Colloid and Interface Science*, 313, 440-448.

Milas, M., Rinaudo, M., and Tinland, B. (1985). "The Viscosity Dependence on Concentration, Molecular Weight and Shear Rate of Xanthan Solutions." *Polymer Bulletin*, 14(2), 157-164.

Nugent, R. A., Zhang, G., and Gambrell, R. P. (2009). "Effect of Exopolymers on the Liquid Limit of Clays and Its Engineering Implications." *Transportation Research Board: Journal of the Transportation Research Board*, 2101, 34-43.

Risica, D., Dentini, M., and Crescenzi, V. (2005). "Guar Gum Methyl Ethers, Part I. Synthesis and Macromolecular Characterization." *Polymer*, 46(26), 12247-12255.

Sharma, B., and Bora, P. K. (2003). "Plastic Limit, Liquid Limit and Undrained Shear Strength of Soil – Reappraisal." *Journal of Geotechnical and Geoenvironmental Engineering*, 129(8), 774-777.

Sutherland, I. W. (1994). "Structure-Function Relationships in Microbial Exopolysaccharides." *Biotech Advances*, 12(2), 393-448.

Tengbeh, G. T. (1993). "The Effect of Grass Roots on Shear Strength Variations with Moisture Content." *Soil Technology*, 6(3), 287-295.

Tolhurst, T. J., Black, K. S., Shayler, S. A., Mather, S., Black, I., Baker, K., and Paterson, D. M. (1999). "Measuring the *in situ* Erosion Shear Stress of Intertidal Sediments with the Cohesive Strength Meter (CSM)." *Estuarine, Coastal and Shelf Science*, 49, 281-294.

Wardhana, K., and Hadipriono, F. C. (2003). "Analysis of Recent Bridge Failures in the United States." *Journal of Performance of Constructed Facilities*, 17(3), 144-150.

Watts, C. W., Tolhurst, T. J., Black, K. S., and Whitmore, A. P. (2003). "In situ measurements of erosion shear stress and geotechnical shear strength of the intertidal sediments of the experimental managed realignment scheme at Tollesbury, Essex, UK." *Estuarine, Coastal and Shelf Science*, 58, 611-620.

Whitcomb, P. J., Gutowski, J., and Howland, W. W. (1980). "Rheology of Guar Solutions." *Journal of Applied Polymer Science*, 25(12), 2815-2827.

Widdows, J., Brinsley, M. D., Pope, N. D., Staff, F. J., Bolam, S. G., and Somerfield, P. J. (2006). "Changes in Biota and Sediment Erodability Following the Placement of Fine Dredged Material on Upper Intertidal Shores of Estuaries." *Marine Ecology Progress Series*, 319(1), 27-41.

Yallop, M. L., Paterson, D. M., and Wellsbury, P. (2000). "Interrelationships between Rates of Microbial Production, Exopolymer Production, Microbial Biomass, and Sediment Stability in Biofilms of Intertidal Sediments." *Microbial Ecology*, 39(2), 116-127.

Zentar, R., Abriak, N.-E., and Dubois, V. (2009). "Fall Cone Test to Characterize Shear Strength of Organic Sediments." *Journal of Geotechnical and Geoenvironmental Engineering*, 135(1), 153-157.

Site Factor for Use of Velocity-Based EFA Erosion Rates

J. F. Perri[1], S. E. Shewbridge[2], R. Millet[3], W. Huang[3], J. Vargas[3], M. Inamine[4], S. Mahnke[4]

[1]Exponent, 500 12th Street, Suite 220, Oakland, CA, 94607 email: jperri@exponent.com
[2]URS Corporation, 1333 Broadway, Suite 800, Oakland, CA, 94612 email: scott_shewbridge@urscorp.com
[3]URS Corporation, 2870 Gateway Oaks Drive, Suite 150, Sacramento, CA, 95833 email: richard_millet@urscorp.com, wilbur_huang@urscorp.com, juan_vargas@urscorp.com
[4]Department of Water Resources, P. O. Box 942836, Sacramento, CA 94236 email: inamine@water.ca.gov, gmahnke@water.ca.gov

ABSTRACT

A mathematical model was developed for estimating riverbed and levee erosion rates based on the results of the Erosion Function Apparatus (EFA) test results of relatively undisturbed soil samples from several California river sites. The mathematical model for erosion estimates was written as a function of shear stresses. An alternative model was used to calculate riverbed and levee erosion rates as a function of channel flow velocity. It is shown that shear stresses imposed by small scale testing apparatuses, such as the EFA, can be significantly larger than those stresses observed in the rivers, for a given flow velocity. Therefore, a 'Site Factor' was developed to account for this difference in stresses, and still maintain the simplicity of a velocity-based erosion model. The velocity-based erosion model can be used as a first order approximation to assess erosion rates under water current loads. Because the use of water velocity is less representative and leads to more uncertainties than using the shear stress, velocity based formulations should be used when shear stress estimates are not readily available. Results of the erosion analyses can then be used to develop a qualitative relative ranking of river bank/berm and levee erosion susceptibility and failure potential.

INTRODUCTION

Historical erosion studies have concentrated in the evaluation of erosion protection. Because the final objective of most of these studies was to evaluate whether erosion was likely to occur, the findings and recommendation of these studied were generally of two types: selection of armor characteristics (e.g., size and shape) to resist the expected loads (wave and/or current) (e.g., Hudson, 1974) or selection of site configurations to reduce the loads at the erodible location (e.g., Dean, 1977; 1991). This lead to recommendation which are, in general, able to predict whether erosion will or will not occur.

The recognition that some erosion processes are beneficial, or too difficult to eliminate, led to the study of equilibrium profiles (e.g., Swart, 1974). The objective was to estimate the equilibrium configuration of sediment transport for natural materials commonly encountered in the coastlines. As a result, the erosion rate of sandy materials has been well studied, and predictions of sand erosion can generally be made.

In recent years, an increased amount of research has been devoted to the study of the erosion processes in non-sandy materials (e.g., Aberle et al., 2006; Hanson and Simon, 2001.). Two important types of failures have accelerated this interest: the relatively large number of bridge failures as a result of scour (e.g., Briaud et al., 2003), and levee erosion (e.g., Briaud, 2008).

Evaluation of erosion rates requires the understanding of the loads to be expected in the field, as well as an understanding of the erosion resistance of the erodible materials. This paper presents a simplified procedure developed for the evaluation of levee erosion, based on readily available hydrodynamic and geotechnical information of the levee systems, as well as the results of erosion rates of different materials, as measured in the lab.

EROSION SCREENING PROCESS

An Erosion Screening Process (ESP) was developed for the DWR Urban Levee Geotechnical Evaluations (ULE) Program. The complete ESP consists of a 3 tier screening process, as presented in Huang et al. (2010). The analyses are completed with the objective of screening the levee vulnerability, and not as a design tool.

Tier 1 consist of an evaluation of the levee geometry, fetch length, and historical geomorphologic performance. If a levee site fails any of the analyses steps in the first tier, or if its historical performance is deemed questionable, the site is evaluated using the second tier of risk factors. In the second tier, comparisons is made between the levee's surface material and river flow velocity and wave action for a given evaluation event. Field reconnaissance is performed to evaluate signs of erosion or unstable conditions, as well as assess the site's vegetation. If a levee site fails any of the three tests in the second tier, it will be advanced to the third tier of factors for further study. On Tier 3, given an evaluation event, an estimate of the erosion potential on the waterside of a levee is made using an Erosion Calculation Spreadsheet. Based on the results of those analyses, the levee section is characterized as having:

1. High erosion risk: The levee site is at immediate risk of an erosional failure during either a flood or a normal flow condition.
2. Moderate erosion risk: The levee site is at risk for failure due to weaknesses, but no immediate threat of failure is apparent.
3. Low erosion risk: Although a geometric deficiency has not been identified, there is either little threat from wind-wave impact and no evidence of historical erosion problems, or the levee's surface material appears adequate to resist velocity and wave loads.

This paper focuses on two alternative approaches to the calculation of erosion rates for Tier 3 of the erosion assessment. The overall methodology for the erosion potential was developed for the U.S. Army Corps of Engineers (USACE) in a risk assessment toolbox (URS, 2007). The methodology currently being implemented builds upon knowledge gained from both previous and concurrent erosion studies conducted by Ayres Associates, USACE, and others. It further adds factors like wind and vegetation.

In essence, for Tier 3, the erosion potential assessment is conducted using six pieces of information:

1. Levee Geometry;
2. Wind Characteristics;
3. Water/Stream/River Current Characteristics;
4. Armor Characteristics;
5. Vegetation Characteristics and
6. Soil Type

Erosion risks to riverine levees will most likely be due to a weakened levee cross section coupled with high flow velocity. In large, open bodies of water like a bypass, wind-wave damage is expected to be a dominant cause of erosion.

EVALUATION OF FLOW INDUCED EROSION: ALTERNATIVE APPROACHES

Because of the complexity of the erosion process, the evaluation of erosion rates was simplified by developing soil erodibility categories. When a soil is identified in the field, absent erosion testing, it can be represented by one of the erosion categories. For this study, and in general agreement with previous studies (e.g., Briaud, 2008; Hanson and Simon, 2001), the following broad erosion categories and typical soils are used:

Very Resistant: Cobbles
Resistant: Gravel (GP-GW)
Moderately Resistant: Clay (CL, CH, SC, GC)
Erodible: Sand (SP, SM and mixtures)
Very Erodible: Silt (ML)

The classification system can be generally presented in terms of erosion rate as a function of velocity, or as a function of shear stress. Although the shear stress formulations is theoretically better founded, there are advantages to representing erosion rates as a function of velocity, as it is often easier to rapidly assess a situation in terms of velocity.

Stress-based formulation

Several erosion studies have been performed in the past that focus on identifying the erosion parameters and correlating those parameters to formulate an expression (i.e., a physical model) for erosion rates (Hanson and Temple, 2001; Hanson and Cook, 2004). The governing equation (1) for this model is:

$$\dot{\varepsilon} = (k\,(\tau - \tau_c)) > 0 \tag{1}$$

Where:

k = erodibility coefficient or detachment rate coefficient (L^3/M-T)
τ = effective hydraulic stress on the soil boundary (M/L^2)
τ_c = critical shear stress (M/L^2) i.e., shear stress at which erosion starts

The erosion rate ($\dot{\varepsilon}$) is a function of both hydraulic (τ) and geotechnical (k, τ_c) parameters. The effective hydraulic stress, τ, mainly depends on the characteristics of the water-soil boundary, current/stream velocity and/or wind wave height and period. Both k and τ_c are functions of the engineering properties of the levee and the foundation materials.

The estimation of erosion rate due to shear stresses imparted to the levee and its foundation due to current/stream velocity requires information on the hydraulic parameters of stream velocity and water-soil interface roughness. Using the conventional assumption of a logarithmic velocity profile (USACE, 1994), the average hydraulic shear stress due to currents (τ_s) can be calculated using Equation 2.

$$\tau_s = \tfrac{1}{2}\, \rho\, f_c\, v^2 \tag{2}$$

Where:

ρ = mass density of water

f_c = current friction factor (dimensionless)

= $2(2.5(\ln(30h/k_b)-1))^{-2}$ (Danish Hydraulic Institute (DHI), 2006)

Where:

h = water depth

k_b = bed roughness

v = flow speed

Critical Shear Stress

Erosion rates as a function of shear stress can be measured in the laboratory using one of several devices such as the Erosion Function Apparatus (EFA, Briaud et. al, 2001a and b). The critical shear stress, τ_c, is defined as the shear stress corresponding to a rate of erosion of 1 mm/hr in the EFA. While useful for analytical studies, this method is impractical for rapid surveys.

Alternatively, the critical shear stress can be estimated using empirical correlations between the critical shear stress and soil index properties. Several empirical correlations between critical shear stress (τ_c) and soil index properties such as grain size, plasticity index and shear strength are available in the literature to estimate the value of τ_c (URS, 2007).

As previously mentioned, in order to simplify the analyses, erosion resistance of the levee and foundation material has been divided into five broad classes related to their ASTM classifications, as shown in Table 1. The erosion calculations used these typical values for critical shear. The values shown in Table 1 are based on the experimental and field-testing results as reported by Briaud et al. (2001a, 2003) and Hanson and Simon (2001).

Table 1 Typical Values for Critical Shear Stress and Coefficient of Erodibility of Soils

Material	ASTM Typical Soil Types	Critical Shear Stress, τ_c, psf (Pa)	Erodibility Coefficient, k, ft^3/lb-hr (m^3/kN-hr)
Levee/Foundation Material			
Very Resistant	Boulders and Cobbles	4.869 (233)	0.005 (0.0318)
Resistant	Gravel (GP-GW)	1.058 (50.7)	0.021 (0.134)
Moderately Resistant	CLAY (CL, CH, SC, GC)	0.094 (4.50)	0.094 (0.598)
Erodible	SAND (SP, SM and mixtures)	0.014 (0.670)	0.409 (2.60)
Very Erodible	SILT (ML)	0.003 (0.144)	1.867 (11.88)

Erodibility Coefficient

One method to estimate the coefficient of erodibility, k, used in Equation 1, is by performing the jet index test (ASTM D 5852). However performing site-specific tests will be impractical for rapid assessment of conditions.

Therefore, in a manner similar to the method used to evaluate critical shear stresses, to simplify the analyses, erodibility of the levee and foundation materials has been divided into five broad classes related to the material's ASTM classification, as shown in Table 1. The erosion calculations used typical values for erodibility coefficients. The values, presented in Table 1, are based on the experimental and field-testing results as reported by Briaud et al. (2001a, 2003) and Hanson and Simon (2001).

Velocity-based formulation

Several erosion studies have been performed in the past that focus on identifying the erosion parameters and correlating those parameters to formulate an expression for erosion rates as a function of velocity (e.g., Briaud, 2008). The governing equation (3) for this model is (a similar formulation can be developed for erosion rate as a function of shear stress):

$$\dot{\varepsilon} = (V / V_1)^{\alpha} \tag{3}$$

Where:

V_1 = Velocity which would cause an erosion rate of 1 unit

V = Site flow velocity

α = slope of the erosion rate versus velocity (in log-log space)

In this formulation, the erosion rate ($\dot{\varepsilon}$) is a function of both hydraulic (V, V_1) and geotechnical (α, V_1) parameters. As will be discussed later in this paper, it is not possible to assign a unique V_1 for a given soil type. In fact, V_1 is generally a function of the induced shear stress, and this is a function of multiple parameters (e.g., see Equation 2). In fact, V_1, mainly depends on the characteristics of the soil type, water depth, water-soil boundary, current/stream velocity and/or wind wave height and period.

Critical Velocity

Erosion rates as a function of flow velocity can be measured in the laboratory using one of several devices such as the Erosion Function Apparatus (EFA, Briaud et. al, 2001a and b). The EFA critical velocity, $V_{c\text{-}EFA}$, is defined as the flow velocity corresponding to a rate of erosion of 1 mm/hr in the EFA (with this definition and units, $V_1 = V_{c\text{-}EFA}$).

Alternatively, the critical velocity can be estimated using empirical correlations between the critical velocity and soil index properties. Several empirical correlations between critical velocity ($V_{c\text{-}EFA}$) and soil index properties such as grain size, plasticity index and shear strength are available in the literature to estimate the value of $V_{c\text{-}EFA}$ (e.g., Briaud, 2008). Figure 1 shows one such correlation, as presented by Briaud (2008).

SITE FACTOR

The EFA device is calibrated using the Moody chart for estimating the shear stresses induced by the flow velocity:

$$\tau = \tfrac{1}{8} \cdot f \cdot \rho \cdot v_{EFA}^2 \tag{4}$$

Where f is the friction factor, ρ is the water mass density and v_{EFA} is the EFA flow velocity.

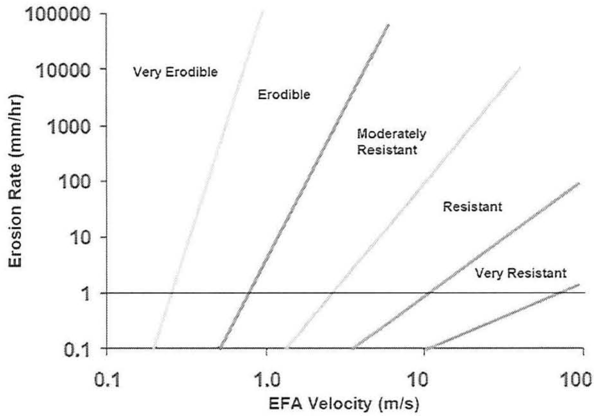

Figure 1. Erosion Rate as a Function of EFA Velocity (after Briaud, 2008)

Because shear stress, rather than flow velocity, is one of the principal loads on the erodible material, in order to develop a velocity-based formulation for erosion rate, it is necessary to estimate the flow velocity which in the field would result in the same shear stresses as in the EFA. Therefore, the objective is to find the river flow velocity (v_h, where the subscript h stands for depth) that, for a given material, causes the same hydraulic shear stresses as the EFA velocity (v_{EFA}). From Equation 2 and 4 follows that:

$$\tau_h = \tau_{EFA} \Rightarrow \tfrac{1}{2} \cdot f_c \cdot \rho \cdot v_h^2 = \tfrac{1}{8} \cdot f_{EFA} \cdot \rho \cdot v_{EFA}^2 \tag{5}$$

It is possible to show that for the material properties (very erodible to very resistant) and for depth between 5 cm (EFA) and 30 m, the stresses calculated with the DHI equation (Equation 2) and Darcy's friction formulae (Equation 4), the calculated hydraulic stresses are within approximately 10%. Therefore, to simplify the formulation of the site factor, Equation 5 can be simplified as (Equation 5 can be used for a more rigorous formulation):

$$\tau_h = \tau_{EFA} \Rightarrow \tfrac{1}{8} \cdot f_h \cdot \rho \cdot v_h^2 = \tfrac{1}{8} \cdot f_{EFA} \cdot \rho \cdot v_{EFA}^2 \tag{6}$$

Therefore:

$$v_{EFA} = \sqrt{\frac{f_h}{f_{EFA}}} \cdot v_h = \frac{v_h}{S}, \text{ Where S is the site factor} \tag{7}$$

For fully developed turbulent flow (it can be shown that for erosion practical cases, and in the EFA, most of the time this is valid), the turbulent portion of the Colebrook equation can be used:

$$\frac{1}{\sqrt{f}} = -2 \cdot \log\left(\frac{\varepsilon/d}{3.7}\right) \tag{8}$$

Where ε is the bed roughness and d is the hydraulic diameter. Therefore, the friction factor can be calculated:

$$f = \left[-2 \cdot \log\left(\frac{\varepsilon/d}{3.7}\right)\right]^{-2} = \left[-2 \cdot \left(\log(\varepsilon) - \log(d) - \log(3.7)\right)\right]^{-2}$$

For a rectangular cross section pipe (like the EFA): $d = \dfrac{4 \cdot A}{p} = \dfrac{2 \cdot a \cdot b}{(a+b)}$

Where A is the cross-sectional area of the flow, and p is the wetted perimeter.

For the EFA:

$$d = \frac{2 \cdot 101.6mm \cdot 50.8mm}{(101.6mm + 50.8mm)} = 67.7mm \approx \frac{1}{4.5} ft$$

Therefore, the friction factor in the EFA is given by:

$$f_{EFA} = \left[-2 \cdot \{\log(\varepsilon) - \log(d) - \log(3.7)\}\right]^{-2} = \left[-2 \cdot \{\log(\varepsilon) - \log(67.7mm) - \log(3.7)\}\right]^{-2} \Rightarrow$$

$$f_{EFA} = \left[-2 \cdot \{\log(\varepsilon\ [mm]) - 2.4\}\right]^{-2} = \left[-2 \cdot \{\log(\varepsilon\ [ft]) - 0.1\}\right]^{-2} \tag{9}$$

For the river:

Several formulations can be used to estimate the shear stress for an open channel. As noted above, given the small differences in the calculated stresses, and to simplify the formulation of the Site Factor, S, the shear stresses for an open channel can be approximated with the Darcy's friction formulae and the Colebrook equation (Equation 8).

For simplicity of the calculations (this is not always necessary, and if needed, the hydraulic parameter can be more accurately calculated) assume a rectangular river section, for which the width is about twice the depth. For these conditions:

$$d = \frac{4 \cdot A}{p} = \frac{4 \cdot (2 \cdot h) \cdot h}{(2 \cdot h + h + h)} = \frac{8 \cdot h^2}{4 \cdot h} = 2 \cdot h$$

Therefore, the friction factor in the river can be estimated by:

$$f_h = \left[-2 \cdot \{\log(\varepsilon) - \log(d) - \log(3.7)\}\right]^{-2} = \left[-2 \cdot \{\log(\varepsilon) - \log(2 \cdot h) - \log(3.7)\}\right]^{-2} \Rightarrow$$

$$f_h = \left[-2 \cdot \{\log(\varepsilon) - \log(h) - 0.9\}\right]^{-2} \tag{10}$$

Site Factor, S:

Combining Equations 9 and 10 into Equation 7, a simple formulation for the Site Factor can be obtained, as a function of material roughness, ε, and channel depth, h:

$$S = \sqrt{\frac{f_{EFA}}{f_h}} = \sqrt{\frac{\left[-2 \cdot (\log(\varepsilon\ [mm]) - 2.4)\right]^{-2}}{\left[-2 \cdot (\log(\varepsilon) - \log(h) - 0.9)\right]^{-2}}} \Rightarrow$$

$$S = \sqrt{\frac{f_{EFA}}{f_h}} = \frac{\log(\varepsilon\ [mm]) - \log(h\ [mm]) - 0.9}{\log(\varepsilon\ [mm]) - 2.4} = \frac{\log(\varepsilon\ [ft]) - \log(h\ [ft]) - 0.9}{\log(\varepsilon\ [ft]) - 0.1} \tag{11}$$

Figure 2 shows calculated Site Factors for several idealized conditions. It can be observed, that if the material particle size is considered to be related to its roughness (Briaud et. al, 2001), then the site factor is between 1.5 and about 5 for water depths between 3 m (~10 ft) and 30 m (100 ft).

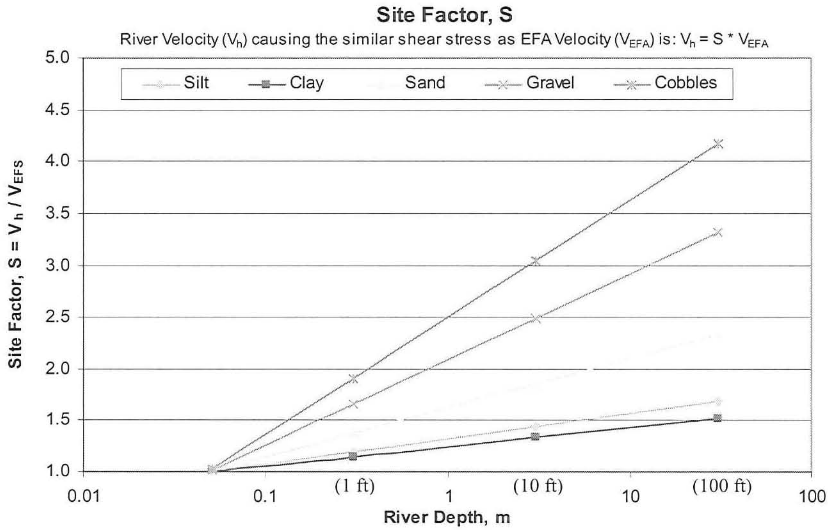

Figure 2. Proposed Site Factor, S, for Various Soil Types

SITE SPECIFIC EXAMPLE CALCULATION

The following site-specific example is based on a known channel geometry and EFA test results obtained for the ULE Program during a soil sample testing program:

1. 6 m (~20 ft) deep channel (approximately rectangular river section),
2. Roughness of 1.5mm (~0.005ft), appropriate for Silts and Clays,
3. EFA results for Silts measured in the DWR program (Shewbridge et al., 2010): $V_1 = 0.157$ m/s, $\alpha = 2.7$ (Equation 3 and Figure 3 - Figure 3 shows EFA test results on Silt and Clay samples from the ULE Program)
4. River velocity of 3 m/s (~10ft/s). appropriate for the American river for the 100-yr event.

From Equation 11, a Site factor is calculated as follows:

$$S = \sqrt{\frac{f_{EFA}}{f_h}} = \frac{\log(\varepsilon\ [mm]) - \log(h\ [mm]) - 0.9}{\log(\varepsilon\ [mm]) - 2.4} = \frac{\log(1.5) - \log(6000) - 0.9}{\log(1.5) - 2.4} \approx 2$$

Therefore, the EFA velocity that would result in the same stresses in the EFA sample as in the river bed can be calculated:

$$v_{EFA} = \frac{v_h}{S} = \frac{3m/s}{2} = 1.5m/s \approx 5ft/s$$

Using Equation 3 with the EFA results adjusted by the site factor, the erosion rate in the river, for this site-specific example, is calculated as 0.44 m/hr (~1ft/hr), compared to 2.9 m/hr (~10ft/hr) using Equation 3 with the EFA results directly, without a site factor correction.

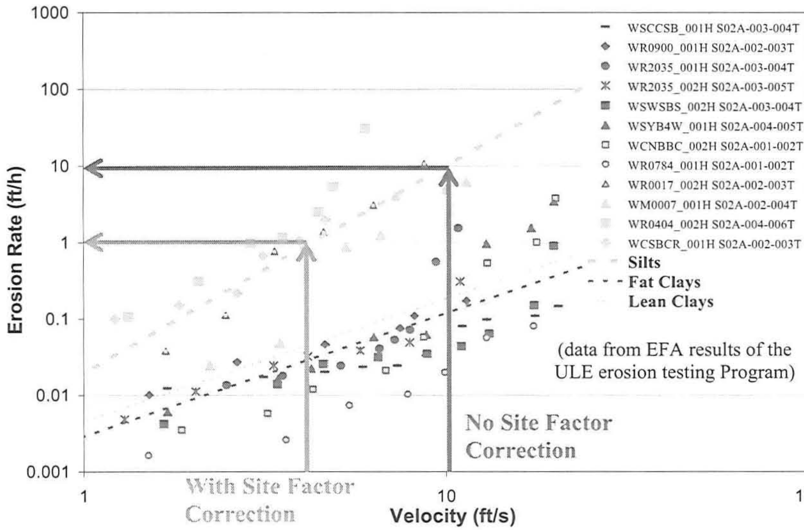

Figure 3. Example Erosion Rate Calculation with Site Factor Use (data from EFA results of the ULE erosion testing Program)

CONCLUSIONS

A site factor to allow for the use of a velocity-based formulation for the calculation of erosion rates in the field was developed and presented. A site factor of 2 implies that the river velocity must be twice the EFA velocity to cause the same shear stresses on the soil. A site factor (or other correction) is required if a velocity based formulation is used to estimate erosion rates in the field, based on laboratory test results. In fact, shear stresses imposed by the EFA for a given flow velocity can be more than an order of magnitude larger than the shear stresses imposed at the riverbed by the same flow velocity. Therefore, for a given flow velocity, velocity-based erosion rates can be more than an order of magnitude larger in the EFA than in the field (specially for Silts).

Stress-based formulations for the erosion rate calculations do not require a site factor. Other factors further compounding the difference between EFA and river condition may include riverbed cross-section (resulting in varying velocity profiles) and vegetation, which are not accounted for in the present formulation.

REFERENCES

Aberle, J., Nikora, V., Walters R. 2006. Data Interpretation for In Situ Measurements of Cohesive Sediment Erosion. Journal of Hydraulic Engineering. ASCE, Bol. 132. pp. 581-588.

Briaud, J.-L. 2008. "Case Histories in Soil and Rock Erosion: Woodrow Wilson Bridge, Brazos River Meander, Normandy Cliffs, and New Orleans Levees", The 9th Ralph B. Peck Lecture, Journal of Geotechnical and Geoenvironmental Engineering, Vol 134, ASCE, Reston Virginia, USA.

Briaud, J.-L., Chen, H.C., Li Y., Nurtjahyo, P., Wang, J. 2003. Complex Pier Scour and Contraction Scour in Cohesive Soils. National Cooperative Highway Research Program Report.

Briaud, J.-L., Ting F., Chen, H.C., Cao Y., Han S. -W., Kwak K. 2001a. Erosion Function Apparatus for Scour Rate Predictions. Journal of Geotechnical and Geoenvironmental Engineering. ASCE, Vol. 127, N. 2, pp. 105-113.

Briaud, J.-L., Ting, F., Chen, H.C., Gudavalli, S.R., Perugu, S.B., Wei, G. 2001b. Apparatus and Methods for Prediction of Scour Related Information in Soils. United States Patent, Patent No. US 6,260,409.

Danish Hydraulic Institute (DHI). 2006. Mike 21 Flow Model. Mud Transport Module, Scientific Background. DHI, Denmark.

Dean, R.G. "Equilibrium beach profiles: characteristics and applications", Journal of Coastal Research 7(1), p. 53-84, 1991

Dean, R.G. "Equilibrium beach profiles: U,S Atlantics and Gulf Coasts" Ocean Engineering report No.12, University of Delaware, Department of Civil Engineering, Newark, 1977.

Hanson, G.H., Temple, D.M. 2001. Performance of Bare-Earth and Vegetated Steep Channels Under Long-Duration Flows. Presented at the 2001 ASAE Annual Meeting. ASAE Paper No. 012157.

Hanson, G.J., Cook, KR. 2004. Apparatus, Test Procedures, and Analytical Methods to Measure Soil Erodibility in Situ. Applied Engineering in Agriculture. American Society of Agricultural Engineers, Vol. 20, No. 4, pp. 455-462.

Hanson, G.J., Simon, A. 2001. Erodibility of Cohesive Streambeds in the Loess Area of the Midwestern USA. Hydrological Processes. V. 15 No 1. pp. 23-38.

Huang, W., Millet, R., Shewbridge, S., Perri, J. F., Vargas, J., Inamine, M., Mahnke, M. 2010. Levee Erosion Screening Process. ICSE5. Procedures.

Shewbridge, S., Perri, J. F., Mineart, P., Millet, R., Huang, W., Vargas, J., Inamine, M., Mahnke, M. 2010. Erosion Screening Process to assess the potential for erosion failure on a levee's waterside slope. ICSE5. Procedures.

Swart, D.H. 1974. Offshore Sediment Transport and Equilibrium Beach Profiles. Delft Hydraulic Lab. Publication 131. Delft University. Delft. 302 pp.

United States Army Corps of Engineers. 1994. Hydraulic Design of Flood Control Channels. EM 1110-2-1601. June 30.

URS. 2007. User's Manual, Erosion Toolbox: Levee Risk Assessment Methodology, USACE Nation Wide Levee Assessment. December.

Surface Erosion: Erodibility Characterisation and Physical Parameters Effects

P.L. Regazzoni, D. Marot and H.H. Nguyen

University of Nantes, Institut GeM, BP 420 44606 Saint-Nazaire Cedex, France; email : pierre-louis.regazzoni@etu.univ-nantes.fr, didier.marot@univ-nantes.fr, hong-hai.nguyen@univ-nantes.fr

ABSTRACT

Erosion is one of the main causes of instabilities within hydraulic earth structures. Two types of erosion can be distinguished: internal erosion and surface erosion. This paper deals with the surface erosion phenomenon and the Jet Erosion Test is used in order to evaluate the erodibility of cohesive soils.

A new energy analysis of the test is developed, linking the expended energy to the erosion phenomenon. The total eroded mass is correlated to the expended fluid energy and a new erosion resistance index is proposed.

The erodibility is evaluated for several natural soil samples which are compacted with the Proctor protocol and which represent a large panel of erosion sensitivity.

Two dissipated hydraulic energy scales appear, and a statistical analysis is carried out which gives a correlation of the erosion resistance index with three physical parameters.

INTRODUCTION

The interaction between water and hydraulic earth structures such as dams, dikes or levees can cause significant damage to these structures. Erosion appears to be one of the main causes of these instabilities (Foster et al., 2000). Two types of erosion can be distinguished: internal erosion which takes place inside the soil matrix, and surface erosion which occurs at the soil/water interface, or at a material interface soil matrix (for example between two different soils).

With the objective to characterize the surface erosion sensitivity of fine soils, an experimental investigation is carried out with the Jet Erosion Test. Twelve natural soil samples which represent a large panel of erosion sensitivity are compacted with the Proctor protocol.

The test interpretation is performed with a new method based on the dissipated hydraulic energy and the eroded mass. The classification of erosion sensibility is defined by a new erosion resistance index.

A multivariate statistical analysis is performed in order to estimate the erosion resistance index as a function of several variables. The results from this study allow the number of variables for the description of the erosion resistance index measurements to be optimised and reduced.

EROSION DEVICE AND EROSION RESISTANCE INDEX

Principle of Jet Erosion Test

The Jet Erosion Test was developed by Hanson and Simon (2001). A hydraulic jet is created by setting a head loss on a diaphragm (see Figure 1). A point gage is adjusted to close off the nozzle, and also allows one to measure the depth of scour below the nozzle. A submergence tank holds the sample. The jet tube is mounted to the submergence tank cover so that the height of the nozzle above the soil surface can be adjusted to different heights prior to the start of a test. The jet tube and cover can also be mounted to a heavy-duty field tank for in situ measurements.

The collected data during the test at specific times include: the depth of scour J measured from a reference level and the head applied to the nozzle, ΔH. Data are recorded at intervals chosen by the operator, depending on the erosion rate. Typical intervals range from 15 s to 30 min, with total test times of 2 hours or less (Hanson and Cook, 2004). With these data, it is possible to relate the hydraulic conditions at interface to the erosion rate at a time t.

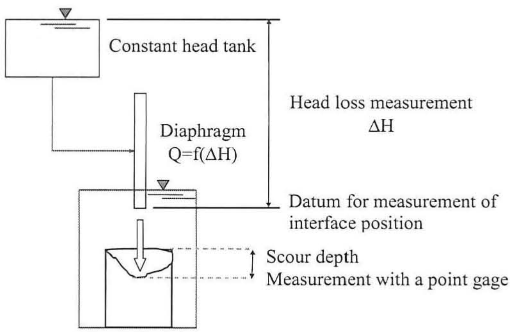

Figure 1. Jet Erosion Test principle.

Water velocity

With the objective to evaluate the water velocity in the area of the impact, two zones are defined (see Figure 2). In the zone I (altitude $Z < J_P = 6.2\ d_0$, where d_0: diameter of the jet at the exit), the water velocity on the axis is constant and equal to exit velocity (axial velocity $u = U_0$, radial velocity $v = 0$). In the zone II ($Z > J_P = 6.2\ d_0$) and far from the interface ($Z < 0.86 - 0.9\ J$), the longitudinal velocity (u) on the axis is proportional to the inverse value of the distance between the jet origin and the altitude considered. According to the measurements made by Beltaos and Rajartanam (1974), a coefficient ($C_d\ d_0$) is introduced in order to obtain a computed velocity in agreement with the measures:

$$u(0,J) = u(0,0)\,\frac{C_d d_0}{Z} \tag{1}$$

where u(0, 0) is the initial velocity at the jet origin, d_0: diameter of the jet at the exit; J: distance between soil-water interface and jet origin.

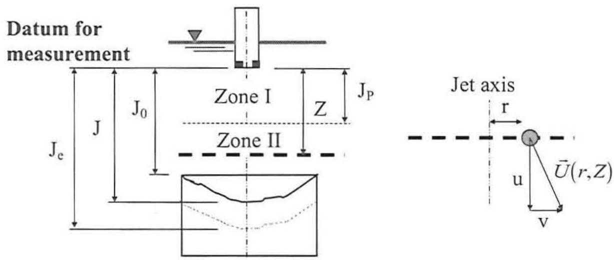

Figure 2. Different measurements during Jet Erosion Test.

In the zone near the interface (J > Z > 0.9 – 0.86 J), the axial velocity (u(r,Z)) decreases to 0 to be converted into radial velocity (v(r,Z)). Beltaos and Rajaratnam (1974) proposed an expression of the vertical velocity on the jet axis:

$$\frac{u(r,z)}{u(0,z)} = \exp\left(-0{,}693\left(\frac{r}{b_u}\right)^2\right) \tag{2}$$

with u(0,J) : water velocity at the distance J from the jet origin on the jet axis in the case of a free jet.
u(r,Z): water velocity at a distance r from the jet axe and a distance Z from the jet origin in the axial direction
ρ_w : water density
b_u : distance from the axis where the water velocity on the axis is divided by two, $b_u = 0{,}093\left(J - J_P\right)$.

Energy analysis

Regazzoni (2009) proposed a method of interpretation based on the energy dissipation between the fluid and the soil. The energy equation for the fluid (neglecting the soil phase inside the volume) can be written as:

$$\frac{dE}{dt} = \frac{d}{dt}\iiint_{Mass}\left(e_{int} + \frac{u^2}{2} + \vec{g}.\vec{x}\right).dM$$

$$= \frac{\partial}{\partial t}\iiint_{Volume}\left(e_{int} + \frac{u^2}{2} + \vec{g}.\vec{x}\right).\rho_W dV + \oiint_S\left(e_{int} + \frac{u^2}{2} + \vec{g}.\vec{x}\right).\rho_W.(\vec{U}.\vec{n}).dS \tag{3}$$

where M: fluid mass, V: fluid volume, e_{int}: internal energy, S: interface between fluid and environment, n: normal vector of interface, U: fluid velocity (components: u, v, w), g: gravity, ρ_w: fluid density, x: coordinates.

Total energy is the sum of the mechanical work W and the energy exchange between the system and the environment E_{Ther}:

$$\frac{dE}{dt} = \frac{dE_{Ther}}{dt} + \frac{dW}{dt} \tag{4}$$

The system can be considered isothermal in time, so internal energy is assumed constant. During the testing time, the system is assumed as adiabatic and the exchange between the system and the environment is neglected $\left(\frac{d\,E_{Ther}}{dt} = 0\right)$. The assumption of a steady state (locally in time) allows neglecting the unsteady term of the kinetic energy. Finally the equation (3) becomes

$$\frac{dW}{dt} = \oiint_S \left(\frac{u^2}{2} + \vec{g}.\vec{x}\right) \rho_w (\vec{U}.\vec{n}).dS \tag{5}$$

The mechanical work W is the sum of: work done by pressure, viscous work in the fluid and work by erosion:

$$\frac{dW_{pressure}}{dt} + \frac{dW_{viscous\ in\ fluid}}{dt} + \frac{dW_{erosion}}{dt} = \oiint_S \left(\frac{u^2}{2} + \vec{g}.\vec{x}\right).\rho_w.(\vec{U}.\vec{n}).dS \tag{6}$$

Two assumptions are made:

-before and after the impact, pressure is assumed hydrostatic,

-the jet deviation is assumed to be the cause of erosion.

The spatial zone concerned by jet deviation is defined by the increasing of radial water velocity. Beltaos and Rajaratnam (1974) noted that radial velocity increases for r/Z < 0.14. So it is assumed that the energy coming from the jet outside of this area (defined by r/Z < 0.14) is dissipated in the fluid.

In the case where $J > J_P$, by combination of equations (6) and (2), the energy equation for the fluid can be expressed by:

$$\frac{dW_{erosion}}{dt} = 2\pi \int_0^{0.14J} \frac{u^2}{2} \rho_w (\vec{U}.\vec{n})\, r\, dr = 2\pi \int_0^{0.14J} \rho_w \frac{u^3(0,J)}{2} \left(\exp\left(-0.693 \left(\frac{r}{b_u} \right)^2 \right) \right)^3 r\, dr \tag{7}$$

In the case of $J < J_P$, the water velocity is assumed to be constant and equal to the speed at the jet exit. So the energy equation is:

$$\frac{d}{dt} W_{erosion} = \pi\, \rho_w u^3(0,0) \left(\left(\frac{J_p - J}{J_p} \right) \frac{d_0}{2} \right)^2 \tag{8}$$

To classify the soil according to the erosion, an erosion coefficient is proposed:

$$\alpha = \frac{\overset{\bullet}{m}_{dry}}{\frac{d}{dt} W_{erosion}} \tag{9}$$

with $\overset{\bullet}{m}_{dry}$: rate of eroded dry mass

By integrating equation (9) over the test duration, the erosion resistance index is built with the erosion energy ($E_{erosion}$) and the eroded dry mass (m_{dry}):

$$I_{\alpha} = -\log\left(\frac{m_{dry}}{E_{erosion}}\right) \tag{10}$$

EXPERIMENTAL INVESTIGATION

Soils properties and testing program

The testing program concerns 12 soils. 8 soils are natural (Regazzoni et al, 2008) and 2 soils were created on the basis of natural soils and 2 soils were created using industrial soil materials. The soils are covering a large part of the Atterberg limits diagram (see Figure 3).

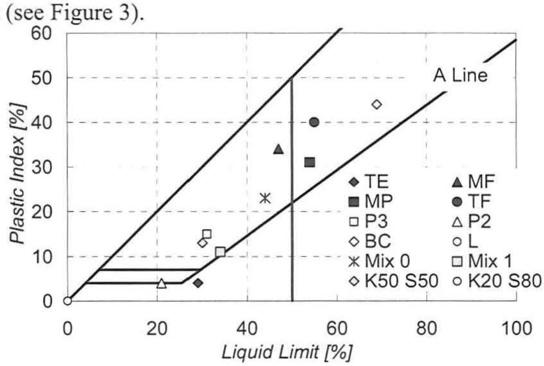

Figure 3. Casagrande diagram.

The optimal dry densities for the Proctor compaction are ranging between 1900 kg/m^3 and 1378 kg/m^3 and the values of optimum water content are between 10 and 24 %. A test consists in a compaction with the standard procedure and a Jet Erosion Test.

The preparation of the sample is made according to the following procedures. First the natural soils are prepared, it means: a drying at 65°C, the crushing and sieving at #4 A.S.T.M. sieve. For all tested soils, water is added and blended to target optimum water content less 1% (in conformity with procedure defined by USBR, 1987). The soil is let 36h (at least) in a plastic bag. The compaction is made in three layers of 25 blows with a normal Proctor rammer. The sample is let in a plastic bag for 12 hours before test.

Results of testing

The tests duration is ranging from 1740 s to 6300 s. We can distinguish two main categories of soil erodibility: an energy erosion soil higher than 600 Joules (see Figure 4) and a low energy erosion soil (see Figure 5).

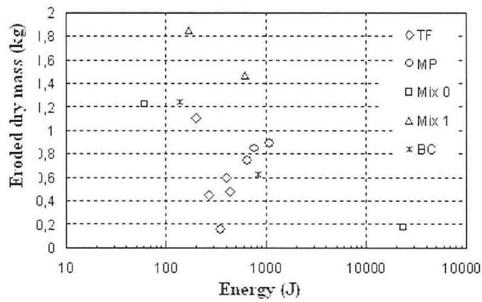

Figure 4. Eroded dry mass vs high energy.

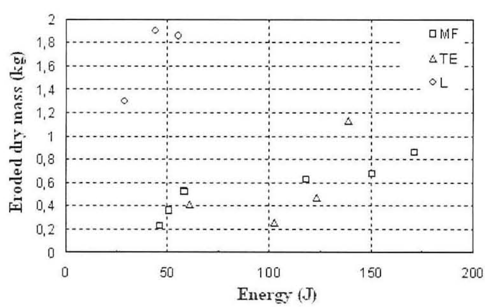

Figure 5. Eroded dry mass vs low energy.

The great difference in erosion sensitivity may be due to the great variability of tested soils.

ESTIMATION OF EROSION RESISTANCE INDEX FROM OTHER SOIL PROPERTIES

Definition of used parameters

The used parameters for the statistical analysis try to represent the soil in several characteristics. The first characteristic considers the grain size distribution. The size curve distribution is introduced by considering the clay fraction (F_{clay}) of the soil (size of particles $d \leq 2$ μm), the silts fraction (2 μm $< d \leq$ 74 μm), the fine sand fraction (74 μm $< d \leq$ 425 μm) and the coarse sand fraction (425 μm $< d \leq$ 4750 μm). The characterization is completed by the Atterberg limits on the soil fraction below 425 μm. For the water in the soil, the water content, w, and the saturation ratio S_r are considered. To describe the soil structure, the compaction, c, and the dry densities are considered:

$$c = \frac{\rho_d}{\rho_S} \tag{11}$$

where ρ_d: dry density of the soil; ρ_s: solid density.

To represent the interaction between clay and water, the clay water content is introduced:

$$w_{clay} = \frac{w}{F_{clay}} \tag{12}$$

Two parameters linking the Atterberg limits to the clay water content are defined:

$$w_{LL} = LL - w_{clay} \tag{13}$$

$$w_{PL} = w_{clay} - PL \tag{14}$$

where LL: liquid limit and PL: plastic limit

With the objective to represent the soil water exchange, the surface exchange S_d is defined by:

$$S_d = 6 \sum \frac{1}{d_{50,Xi}} p_i \, c \tag{15}$$

with $d_{50,Xi}$: average diameter of the considered fraction (for the clay, we consider 2 μm); for the sand, the silt, average diameter is computed with grain size distribution; p_i: percentage in composition of the considered fraction.

Principle of statistical analysis

Multivariate analysis allows the full set of variables related to the measurements to be reduced to a subset representing the principal components assuming a linear correlation between the variables. Each parameter is represented in a factor space, and the geometrical representation associates a vector to each parameter. The scalar product of two associated vectors is equal to the correlation coefficient of the two parameters. An automatic classification is used to define all variables according to the most useful factors. Figure 6 shows the variables in first factor plane. The variables list is given below:

0 : Iα : Erosion resistance index.	5 : Silt fraction	9 : $\log(S_d)$: logarithm of the specific area
1 : w_{LL}	6 : Dry density	10 : w : Water content
2 : w_{PL}	7 : Saturation ratio	11 : Fine sand fraction
3 : w_{Argile} : water content of the clay	8 : Compaction	12 : Coarse sand fraction
4 : F_{clay}: Clay fraction		

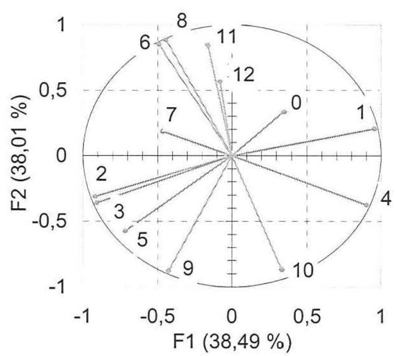

Figure 6. Representation of the variables in first factor plane.

Thus in each plan, the interpretation of parameters is made according to the position from an unit radius circle. Two variables are in linear relationship when their positions are near the unit circle, and very close to each other or diametrically opposite (for example variables 6 (ρ_d), 8 (c) and 10 (w) on Figure 6). Two variables are independent when their representations are in quadrature (for example variables 4 (F_{clay}) and 9 ($\log(S_d)$) on Figure 6).

Now, we are eliminating the variables which are correlated, or seem meaningless by their redundancy information with other variables.

By leading a new multivariate analysis, three parameters are kept and the correlation with erosion resistance index is:

$$I_\alpha = -0.97 + 0.47\, w_{LL} - 0.36\, c + 5.41\, S_r \qquad (16)$$

The obtained correlation coefficient (R^2) between the prediction and the measurement is 0.35 with a number of items N=38. By observing the distribution of the error (cf. Figure 7), it appears that the problematic soils are represented by MF, Mix 0, Mix 1. These soils are dispersive, so now we take into account the dispersive property of the soils.

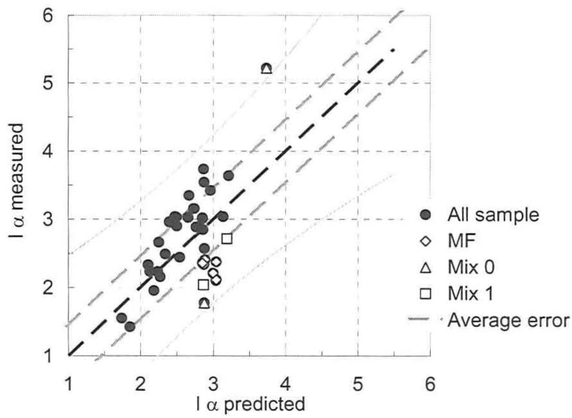

Figure 7. Erosion resistance index, measured values vs predicted values.

A new correlation is defined for non-dispersive soils:

$$I_\alpha = -2.31 + 0.69\, w_{LL} + 1.41\, c + 6.07\, S_r \qquad (R^2 = 0.59, N = 27) \qquad (17)$$

For the dispersive soils the expression of estimated value of I_α is:

$$I_\alpha = -1.36 + 8.69\, w_{LL} + 2.68\, c + 2.08\, S_r \qquad (R^2 = 0.81, N = 11) \qquad (18)$$

As a conclusion of this statistical analysis, by distinguishing between dispersive and non-dispersive soils, we identify the main parameters for a soil analysis in relation to the surface erosion phenomenon. Namely: compaction saturation ratio and difference between clay water content and liquid limit.

CONCLUSION

A Jet Erosion Test device is used in order to characterize the sensitivity to erosion of twelve fine soils which cover a large part of the Atterberg limits diagram. The tested samples are compacted with the standard Proctor procedure at optimum water content less 1%. Study of energy exchanges between fluid and soil leads to propose a new analysis of Jet Erosion Test and a new erosion resistance index is proposed.

Several physical parameters are determined and a statistical analysis is performed in order to identify the main parameters for a correlation with erosion resistance index.

By distinguishing the dispersive behaviour from non-dispersive behaviour, the multivariate statistical analysis leads to an expression of the erosion resistance index as a function of three physical parameters: compaction, saturation ratio and difference between clay water content and liquid limit. Thus this method allows reducing the number of variables for the description of the erosion sensitivity.

In contrast to the precedent models based on stress, energy model leads to a same classification of soil surface erodibility for two types of apparatus: Jet Erosion Test and Hole Erosion Test (Regazzoni, 2009). Moreover, the analysis based on energy dissipation offers the potential for a consistent interpretation of internal erosion test (Le et al, 2010).

ACKNOWLEDGEMENT

The authors wish to acknowledge Electicité de France (EDF-CIH) for the funding of the work and for their advice.

BIBLIOGRAPHY

Beltaos S., Rajaratnam. N. (1974). "Impinging circular turbulent jets." *Journal of the Hydraulics Division*, HY10: 1313-1328.

Foster, M., Fell, R. and Spannagle, M. (2000). "The statistics of embankment dam failures and accidents." *Canadian Geotechnical Journal*, 37, 1000-1024.

Hanson G.J, Simon A. (2001). "Erodibility of cohesive streambeds in the loess area of the Midwestern USA." *Hydrological Processes*, 15 (1): 23-38.

Hanson G. J., Cook K. R.(2004). "Apparatus, Tests procedures, and analytical methods to measure soil erodibility in-situ." *Applied engineering in Agriculture*, 20 (4): 455-462.

Le V.D., Marot D., Thorel L., Garnier J., Audrain P. (2010) "Centrifuge modelling of an internal erosion mechanism." *5th International Conference on Scour and Erosion (ISCE-5),* 7-10 Nov, San Francisco, in press.

Regazzoni P.-L., Marot D., Wahl T., Hanson G. J., Courivaud J.-R. (2008). "Soils erodibility: a comparison between the Jet Erosion Test and the Hole Erosion Test." *Proc. Inaugural International Mechanics Institute (EM08)*, Conference (A.S.C.E.), 18-21 May, Minneapolis, USA.

Regazzoni P.-L. (2009). Confrontation et analyse d'érodimètres et caractérisation de la sensibilité à l'érosion d'interface. *PhD thesis,* Université de Nantes, 155 p.

USBR, United States Department of the Interior Bureau of Reclamations (1987). "Design of small dams." *Water Resources Technical Publication.*

Prediction of Exposure Risk for Buried Pipelines due to Surface Erosion

E. Gavassoni[1] and C. B. Garcia[2]

[1]PETROBRAS TRANSPORTES, Gas pipeline rights-of-way maintenance division. R. Darcy Grijó, 50 – sl. 904 – Jd.da Penha, Vitória – ES, Brazil – 29060440; PH (5527) 3235-4116; email: gavassoni@petrobras.com.br

[2]PETROBRAS TRANSPORTES, Gas pipeline project division, Av. Pres. Vargas, 328, Centro, Rio de Janeiro, RJ, Brazil – 20091060; PH (5521) 3211-9215; email: cbgarcia@petrobras.com.br

ABSTRACT

Pipeline right-of-way maintenance activities face great challenges that have come from different climates, slopes, soils and other environmental conditions. Control of surface drainage and erosion is an important element in the restoration and maintenance of pipeline right-of-ways, since erosion can result in risk of pipe exposure and its consequences. Evaluation of this risk can be a powerful tool to ensure reliability of buried pipelines. The universal soil loss equation is used as a model to estimate the rates of erosion at sections of rights-of-way of a gas pipeline right-of-way near Vitória city in southeast of Brazil. The confrontation of these rates to the actual pipe cover depths is used as a basis to derive a probabilistic procedure for determining the time period over which exposure may occur for a given level of uncertainty. Then, risk can be estimate as a product of the probability (or frequency) of product leakage due to pipeline exposure and the associated consequences of this event. Such risk definition is used to estimate results in an effective guideline to engineers, since it leads to the achievement of optimum and safe erosion control and superficial drainage system projects and results in efficient mitigation planning programs. The results obtained are very promising and show relevant correspondence with the erosion process and cover depth reduction identified on the right-of-way.

Keywords: *Erosion, Risk, EUPS, Pipeline, Right-of-way.*

INTRODUCTION

Minimum cover depths are an important assurance of the security of buried pipelines, since it is designed to dissipate the surface overload that can be transmitted to the buried pipe.

One of the most important activities of the pipeline right-of-way engineering is to treat and prevent erosion process along the rights-of-way. As a linear construction these rights-of-way crosses different kinds of climate, vegetation, soil, topographic characteristics and other environmental conditions that increase the challenges that the engineer faces when those problems need to be solved.

A precise prediction method is an efficient toll to guide the engineer design; however the most common approach only considers the soil loss rates by using the universal soil loss equation without considering the actual soil cover depths (Tansamrit, 2000; Morgan et al., 2003). It is very important to confront values of cover depths and soil loss equations to estimate precisely the risks of exposure due surface erosion.

This works estimate such risks using a risk matrix based method and also an approach based on the concept of soil loss rate to evaluate the actual condition related to the exposure risks along pipeline rights-of-way. The methods are exemplified using the gas pipeline Cabiúnas – Vitória right-of-way.

METHODOLOGY

Firstly the soil loss equation is briefly discussed, followed by the survey of cover depth along pipeline rights-of-way and then the methods of risk estimation are presented.

Soil loss rates

The soil loss rates can be estimated by means of the universal soil loss equation, expressed by:

$$A = RKLSCP \tag{1}$$

Where:
A = Soil loss rates - $Mg.ha^{-1}.year^{-1}$;
R = Rainfall and runoff factor - $MJ.mm.h^{-1}.ha^{-1}.year^{-1}$;
K = Soil erodibility factor - $Mg.h.MJ^{-1}mm^{-1}$;
LS = Topographic factor – dimensionless factor;
C = Cover and management factor – dimensionless factor;
P = Support practice factor – dimensionless factor.

The rainfall and runoff factor consider the climate aspects in the evaluation of erosion rates by the universal soil loss equation. The rainfall and the runoff deriving from it amount of precipitation is considered by this factor, depending on the distribution in the time and in the space of such precipitation. According to Gerra *et al.* (1999) the methodology developed by Wischmeier and Smith (1978) is the most appropriated way to consider the rainfall erosivity. However, the lack of intensity rainfall dates, which is necessary for the R factor by this method, turns impracticable its use in many regions in Brazil. The most common way to overcome this lack of data is to use pluviometric data encountered with more facility. This pluviometric data based methods correlates the R factor to the monthly and annual amount precipitation averages by equations that are only valid at the area where the data for the correlation was picked-up from.

The soil erodibility reveals the capacity of the soil to suffer or to resist the erosion action of rainfall and runoff. The soil erodibility factor is evaluated as a function of the texture of the soil using the relations developed by Roemkes (2003).

The topographic factor, also known by LS factor is dimensionless parameter that considers the slope length and steepness. According to Bertoni and Lombardi Neto (2008) the most suitable equation for soil loss rates evaluation in Brazil is:

$$LS = 0.00984c^{0.63}D^{1.18} \tag{2}$$

where c is the slope length and D is the slope steepness.

The cover and management factor express the ratio between soil loss rates in a cultivated or vegetated area with others with bare soils.

The support practice factor is a dimensionless factor that considers how support and agricultural practices reduces the soil loss at cultivated areas.

Pipe cover depth

Soil cover depths are designed to dissipate the overloads that can be transmitted to the buried pipe. According to Standard PETROBRAS N-464 Rev. H (2007) the procedure of buried pipelines construction should obey the following minimum soil cover depths, shown by Table 1.

Table 1 – Minimum soil cover depths according to N-464.

Location	Cover (m)
Industrial, commercial, and residential areas	1.5
Rock excavation	0.6
Any other area	1.0

Exposure risks evaluation

When soil loss rate at a determined point is considered together its actual soil cover depth one can evaluate the risks of the pipeline becomes exposed at this same point due surface erosion process. This kind of analysis can be done in two different ways: the first is to use risk matrices. The risk matrix used in the study is an adaptation of the Risk Assessment Matrix from military standard MIL-STD-882B developed by Department of Defense of USA. The original matrix provides a systematic method for assigning a hazard level to a failure event based on the severity and frequency of the event. Associating frequency and consequence categories, a hazard level is determined, represented by a risk category. Risk categories assist risk-management team members in differentiating credible high-hazard threats that may result in loss of life and property from less probable risks, therefore aiding management in risk versus cost decisions. A risk matrix is used in the risk assessment process; it allows the severity of the risk of an event occurring to be determined.

Although risk matrices experience problems like poor resolution and errors due to subjective interpretation, they can be used as an additional tool for managing pipeline right-of-way maintenance and integrity. Instead of hazards and probabilities this study uses the soil loss rates and the soil cover depths to categorize the exposure risks of a buried pipeline due surface erosion.

Another different approach to consider the exposure risks at buried pipelines is to use the concept of soil loss rate. Regarding the units of the parameter A in eq. 1 one can write:

$$A = \frac{M}{Ta} \tag{3}$$

where M is the mass of an amount of soil lost in a determined period of time T, over an area of surface equals to a.

If the soil type and soil loss rate is considered constant over the entire area a, and the mass of lost soil M is equal to:

$$M = \rho H a \tag{4}$$

where ρ is the specific mass of the soil and H is the soil cover depth, the soil loss rate can be rewrite as:

$$A = \frac{\rho H}{T} \tag{5}$$

Equation (5) can be re-arranged and the time until exposure of the buried pipeline can be estimated as:

$$T = \frac{\rho H}{A} \tag{6}$$

If the soil loss rate in equation (6) is assumed to be equal to the tolerance value and the depth of cover is assumed to be equal the minimum cover depth value, one can define a standard or allowed time until exposure:

$$T_{al} = \frac{\rho H_{\min}}{A_{tol}} \tag{7}$$

By dividing equation (6) by equation (7) it is possible to settle a time dimensionless parameter τ, expressed by:

$$\tau = \frac{T}{T_{al}} = \left(\frac{H}{H_{\min}}\right)\left(\frac{A_{tol}}{A}\right) \tag{8}$$

The time parameter defined by eq. (8) allows a joint analysis between soil loss rates and cover depths in the process of buried pipeline exposure due surface erosion. If τ is greater or equal to 1 one can expect that risks of exposure at this point is considered very low.

The derivation of this methodology considers that the soil loss is evenly distributed across an area. Even though at pipeline rights-of-way the soil conditions are different due to the presence of the pipeline trench, the assumption of an average soil loss across the area is acceptable, because the company approach to construction affects all the width of the right-of-way at the superficial soil layers. And the deeper layers at pipe trench tend to become similar to the natural soil of the right-of-way, some differences will occur when the erosion process is faster than the soil before prior construction characteristics are recovered.

EXAMPLE OF APPLICATION

The gas pipeline Cabiúnas-Vitória (GASCAV) right-of-way is used as case of study to show how the proposed methods are used to determine the risks of pipe exposure due surface erosion. This pipeline right-of-way was choose as example because it was recently constructed, this fact allows a good correlation between the predict soil loss rates and the significant erosion problems identified at the final inspection of the right-of-way implementation (Gavassoni and Zambom, 2009).

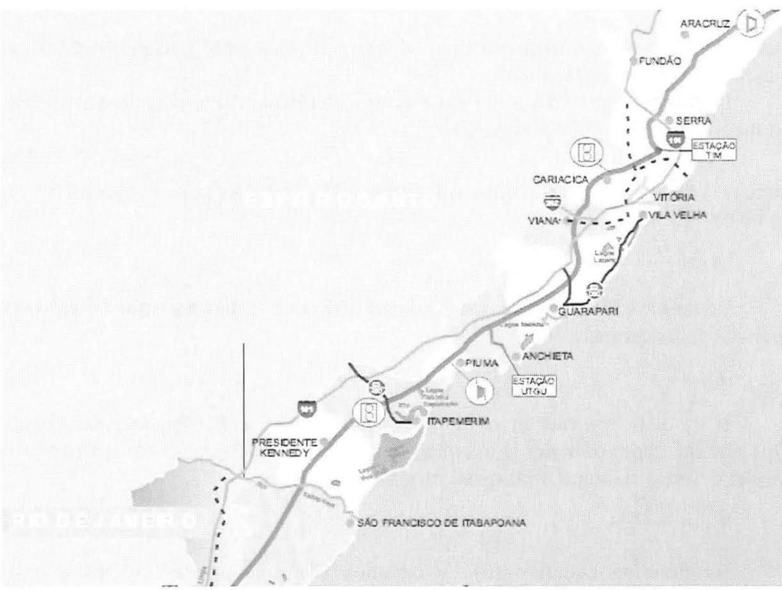

Figure 1 – GASCAV right-of-way.

Study site description

The considered stretch of the GASCAV right-of way on this study ranges from the border between the Rio de Janeiro and Espírito Santo States at the southeast part of Brazil to the north zone of the city of Vitória the Espírito Santo capital. This stretch of 162 km has a constant length of 20 m resulting in an area of 3.24km^2 (324 ha). The map of the GASCAV right-of-way is shown by Figure 1. The right-of-way crosses an area inhabitant by 1.4 million of people (IBGE, 2008).

The terrain conditions crossed by the GASCAV right-of-way consists mostly of plain lands mainly in the south part of Espírito Santo State and at some points the pipeline crosses the foothills the Castelo mountain range which occupies 40% of the area of the Espírito Santo State. Such foothills areas are responsible by the critical topographic factor values encountered in the soil loss predicted rates.

The climate in the study site is classified as a tropical wet and dry. This means that the average amount of precipitation is about 1000 mm and that there is a definite dry season, which in this region is from April to August. The rain gauges installed at points in the Castelo mountain range the amount of precipitation is higher, like 1500 mm.

The soil uses activities consist of agriculture and animal husbandry.

Soil loss results

The parameters of soil loss equation and soil loss rates estimated for the GASCAV right-of-way are shown in this section.

According to the map proposed by Silva (2004) the appropriated equation for the annual rain erosivity at the GASCAV area is that one proposed by Leprun:

$$R = \sum_{i=1}^{12} 0{,}13(p_i)^{1{,}24} \tag{9}$$

where p_i is the monthly average of amount of precipitation of each pluviometric station.

The historical series of pluviometric data for a fifty years period was taken from the HidroWeb, the digital collection of pluviometric data of the Brazilian Federal Water Agency (ANA, 2009). Seven pluviometric stations were used in this study. The area of influence of each pluviometric station was determined by the use of the Thyssen polygons method.

The soil erodibility was evaluated via the soil texture results. These results were obtained by sieve analysis on the samples collected at the penetration tests performed at every kilometer of the right-of-way in the pipe construction phase.

Topographic factor values for the entire GASCAV right-of-way were evaluated by means of eq. 2, where the *c* and *D* values were taken from the "As Built" projects of the right-of-way.

Soil loss rates are then estimated by eq. 1 and shown at Table 2. The soil loss rates are classified according to the intervals proposed by Silva *et. al*. (2007). The result of the combination of the USLE factors revealed that there is a predominance of the class that indicates "low" soil loss expectation (that means a soil loss expectation lesser than 10 $Mg.ha^{-1}.year^{-1}$). This class occurs in 44.84% of the area. The class "medium to high" (50.1 - 120 $Mg.ha^{-1}$ $year^{-1}$) is the second predominant class and occurs in 23.77%, followed by class "medium" (15.1 – 50 $Mg.ha^{-1}.year^{-1}$) with 14.64%, "high" (120.01 – 200 $Mg.ha^{-1}$ $year^{-1}$) with 10.43%, "moderate" (10.01 – 15 $Mg.ha^{-1}$ $year^{-1}$)with 3.68% and "very high" (> 200 $Mg.ha^{-1}.year^{-1}$) with 2.68%.

Table 2 – GASCAV soil loss rates

Soil Loss (Mg/ha/year)	Class	Extension (km)	% of area
0.0 - 10.0	Low	72.60	44.84
10.1 - 15.0	Moderate	5.95	3.68
15.1 - 50.0	Medium	23.71	14.64
50.1 - 120.0	Medium to High	38.50	23.77
120.01 - 200.0	High	16.89	10.43
> 200.0	Very High	4.34	2.68

Pipe cover depth results

Soil cover depths were surveyed at the phase of construction of the pipeline. This survey was performed with the use of topographic devices at least every 12 m of the pipeline, where are located the pipe joints. The entire GASCAV right-of-way is located at rural locations, where the minimum soil cover depth required by N-464 is equal to 1.0 m. The results of the cover depth survey were divided into six different classes according to chosen ranges and are shown in Table 3. Rock excavation, crossings of inland bodies of water, public paved roads and railroads points are not considered here because there is no bare soil to suffer surface erosion process. The ranges of table 3 are product of a technical group of the company and they are based on the company risks management.

Results from Table 3 show that the class I is the predominant with 33.14% of the points, followed by class II with 28.66%, class III with 27,07%, class IV with 9.91%, class V with 0.96% and class VI with 0.26%.

The 11,160 points surveyed along the GASCAV right-of-way show that 98.78 % of these points are higher than those required by Standard N-464. However, depending on the soil loss rates at these points, one may expects a accelerated decreasing of soil cover depth by erosion processes, this fact is more important in the case of the points whose cover depth is slightly higher than those minimum values required by N-464. This fact suggests that the soil loss rates and cover depths should be analyzed together, not as distinct matters when risks of exposure or covers depths bellow minimum values.

Table 3 – GASCAV soil cover depths

Class	Cover Depth - H (m)	Number of Points	%
I	$H > 1.75$	3698	33.14
II	$1.50 < H \leq 1.75$	3199	28.66
III	$1.20 < H \leq 1.50$	3021	27.07
IV	$1.00 < H \leq 1.20$	1106	9.91
V	$0.75 < H \leq 1.00$	107	0.96
VI	$H \leq 0.75$	29	0.26
	Total	11160	-

Exposure risks results

The exposure risk matrix developed has as rows the soil cover depths classes and as columns the soil loss rates classes. The resulted matrix with the risk categorization is shown in Table 4. Even though Tables 2 and 3 consists of six classes of soil loss taxes and cover depth respectively the results on the risk matrix are divided on three groups to obtain a simple analysis of the results when the procedure is applied to real pipelines.

The points are now categorized according to the risk matrix shown by Table 4 and the results are shown in Table 5. According to the categorization presented by Table 5, the classification of exposure risk for the GASCAV right-of-way is shown in Table 6. Most of the GASCAV right-of-way is characterized by low risks of exposure due surface erosion with 52.69% followed by medium risks with 26.59% and high risks with 20.78% of the 11,160 where the cover depth was surveyed.

Using now the dimensionless parameter τ, for time until exposure, the risks classification is evaluated using the tolerance for soil loss rate equals to 10 Mg/ha/year and for the minimum cover depth the value required by the Standard N-464 of 1.0 m. The values of τ are divided into three categories, high, medium and low risks. The results are shown in Table 7 and are very similar to the results obtained via the matrix of risks. The substantial amount of points classified by high and medium risks of exposure due surface erosion both by the method using the matrix of risks and the method using the τ parameter indicates that conservative and preventive practices must be taken to decrease the amount of problems in caused by surface erosion at the GASCAV right-of-way.

Table 4 - Exposure risk categorization (L = low risk, M=medium risk, H=high risk)

	Soil Loss rates					
Cover Depth	Low	Moderate	Medium	Medium to High	High	Very High
Class I	L	L	M	M	H	H
Class II	L	L	M	M	H	H
Class III	L	L	M	H	H	H
Class IV	L	L	M	H	H	H
Class V	L	M	M	H	H	H
Class VI	M	M	H	H	H	H

Table 5 - Exposure risk categorization results for the GASCAV right-of-way.

	Soil Loss rates					
Cover Depth	Low	Moderate	Medium	Medium to High	High	Very High
Class I	1601	224	511	871	368	123
Class II	1582	168	447	622	251	129
Class III	1632	58	446	620	342	145
Class IV	520	13	53	140	96	62
Class V	76	0	6	15	1	9
Class VI	11	0	5	7	1	5

Low
Medium
High

Table 6 - Exposure risks classification via Risk Matrix

Risks Level	Number of Points	%
Low	5874	52.63
Medium	2967	26.59
High	2319	20.78
Total	11160	-

Table 7 - Exposure risks classification via τ parameter

τ	Class	N de Pontos	%
$\tau > 0.75$	Low	6002	53.78
$0.75 \geq \tau > 0.15$	Medium	2985	26.75
$0.15 \geq \tau$	High	2173	19.47
-	**Total**	11160	-

CONCLUSIONS

Buried pipeline may be exposed by action of surface erosion processes. These processes can be mitigated and prevented if a correct evaluation of risks is carried on the pipeline rights-of-way. A precise exposure risk analysis must evolve the joint influence of the actual cover depth and the potential soil loss rate at every point. The methodologies used in this study use the universal soil loss equation with the surveyed values of cover depth at determined points along the pipeline right-of-way. Two approaches are followed on this study, the first make use of a matrix of risks and the second uses the concept of soil loss rate to create a dimensionless parameter related to the time until exposure of the pipe.

Both approaches are demonstrated in the risks analysis of the GASCAV right-of-way. The results show that conservational and preventive practices must be used to reduce the levels of medium and high risks that in both methods are approximately equal to 47% of the 11,160 of surveyed depth cover along the GASCAV right-of-way.

Further work will include this evaluation of other rights-of-way pipelines and the risks analysis of cover depth loss until a value below to those required by technical standards. Test investigation on soil loss tolerances and soil loss equation paramenters also are necessary to determine more appropriate values related to surface erosion in pipeline rights-of-way.

REFERENCES

ANA, Agência Nacional de Águas. (2009). "Sistema de informações hidrológicas". http://hidroweb.ana.gov.br/.

Bertoni J. and Lombardi Neto, F. (2008). "Conservação do solo". Ícone Editora, São Paulo – SP, 355 p.

Gavassoni, E. and Zambon, A. (2009). "Potencial erosivo da faixa de dutos do gasoduto Cabiúnas-Vitória (GASCAV). *Proc., XVIII Simpósio Brasileiro de Recursos Hídricos* (CD-ROM).

Guerra, A. J. T.; Silva, A. S. and Bothelho, R. G. M. (1999). "Erosão e Conservação dos Solos." Bertrand Brasil, Rio de Janeiro – RJ, 339 p.

Morgan, R. P. C.; Mirtskhoulava, T.S.; Nadirashvili,V.;Hann, M. J. and Gasca, A. H. (2003). "Spacing of berms for erosion control along pipeline rights-of-way." *Biosystems Engineering* 85 (2), 249-259.

Standard PETROBRAS N-464 Rev. H. (2007). "Construction, installation and commissioning of pipelines on land", 78p.

Römkens, M. J. M.; Poesen, J. W. A. and Wang, J. Y. (1988). "Relationship between the USLE soil erodibility factor and soil properties." *Land Conservation for Future Generations* (Rimwanich S ed), 371-385.

Silva, A, M. (2004). "Rainfall erosivity map for Brazil" *Catena*, 57, 251-259.

Silva, A.M.; Casatti, L.; Alvares, C. A.; Leite, A. M.; Martinelli, L. A. and Durrant, S. F. (2007). "Soil loss risk and habitat quality in streams of a meso-scale river basin". *Scientia Agricola* 64 (4).

Tansamrit, S. (2000). "The use of vetiver grass system for erosion control and slope stabilization along the Yadana gas pipeline right-of-way". *Proc. of the Seventh International Symposium on Environmental Concerns in Rights-of-Way Management* (CD-ROM).

Wischmeier, W. H.and Smith, D. D. (1978). "Predicting rainfall erosion losses – a guide to conservation planning". U.S. Department of Agriculture, *Agriculture Handbook* 537, 58p.

Piping Potential of a Fibrous Peat

Benjamin Adams[1] and Ming Xiao[2]

[1] Graduate student, Department of Civil and Geomatics Engineering, California State University, Fresno. USA. Email: runinguy@csufresno.edu.
[2]Assistant Professor, Department of Civil and Geomatics Engineering, California State University, Fresno. USA. Email: mxiao@csufresno.edu. Phone: (559) 278-7588.

ABSTRACT

The experimental research presented in this paper aims to develop an understanding of the piping mechanisms of a fibrous peat. The organic matter content of the peat is 22.6%. The peat is compacted to 98% of its maximum dry density within a 7.0cm diameter transparent acrylic cylinder. A hole 0.64cm in diameter that penetrates the entire length of the specimen is preformed to simulate an initial piping channel. A constant-head hole-erosion test is performed on the peat specimen. Upon completion of the test, no significantly measurable enlargement of the preformed hole is observed. A comparison is then made with a sandy soil with the same grain size distribution but no organic matter content. The sand is compacted to 100% of its maximum dry density and tested under the same experimental conditions. Erosion of the piping hole progresses quickly toward the perimeter of the mold. To better understand the effect that organic matter may have on erosion resistance, the sand and the peat are mixed to create a composite soil exhibiting similar soil properties. The newly constituted soil is compacted to its maximum dry density and tested under the same experimental conditions. Only a slight increase in the hole size is observed after the test. The preliminary study suggests that (1) the presence of organic matter in soils may cause initial piping erosion rates to decrease toward a stable value; (2) organic matter content appears to play a role in a soil's resistance to piping progression; the presence of a small percentage of organic matter results in a drastic increase in a soils ability to resist this form of erosion.

INTRODUCTION

Internal erosion in soil can severely weaken dams, dikes, and levees, and can lead to eventual failure and breaching of these hydraulic earth structures. While the mechanisms contributing to internal erosion in mineral soils are still not fully understood, an even less known process is that of internal erosion in organic soils such as peat. Peat is prevalent, with deposits being found in many parts of the world, including 42 states within the United States (Mesri and Ajlouni, 2007). The intention of this research is to provide a preliminary understanding of the mechanisms involved in internal erosion in peat, and the potential for internal erosion that peat possesses. This information could aid in risk analysis and design procedures of hydraulic earth structures.

In recent years, many researchers have continued to study subsurface soil erosion of various combinations of gravel-sand-silt-clay mixtures and the effects of various soil properties on the erosion process. One form of internal erosion is referred to as piping. This type of erosion occurs when concentrated seepage, either through cracks formed due to differential settlement or poor compaction around conduits, or through zones of high permeability within the soil mass, reaches an exit point and carries away both fine and coarse soil particles. This erosion progressively advances upstream along the path of seepage, forming a hollow tube-like channel within the soil mass. This creates the potential for increased seepage and erosion within the hollow pipe and eventual disintegration of the earth embankment or collapse of the open flow tunnel and the structure itself. In a survey of 11,192 dams, Foster et al. (2000) concluded that approximately 46% of all dam failures could be attributed to internal erosion. In reanalyzing this survey, Richards and Reddy (2008) determined that approximately 31% of dam failures resulted from the piping mode of failure. Figure 1 shows the Upper Jones Tract levee failure, which took place on June 4, 2004 near Stockton, California. The failure occurred on a sunny morning on which no seismic activity was recorded in the area. Although the exact cause of the incident was never determined, it is speculated that internal piping channels and a high water level led to the failure. After construction of a pumping system, five months were required to dewater the flooded farmland that had been protected by the levee, and the entire cost of the repair came to $90 million.

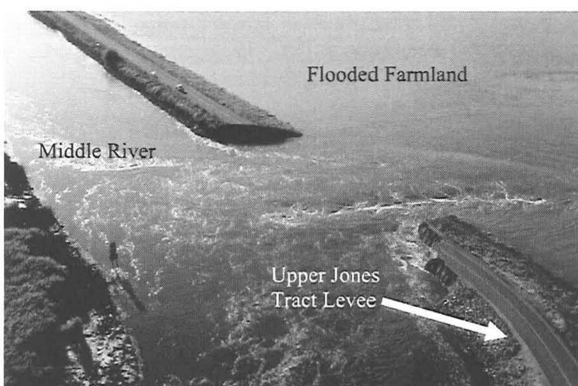

Figure 1. Upper Jones Tract levee breach; June 4, 2004 (DWR, 2004)

The susceptibility to internal erosion of levees built on or near peat deposits is currently unknown. Peat has always been considered an unsuitable building material due to its high compressibility, and its engineering properties have been relatively unstudied. This highly organic soil can attribute its organic content to the decomposition of fragmented plant and animal remains that can accumulate in lush, vegetative environments. Although the same fundamental principles that govern inorganic mineral soil behavior may be applicable to organic peats, the basic engineering properties of peat are significantly different from those of mineral soils (Mesri and Ajlouni, 2007). After a comprehensive review of previous research on peat soils, in conjunction with their own research on two types of peat, Mesri and Ajlouni (2007) pointed out the extremely high in situ permeability and void ratios that are typically exhibited by peat. Another typical characteristic of peat, resulting from its high in situ void ratio coupled with the high water holding capacity of the organic material, is its high compressibility under overburden stress. Peats usually have low specific gravity. The combination of low density, high void ratio, and high permeability seems to suggest that peat might be susceptible to internal erosion.

Due to the potentially complex interaction of the mechanisms possibly involved in internal erosion, i.e. grain size distribution, compaction, hydraulic gradient, cohesion, internal friction angle, and organic content, a systematic study is necessary in order to understand the effects that each of these parameters might play in a soils internal erosion potential. In this paper, we present our preliminary findings on the internal erosion potential of peat and its comparison with that of a mineral soil.

TEST MATERIALS AND SOIL CHARACTERIZATION

Three types of soils are studied in order to examine the various soil characteristics possibly affecting internal erosion potential in peat. The basic characteristics of each soil are shown in Table 1.

Table 1. Basic Soil Properties

Soil Property	Kerman Peat	Fine Grained Sand	Composite
Organic matter content (%)	22.6	0.0	5.0
Maximum dry density (g/cm^3); optimum moisture content (%) (Harvard Miniature compaction)	0.94; 46.0	1.94; 9.5	1.59; 16.0
Cohesion (drained direct shear)	27.3 kN/m^2 (or 4.0 lb/in^2)	22.0 kN/m^2 (or 3.2 lb/in^2)	10.6 kN/m^2 (or 1.5 lb/in^2)
Internal friction angle (°) (drained direct shear)	32.9	38.8	41.3

The soil here referred to as Kerman Peat is light in color, contains visible organic fibers and large soil particles, and is non-plastic. It was sampled from a dry riverbed in Kerman, CA. The peat was sampled and immediately placed in airtight containers at room temperature (20-22°C) for storage and testing. The grain size distribution (GSD) of the peat (from wet sieving and hydrometer analysis) is shown in Fig 2. The mineral soil here referred to as Fine Grained Sand was created by deliberately manipulating the grain size distribution of a fine-grained sandy soil intended for use in urban construction. The sand was separated into the portions retained on sieves of selected sizes, and the grain size distribution of the peat was used to develop the mixing ratio necessary to achieve a sandy soil with the same gradation. Figure 2 shows the similarity in grain size distribution between the peat and the sand. Note that the portion of the sand passing the No. 200 sieve (0.075 mm) is an average of the slightly varying results obtained from multiple hydrometer tests on the Kerman Peat.

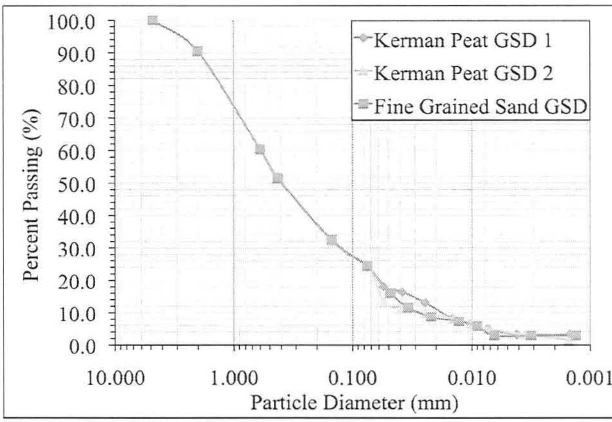

Figure 2. Grain size distributions of Kerman Peat and Fine Grained Sand

The third soil, here referred to as the composite soil, was also created in the laboratory and was a mixture of the sand and the peat. The two soils were mixed at a mass ratio of 22% peat to 78% sand, creating a sandy soil having 5% organic content by mass. Since the two soils with the same grain size distribution were the only components used in creating this composite soil, the mixture exhibits basic soil properties similar to those of its constituents. The purpose of creating the mineral soil (with 0% organic matter content) and the composite soil (with 5% organic matter content) is to examine the possible effect of organic matter content on internal erosion resistance.

In order to study the effect of cohesion and internal friction angle on the soils' internal erosion, drained direct shear tests are conducted on the peat, the sand, and the composite soil, which are compacted at their optimum moisture content and at compaction ratios of 98%, 100%, and 100%, respectively. The results are shown in Table 1.

EXPERIMENTAL METHODOLOGY

To conduct the erosion tests, the improvised hole-erosion test (HET) apparatus shown in Figure 3 has been developed. The device is modeled after the apparatus developed by the researchers at the University of New South Wales (Wan and Fell, 2004a; 2004b). The test is conducted on specimens measuring 7.0cm in diameter and 13.5cm in length. Clear acrylic tubing and end caps, which allow for easy observation of the specimen during all phases of testing, are used for the specimen mold. The end caps are designed in such a way that eroded soil particles are able to exit from the specimen unhindered. The hole diameter of the influent end cap is drilled to the same size as that of the simulated piping channel allowing for direct introduction of eroding fluid into the channel. This straight hole measuring 0.64cm in diameter is preformed during the specimen compaction using a metal rod. The soil specimen is compacted directly within the mold in thin, uniform layers at optimum moisture content. De-ionized water is introduced via a constant head reservoir, and the effluent with eroded soil particles is collected in buckets directly beneath the specimen. With the downstream side of the specimen open to atmosphere, a constant hydraulic gradient of four is established for conducting the erosion tests, simulating possible field conditions.

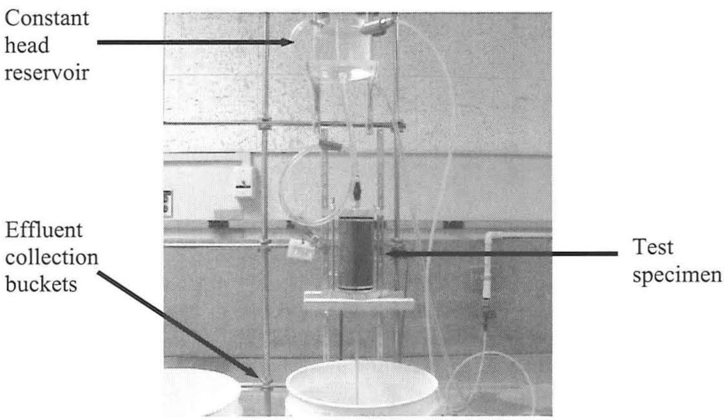

Figure 3. HET apparatus and test specimen

Throughout the duration of each test, effluent is collected for predetermined incremental lengths of time. Based on the mass of water collected during each increment, the corresponding effluent volume can be calculated. Also determined in each time increment is the total dry mass of eroded soil. This mass is obtained through decanting and drying of the effluent with eroded particles. Then, average seepage and erosion rates for each increment of time can be determined. Table 2 summarizes the test conditions for each soil type.

Table 2. Erosion Test Parameters

Test Parameter	Kerman Peat	Fine Grained Sand	Composite
Duration of test (min)	60	3	60
Duration of each increment (min)	5.0	0.5	5.0
Hydraulic gradient	4	4	4
Compaction ratio (%)	98	103	100

RESULTS AND DISCUSSION

At the end of each erosion test, the condition of the piping hole is recorded. As shown in Figure 4(a), no measurable difference is observed in the preformed piping hole after the peat specimen experiences a full hour of eroding flows. Figure 4(b) shows that after experiencing only three minutes of the same flow conditions, the initial hole in the sand specimen has eroded to the perimeter of the mold. The soil and test parameters (grain size distribution, cohesion, internal friction angle, and compaction ratio) are similar in both specimens. However, a drastic variation in the erosion potential is observed between the two soils. The composite soil specimen, also having similar soil parameters but differing in organic content, is shown in Figure 4(c). This soil is also tested for a duration of 60 minutes and shows an intermediary level of piping hole enlargement and soil erosion, which is only slightly greater than that of the peat specimen. A summary of the test results is presented in Table 3.

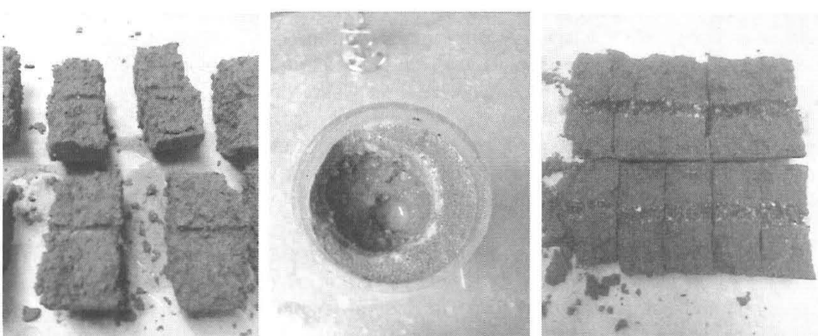

(a) Peat specimen (b) Sand specimen (c) Composite specimen

Figure 4. Post-erosion condition of test specimens with piping holes

Table 3. Erosion Test Results Summary

Test Results	Kerman Peat	Fine Grained Sand	Composite Soil
Maximum erosion rate (g/min)	0.12	38.80	0.94
Average erosion rate during all increments (g/min)	0.03	24.00	0.13
Hole condition at the end of test	No visible change [Fig. 4(a)]	Considerable erosion [Fig. 4(b)]	Slight enlargement [Fig. 4(c)]

Figure 5 shows the variation of average erosion and seepage rate with time during each test. Each point represents the average erosion or seepage rate for the duration of that particular time increment. The initial point of each test in Figure 5(a) may not be reliable — during the formation of the piping channel at specimen compaction, the removal of the metal rod used to form the piping hole can cause soil particles to dislodge from the wall of the hole. The assembly of the cylinder and the end caps can also cause a slight disturbance of the specimen. These loose particles are easily washed from the specimen upon the initiation of the test (due to water hammer) and are collected in the first effluent bucket, causing the eroded soil mass to be unrealistically high. This is supported by the fact that for each soil type, the first point is significantly higher than subsequent points. This possible procedural error also affects the reported maximum and average erosion rates.

Figure 5(a) shows that the erosion rates of both the peat and the composite soil follow a decreasing trend toward a stabilizing value, while the sand erosion rate appears to be increasing at the end of the test. The generally increasing and then stabilizing seepage rates observed in the peat and the composite soil tests, as shown in Figure 5(b), also indicate the progression of the piping channel. As the piping hole enlarges due to initial erosion, the seepage rate increases. Once the erosion rate has decreased, the hole size stabilizes and the seepage rate through the hole also stabilizes. Due to the high erosion potential of the sand and the subsequently low number of data points for this test, a clear trend is more difficult to distinguish. Most important to recognize, however, is the high erosion potential of this non-organic soil.

These results indicate the possible effect of organic matter content on a soil's erosion resistance — soils with higher organic matter content erode less under the same soil compaction and hydraulic conditions. Soil organic matter has been shown to affect erosion resistance. Organic matter binds mineral particles into a granular soil structure; part of the soil organic matter that is especially effective in stabilizing these granules consists of certain glue-like substances produced by various soil organisms (Brady and Weil, 2002; Haynes and Beare, 1996). Application of compost in *surface* erosion control employs this principle. Mazurak et al. (1975) reported that application of organic wastes decreased the amount of soil particles detached by raindrop impact. Xiao and Gomez (2009) also found that *surface* erosion resistance of composts increases with the increase of organic matter content. It seems the surface erosion mechanisms could be extended to the internal piping erosion. Closer examination of the post-erosion piping hole of the composite soil [Figure 4(c)] shows larger granular sand particles (in lighter color) remained on the wall of the hole, indicating the "binding" of organic particles with the mineral particle, preventing them from eroding.

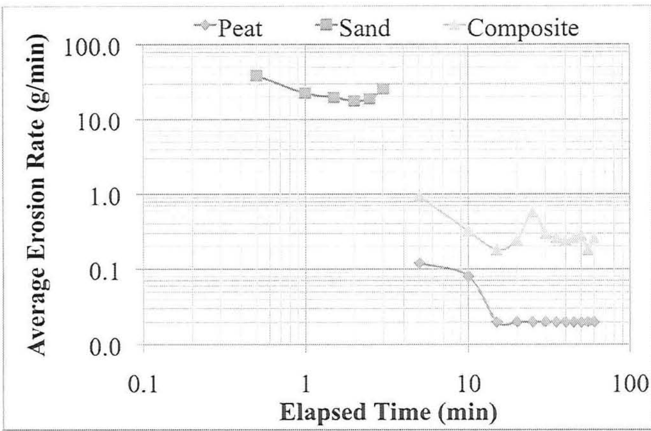

(a) Erosion rate with time

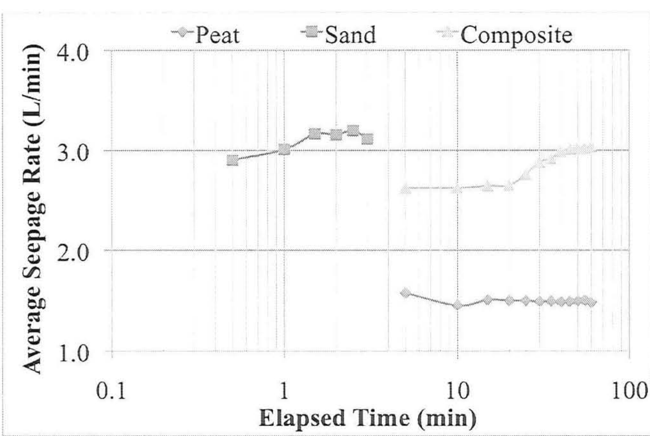

(b) Seepage rate with time

Figure 5. Average erosion rate and seepage rate based on HET results for the three tested soils

Shear strength parameters were analyzed within the context of piping erosion. It appears that inter-particle friction may not play a significant role in piping erosion resistance given that soil solids at the soil-water interface along the open channel are subjected to nominal effective stress; therefore, internal friction angles of the three types of soil (Table 1), albeit different, may not be attributed to the erosion difference. The impact of cohesion on erosion resistance is inconclusive, based on the results shown in Figure 5(a). The composite soil with lower cohesion of 10.6 kN/m^2 but higher organic matter content (5%) has significantly higher erosion resistance than that of sand, whose cohesion is higher (22.0 kN/m^2) but organic matter content is less (0%).

The study reported in this paper did not consider the effects of particle shape and structure on the erosion process. Although the three soil types have the same grain *size* distribution, the individual particle shapes are quite different — sand solids are either round or angular in shape, while the peat particles are mostly flakes. Moreover, Mesri and Ajlouni (2007) demonstrated that fibrous peat particles have a hollow, perforated cellular structure. The authors are conducting further study to understand the relationships between organic content, particle shape and size, and resistance to piping erosion.

CONCLUSIONS

This paper presents the findings of a preliminary study of the mechanisms involved in piping erosion and the role that organic matter content may play in resisting piping progression. Hole erosion tests were carried out on three soils having varied organic matter contents but the same grain size distribution using an improvised hole erosion test apparatus. The research presented in this paper suggests the following conclusions:

1. The presence of organic matter in soils may cause initial piping erosion rates to decrease toward a stable value.
2. Organic matter content appears to play a role in a soil's resistance to piping progression. The presence of a small percentage of organic matter, i.e., 5%, results in a drastic increase in a soils ability to resist this form of erosion.

REFERENCES

Brady, N.C., and Weil, R.R. (2002). *The Nature and Properties of Soils*, 13th edition. Prentice Hall.

California Department of Water Resources (DWR) (2004, June). "*Photographs of the Upper Jones Tract Levee Break in the Sacramento-San Joaquin Delta.*" Retrieved December 16, 2009, from www.water.ca.gov/news/newsreleases/2004/061604floodpic.pdf

Foster, M., Fell, R., and Spannagle, M. (2000). "The Statistics of Embankment Dam Failures and Accidents." *Canadian Geotechnical Journal*, 37(5): 1000-1024.

Haynes, R.L., and Beare, M.H. (1996). "Aggregation and organic matter storage in meso-thermal, humid soils." Structure and organic matter in agricultural soils. Advances in Soil Science, ed. M.R. Carter and B.A. Stewart, 213-263. Boca Raton, FL: Lewis-CRC Press.
Mazurak, A.P., Chesnin, L., and Tiarke., A.E. (1975). "Detachment of soil aggregates by simulated rainfall from heavily manured soils in eastern Nebraska." *Soil Science Society of America Journal*, 39:732-736.
Mesri, G., and Ajlouni, M. (2007). "Engineering properties of fibrous peats." *Journal of Geotechnical and Geoenvironmental Engineering*, 133 (7): 850-866.
Richards, Kevin S. & Reddy, K.R. (2008). "Experimental Investigation of Piping Potential in Earthen Structures" *Geotechnical Special Publication #178*, GeoCongress 2008: Geosustainability and Geohazard Mitigation, pp. 367-376
Wan, C. F., and Fell, R. (2004a). "Investigation of Rate of Erosion of Soils in Embankment Dams" *Journal of Geotechnical and Geoenvironmental Engineering*, 130 (4): 373-380.
Wan, C. F., and Fell, R. (2004b). "Laboratory Tests on the Rate of Piping Erosion of Soils in Embankment Dams" *Geotechnical Testing Journal*, 27 (3): 295-303. ASTM International, West Conshohocken, PA, DOI: 10.1520/GTJ11903.
Xiao, M. and Gomez, J. (2009). "Rainfall erosion resistance and stability of various composts." *Journal of Soil and Water Conservation*, 64(4): 233-242.

Comparison of Geosynthetic Rolled Erosion Control Product (RECP) Properties between Laboratories

J.L. Smith[1], S.K. Bhatia[2] and C.J. Sprague[3]

[1]Assistant Professor, Sustainable Construction Management and Engineering, SUNY College of Environmental Science and Forestry, 205 Baker Laboratory, 1 Forestry Drive, Syracuse, NY 13210; PH (315) 470-6866; email: jsmith@esf.edu
[2]Professor, Civil and Environmental Engineering, Syracuse University, 105 Link Hall, Syracuse, NY 13214; PH (315) 443-3352; email: skbhatia@syr.edu
[3]TRI/Environmental, Inc., P.O. Box 9192, Greenville, SC 29604 ; PH (864) 242-2220; email: jsprague@tri-env.com

ABSTRACT

Geosynthetic rolled erosion control products (RECPs) are used extensively to minimize soil erosion and enhance the growth of vegetation on slopes and in channels. RECPs suitable for these applications come in a variety of different fiber and structure types, ranging from coir erosion control blankets (ECBs), jute open weave textiles (OWTs), to polyolefin turf reinforcement mats (TRMs). Although there is a wide variety of products available, engineers are often given little guidance on the selection of RECPs beyond maximum allowable slope, velocity, and shear stress. RECPs can vary significantly in basic index properties and overall field performance. More than a decade ago, the Erosion Control Technology Council (ECTC), in conjunction with TRI/Environmental, Inc. (TRI), developed several index tests in an effort to compare and standardize RECPs. Although these tests are used extensively to characterize different RECPs, no studies have been conducted that evaluate the repeatability, reproducibility, or usefulness of these tests beyond those conducted at TRI. This paper presents the results of a comparative study of two index tests (light penetration and water absorption) for several different RECPs between Syracuse University and ECTC. These tests were selected for evaluation because the properties these tests measure have been identified by several researchers as being important to the performance of RECPs. Based on the results of the evaluation, a new test for evaluating the water absorptive behavior of RECPs is proposed.

INTRODUCTION

Soil erosion is the detachment and transport of soil particles from the ground surface by raindrops, water, or wind. Of these, the detachment of soil by raindrop impact has been identified as being the most important and most damaging (Ellison 1944). In the raindrop erosion process, soil particles are detached from the ground surface by raindrops; entrained in the sediment load; transported by thin films of water; and deposited (Toy et al. 2002.)

Soil particle movement is initiated when the kinetic energy of the rainfall is transferred to individual soil particles, breaking the bonds between soil particles and causing their detachment. One of the most effective ways of reducing the erosivity of raindrops is to provide ground cover than can intercept raindrops, dissipating their energy before they can reach the underlying soil particles (Toy et al. 2002, et al.) A second component is to reduce the transport capacity of the underlying overland flow, which can be achieved through intimate contact of the ground cover with the underlying soil surface. This contact provides resistance against overland flow by providing tortuous flow paths that reduce the velocity and erosive potential of the flow.

RECPs provide immediate ground cover to protect against raindrop impact. Many researchers have noted the importance of RECP surface coverage to rainsplash erosion performance in bench-scale tests (e.g. Ziegler et al. 1997, Ziegler and Sutherland 1998, Ogobe et al. 1998, Rickson 2002). Similarly, these researchers have also documented the importance of high water absorbency of RECP fibers to improve their contact with the underlying soil.

The two index tests that were developed by ECTC to provide information on ground cover percentage and water absorption capacity of RECPs are the light penetration test and the water absorption test, respectively. Smith et al. (2005) related light penetration and water absorption index test results to the performance of six different RECPs installed in a drainage channel in central New York in terms of both soil erosion and vegetative growth. It was found that percentage area cover and water holding capacity/percentage wet weight play a direct role in initial soil erosion protection and long-term vegetation establishment.

This paper presents a critical review of two ECTC index tests (light penetration and water absorption) based on a comparison of laboratory test results for several different RECPs between Syracuse University and ECTC. The tests are evaluated for their repeatability, reproducibility, and usefulness in characterizing and comparing different RECPs. Based on the results of the evaluation, a new test for evaluating the water absorptive behavior of RECPs is proposed.

MATERIALS

Twelve different RECPs from four different manufacturers were selected for the study. The RECPs were selected based on fiber type and manufacturing process. Eight of the RECPs are erosion control blankets (ECBs): temporary degradable RECPs composed of processed natural or polymer fibers mechanically, structurally, or chemically bound to form a continuous matrix (ECTC 2001) (see Figure 1a). Two of the ECBs are composed of curled wood excelsior fibers (W1 and W2); one is composed of blended wood and synthetic polypropylene (PP) fibers (WS1); one is composed of straw fiber (S1); two are composed of 70% straw and 30% coconut blended fibers (SC1 and SC2); and two are composed of coconut fibers (C1 and C2).

Two of the RECPs are open weave textiles (OWTs): temporary, degradable RECPs composed of processed natural or polymer yarns woven into a matrix (ECTC 2001) (see Figure 1b). One of the OWTs is composed of coconut fibers (C3) and one is composed of jute fibers (J1). Two of the RECPs are turf reinforcement mats (TRMs): long-term, non-degradable RECPs composed of UV-stabilized, non-degradable, synthetic fibers, nettings, and/or filaments processed into 3-D reinforcement matrices (ECTC 2001) (see Figure 1c). One of the TRMs is composed of a coconut matrix (T1) and one is composed of a synthetic PP matrix (T2). A description of the RECPs and their average physical properties, as measured in this study, are presented in Table 1.

The RECPs tested in this study were obtained from the manufacturers in both rolls and in sections taken from entire roll widths. Sampling was conducted across the roll widths in accordance with ASTM D4354. Care was taken during sampling to maintain the structural integrity of the specimens and to ensure that specimens were representative of the provided materials.

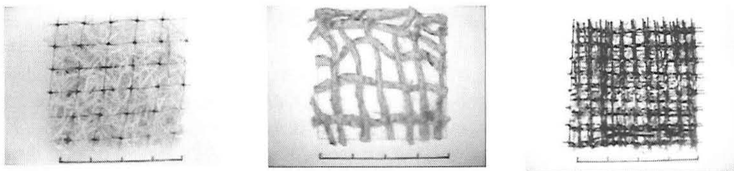

(a) ECB (b) OWT (c) TRM

Figure1. Typical RECP structure types (10 cm by 10 cm specimens)

Table 1. RECPs and their average physical properties as measured in this study

RECP	Structure Type	Fiber Type	Mass per Unit Area $(g/m^2)^{1,2}$	Thickness (mm) [1,3]	Light Penetration (%)[1,4]	Water Absorption (%)[1,5]
W1	ECB	Wood	346 ± 40	10.07 ± 1.84	41.5 ± 9.2	228 ± 7
W2	ECB	Wood	623 ± 135	10.95 ± 2.06	12.4 ± 2.9	243 ± 13
WS1	ECB	Wood/ Synthetic	164 ± 13	3.57 ± 0.28	20.2 ± 3.5	1896 ± 72
S1	ECB	Straw	243 ± 22	8.54 ± 1.48	27.2 ± 4.7	556 ± 49
SC1	ECB	Straw/ Coconut	312 ± 65	5.55 ± 1.30	20.4 ± 7.1	666 ± 197
SC2	ECB	Straw/ Coconut	278 ± 23	8.29 ± 1.70	14.4 ± 5.0	764 ± 186
C1	ECB	Coconut	254 ± 12	4.83 ± 0.77	20.6 ± 10.7	913 ± 179
C2	ECB	Coconut	247 ± 19	4.81 ± 0.65	20.5 ± 5.5	1218 ± 212
C3	OWT	Coconut	741 ± 20	8.68 ± 0.55	22.7 ± 0.6	297 ± 34
J1	OWT	Jute	422 ± 17	4.41 ± 0.43	50.1 ± 4.2	601 ± 54
T1	TRM	Coconut	388 ± 24	13.11 ± 1.13	18.4 ± 3.1	241 ± 58
T2	TRM	Synthetic	580 ± 35	14.24 ± 1.13	24.6 ± 3.7	42 ± 9

[1]Average is given ± 1 standard deviation from the mean (±1SD); [2]ASTM D6475 (ECBs and OWTs) and ASTMD6566 (TRMs); [3]ASTM D5199 (ECBs and OWTs) and ASTM D6525 (TRMs), as modified by ECTC (2001); [4]ASTM D6567, as modified by ECTC (2001); [5]ASTM D1117, as modified by ECTC (2001)

TEST METHODS

Light penetration testing was performed in accordance with ECTC (2001), which is based on ASTM D6567. In the test, light is projected through frosted glass to dissipate the light, and then through a 20.3 cm x 25.4 cm RECP specimen in a closed container (see Figure 2). The amount of light that passes through the RECP is measured using a light meter in terms of foot candles. The percentage light penetration is calculated as the ratio of the amount of light that passes through a RECP specimen to the amount of light that passes without a RECP specimen. Five specimens were tested for each RECP.

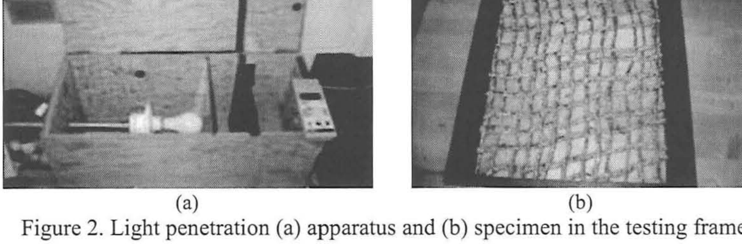

(a) (b)

Figure 2. Light penetration (a) apparatus and (b) specimen in the testing frame

Water absorption testing was performed in accordance with ASTM D1117, which was modified by ECTC (2001.) In the test, 20.3 cm x 20.3 cm RECP specimens are placed on a screen and submerged in water for 24 hours (see Figure 3). The RECP specimens are then removed, allowed to drain for 10 minutes, and weighed. The water absorptive capacity is calculated as the ratio of the water held by a RECP specimen to the original dry weight of the sample. Five specimens were tested for each RECP.

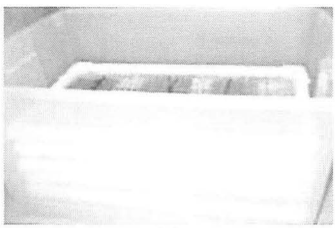

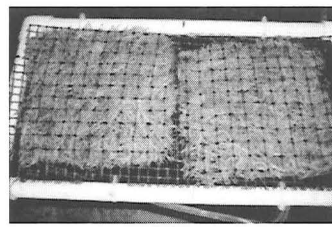

(a) (b)

Figure 3. Water absorption (a) reservoir and (b) testing frame

RESULTS

Light penetration

Light penetration testing was conducted to provide information on the amount of ground cover a RECP would provide to an underlying soil surface. Light penetration is inversely related to ground cover. A comparison of the range of light penetration results obtained for each group of RECPs tested (ECBs, OWTs, and TRMs) is presented on Figure 4.

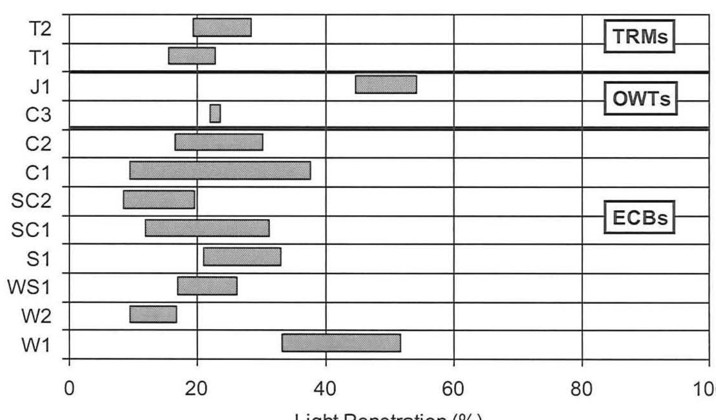

Figure 4. Range of light penetration results

As shown on Figure 4, there was some degree of variability in light penetration results for the RECPs tested. In terms of variability, the ECBs fell within three groups. The first group (W2, WS1, S1, SC2) showed relatively little scatter in results, with results varying less than ±5% (±1SD.) The second group (W1, SC1, C2) showed moderate scatter in results, with results varying between

5% to 10% (±1SD.) One ECB (C1) varied more than 10% (±1SD.) In general, it is believed that the variability in results resulted from: (1) variations in mass per unit area across and between specimens (see Figure 5); and (2) difficulties in specimen handling and supporting with some of the ECBs in the specimen apparatus (repeatability). In particular, there were difficulties in securing ECBs that contained loose arrangements of fibers, such as straw fiber ECB S1. In general, as mass per unit area increased, light penetration decreased for the ECBs tested.

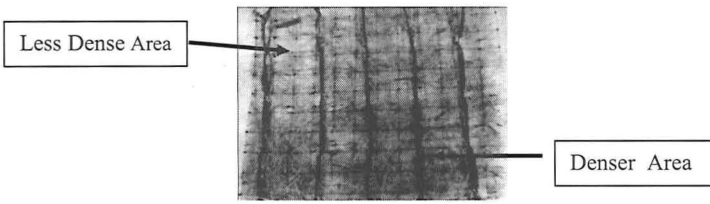

Figure 5. Variability within a RECP light penetration specimen (C1)

The OWTs tested included coconut fiber C3 and jute fiber J1. It is believed that the variability in OWT results is directly related to the rigidness of the structures. C3 consisted of coir fibers that were twisted into yarns, creating a fairly rigid structure, with regular openings. Results for C3 varied relatively little, with results varying only 0.6% (±1SD.) J1 also showed little scatter, with results varying less than 5% (±1SD.) However, there was a greater degree of scatter with J1 in comparison to C3 because of difficulties installing J1 in the apparatus because of the flexible nature of the fibers that made up its structure (see Figure 6.) The fibers were easily distorted during specimen preparation and during installation. Similarly, there was little scatter in results for the TRMs T1 and T2, with results varying less than 5% (±1SD.) It is believed that the rigidness of the three-dimensional structure held fibers in place during testing.

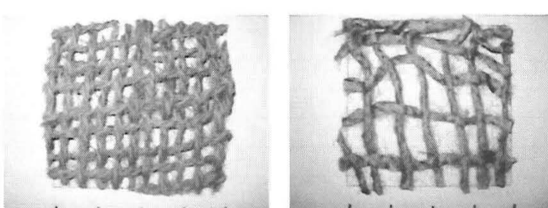

(a) C3 (coconut) (b) J1 (jute)

Figure 6. Comparison between the two OWTs tested

To evaluate reproducibility, light penetration results obtained by Syracuse University are compared to those obtained by ECTC (AASHTO 2005) for ten RECPs on Figure 7. As shown, light penetration results obtained by Syracuse University were slightly different for half of the RECPs tested (W1, S1, C2, T1, T2) and generally higher than those obtained by ECTC.

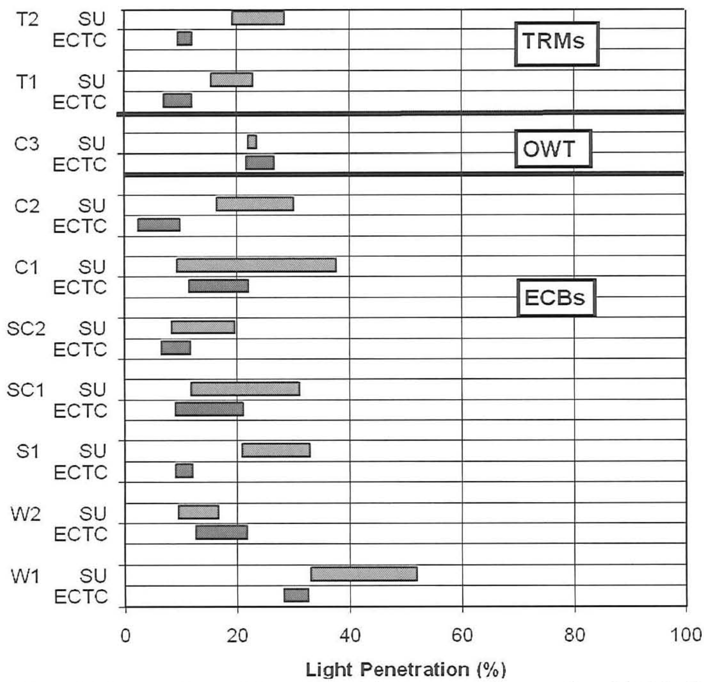

Figure 7. Comparison of the range of light penetration results with ECTC

As shown on Figure 7, in terms of the ECBs, it is, again, believed that variations in mass per unit area across and between specimens lead to variations in results between laboratories. Specimen handling could have also played a role in variations in results. In terms of the OWTs, results were available for coconut fiber C3 for both laboratories. As expected, there was very little scatter in results for both laboratories, with good reproducibility. In terms of the TRMs, it is interesting that light penetration results obtained by Syracuse University were higher for both T1 (coconut matrix) and T2 (synthetic matrix) than by ECTC. Again, this could be due to specimen variability.

In summary, light penetration is a useful property for distinguishing and comparing different RECPs. The method was able to distinguish between the wood ECBs (W1, W2), coconut (C3) and jute (J1) OWTs, and coconut (T1) and synthetic (T2) TRMs, although was limited in distinguishing between the straw (S1), straw/coconut (SC1, SC2), and coconut (C1, C2) ECBs.

Water absorption

Water absorption testing was conducted to provide information on the absorptive capacity of the RECPs. A comparison of the range of water absorption results obtained for each group of RECPs tested (ECBs, OWTs, and TRMs) is presented on Figure 8.

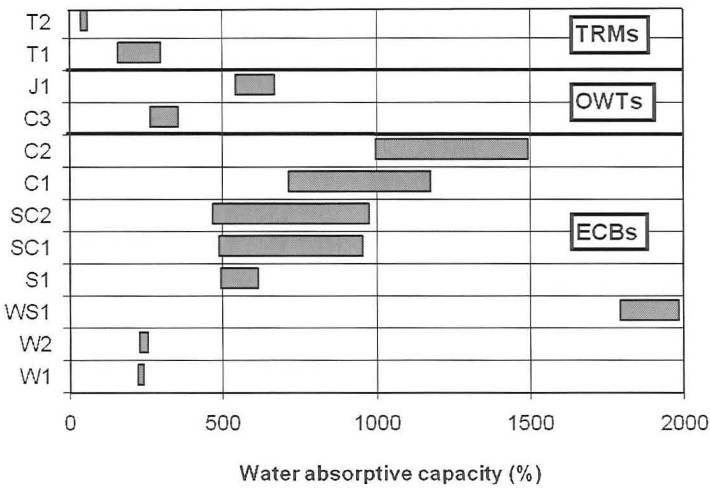

Figure 8. Range of water absorption results

As shown on Figure 8, scatter in water absorption results ranged from very little (W1, W2), to moderate (WS1, S1), to excessive (SC1, SC2, C1, C2) in the ECBs. The little scatter in results for the wood ECBs (W1 and W2) can be attributed to the ability of the wood fibers to hold water once it is absorbed. There was very little dripping or loss of water due to specimen handling during weighing. This was not the case for the straw/coconut (SC1, SC2) and coconut (C1, C2) ECBs. Any tilting of the testing frame from horizontal resulted in loss of water from the specimen fibers. The similar results for W1 (346 g/m^2) and W2 (623 g/m^2) were surprising because it was expected that the denser W2 would have held more water than W1. It is also interesting that the coconut OWT (C3) held less water than the coconut ECBs (C1 and C2). It is believed that higher water pressure is needed for water to penetrate the tight, twisted yarns of C3. The relatively little scatter and low water absorptive capacity of the TRMs (T1, T2) are not surprising because synthetic structures do not absorb appreciable amounts of water.

To evaluate reproducibility, water absorption results obtained by Syracuse University are compared to those obtained by ECTC (AASHTO 2005) for ten RECPs on Figure 9. In terms of the ECBs, water absorption results were generally similar between laboratories for the wood ECBs (W1, W2). However, results varied for the straw (S1), straw/coconut (SC1, SC2), and coconut (C1, C2) ECBs. The wide range in results in comparison with ECTC results is surprising. However, these ECBs are difficult to test in that any tilting of the testing frame from horizontal would result in the loss of water. For example, if the testing frames were not level during drip-drying, significant loss of water could have resulted. Similar to water absorption results at Syracuse University, ECTC's results for the coconut OWT (C3) were also in a relatively narrow range. This is attributed to the twist of the coconut fibers in C3 that held onto absorbed water.

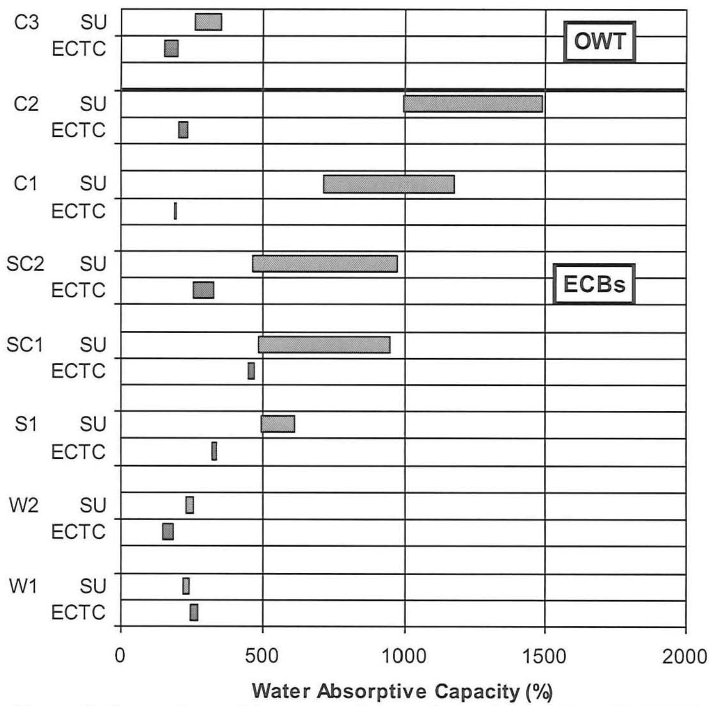

Figure 9. Comparison of the range of water absorption results with ECTC

Water uptake (New test)

Because of difficulties associated with the water absorption test, water uptake testing was conducted on the natural-fiber RECPs to evaluate their water absorption properties. Water uptake testing is commonly used to characterize building materials, but is not used to characterize RECPs.

Water uptake tests were conducted in accordance with ASTM D5802. In the test, 12.7cm by 12.7cm RECP specimens are weighed and placed in air-dried specimen Plexiglas containers with fine-mesh metal screens on the bases (see Figure 10.) The weighed containers are then placed in a reservoir that is filled with water to a height where it would just be in contact with the bottom of the RECP. The containers with RECP specimens are then weighed at time intervals that coincide with a square root of time scale for a period ranging from one hour to several hours, depending on the RECP being tested, to measure the amount of water absorbed by the material over time. This measurement provides information on the amount of "free" water or water that is loosely held within and between the RECP/fibers and easily drains from the RECP/fibers. To go one step further, RECP specimens were also weighed after being held vertically for 10 seconds to measure "held" water, the water that is physically "held" by the RECP/fibers and does not readily drain.

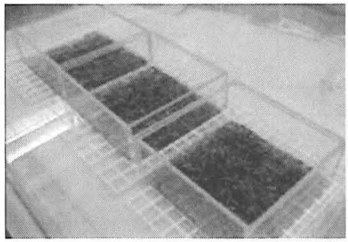

Figure 10. Water uptake (a) reservoir with three specimen containers

Typical water uptake results are shown on Figure 11. As shown, the water uptake test presents very interesting results. For example, the straw (S1), straw/coconut (SC1), and coconut (C1) show different performance in terms of total water uptake, when the products are used in a horizontal orientation. However, this data indicates that the three products would behave similarly in terms of water absorptive behavior when installed in a non-horizontal orientation. This test also demonstrates the differences between coconut ECB (C1) and coconut OWT (C3). Both coconut RECPs absorbed similar amounts of water; however, the coconut ECB (C1) released most of its water when the orientation changed. The OWT (C3), which contained twisted coir fibers, held onto its absorbed water. These differences may have important design implications that are not measured in the water absorption test.

In summary, water absorption is an important property that is distinctive for different fiber types. The ability of natural fibers to absorb water increases their weight and ability to drape, improving the contact between the RECP and the underlying soil. Second, when fibers absorb water, they swell, increasing the amount of ground cover they provide. Third, the ability of a RECP to hold water allows seeds to germinate quickly and vegetation to grow. Because of this, it is important that the water absorptive test be repeatable, reproducible, and useful.

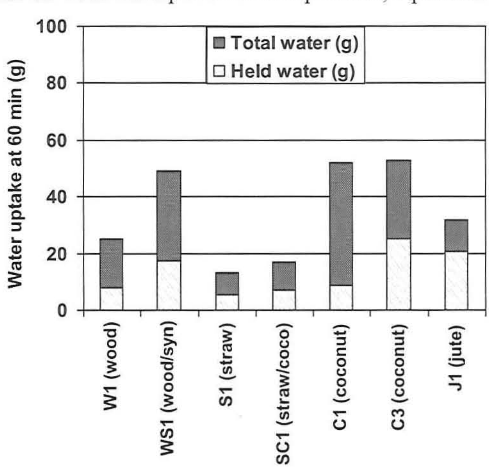

Figure 11. Water uptake results

CONCLUSION

In summary, the index tests provide a straight forward way to characterize and differentiate RECPs, although to varying degrees. The ECTC light penetration test was able to distinguish between the wood ECBs, wood/synthetic ECBs, coconut, and jute OWTs, and coconut and PP TRMs, although was limited in distinguishing between the straw, straw/coconut, and coconut ECBs. The method also showed a relatively slight to moderate range in results.

Water absorption appears to be an important property that is distinctive for different types of fibers. The ECTC water absorption method was able to distinguish between the wood/synthetic ECBs, coconut ECBs, coconut and jute OWTs, and coconut and PP TRMs, although was limited in distinguishing between the straw, straw/coconut, and coconut ECBs. The method also showed significant variability for some products, due to product variability and sensitivity of the test.

The water uptake test in conjunction with the ECTC water absorption test is promising for evaluating RECP performance. Although some field and laboratory studies have shown the usefulness of these tests for performance, more studies are needed to substantiate these studies.

ACKNOWLEDGEMENTS

The authors would like to acknowledge support received from the National Science Foundation (Award #3535848), the Department of Education (Foreign Language and Area Studies Fellowship in South Asia), and the Syracuse University Graduate School (University Fellowship Award). The authors would like to thank Sam Allen (TRI) and Jarrett Nelson (TRI) for their technical assistance with the index tests. The authors would also like to gratefully acknowledge Tony Johnson (American Excelsior Company), Bob Moran (Belton Industries), Roy Nelsen (North American Green), and Marc Theisen (Profile Products) for providing materials used in this study.

REFERENCES

Ellison, W.D. (1944). "Studies of raindrop erosion." *Agricultural Engr.*, 131-136.

ECTC. (2001). "Standard terminology for RECPs." http://www.ectc.org/guide/chap3.htm.

Ogobe, O., Essien, K.S., and Adebayo, A. (1998). "A study of biodegradable geotextiles used for erosion control." *Geosynthetics Internat'l.*, 5:545–553.

Rickson, R.J. (2002). "Salient properties of erosion control geotextiles." *Proceedings 33rd Annual Conference*, IECA, Orlando, 499-506.

Smith, J.L., Bryz-Gornia, C.J., Bhatia, S.K., and Walowsky, D. (2005). "A comparative study of RECPs: lab testing and field performance." *GeoFrontiers 2005*, TX, Jan.

Toy, T.J., Foster, G.R., and Renard, K.G. (2002). *Soil Erosion: Processes, Prediction, Measurement, and Control*. Wiley, NY.

Ziegler, A.D., Sutherland, R.A., and Tran, L.T. (1997). "Influence of rolled erosion control systems on temporal rainsplash response – a laboratory rainfall simulation experiment." *Land Degradation & Development*, 8:139-157.

Ziegler, A.D. and Sutherland, R. A. (1998). "Reduction in interrill sediment transport by rolled erosion control systems." *Soil and Tillage Research*, 45 (3-4): 265-278.

Comparison of the Rate of Evaporation from Six Rolled Erosion Control Products

R.E. Cutts[1], A.M. ASCE, S.E. Burns[2], M. ASCE, P.E., J.D. Griffith[3], P.G., P.E., and B.R. Ehrman[4], P.E.

[1]PSI, Inc., 2930 Eskridge Road, Fairfax VA 22031; PH 1 (703) 698-9300; email: ross.cutts@gmail.com
[2]School of Civil and Environmental Engineering, Georgia Institute of Technology, Atlanta, GA 30332-0355; PH 1 (404) 894-2285; email: sburns@gatech.edu
[3]Georgia Department of Transportation, 600 West Peachtree NW Atlanta, GA 30308; PH 1(404) 631-1547; email: jogriffith@dot.ga.gov
[4]Georgia Department of Transportation, 600 West Peachtree NW Atlanta, GA 30308; PH 1(404) 631-1669; email: behrman@dot.ga.gov

ABSTRACT

Rolled Erosion Control Products (RECPs) are temporary degradable or long-term non-degradable materials designed to reduce soil erosion and assist in the growth, establishment, and protection of vegetation. Although the diversity of products within the RECP category is beneficial from a cost competitive standpoint, it is often difficult for a designer to distinguish between the function of the materials due to the sheer number of products available. Six RECPs were tested in this experimental study to quantify the level of evaporation protection conferred to the underlying soil by the presence of an RECP. Moist soil was placed in polyethylene test containers to ensure one-dimensional vertical flow of the soil moisture during evaporation. Each RECP was tested in two conditions: full sun and buried in topsoil in shade. Additionally, a control test was performed on the soil, with no RECP covering. The mass of the soil container was monitored as a function of time and temperature throughout the day. Soil temperature remained fairly constant throughout the test, at approximately 32°C (89°F), while air temperature ranged from 30-37°C (86–99°F). In all cases, the presence of the TRM dramatically reduced the rate of evaporation, both when shaded and when exposed to full sun.

INTRODUCTION

RECPs play a significant role in engineering projects where erosion control is of importance. RECPs are designed to reduce erosion in channels and slopes and to encourage rapid revegetation to further reduce a soil's susceptibility to erosive forces. Available products are manufactured to exist in a diverse range of environmental conditions, so they have a large variation in their characteristic properties. RECPs designed for long-term, non-degradable applications are typically known as turf reinforcement mats (TRMs), and temporary degradable RECPs made for short-term applications are known as erosion control blankets (ECBs). Depending on their function, the products are manufactured with a variety of materials, ranging from ultraviolet-stable or photodegradable polyethylene to natural fibers that are readily biodegradable.

In addition to shielding soil from the erosive forces of rain, RECPs also function to reduce the rate of evaporation from soils. Evaporation is a complex function of system properties including temperature, humidity, air velocity, and the characteristics of the porous media (Shokri et al., 2008). The parameter of interest is typically the rate of evaporation, which is characterized by two primary stages: a high water content stage where the rate of evaporation is relatively constant and similar to that of free, bulk water, and a low water content stage where the rate of evaporation is controlled by the rate at which water can move through the pore space; that is, the rate of diffusive mass transfer of water (Shokri et al., 2009). This study focused on evaporation from low water content soils, in which the water in the soil is held in a meniscus in the pendular state. When a soil is in the pendular state, water occurs as a coating at the contacts of soil particles, and the pore space of the soil is occupied primarily by air (Cho and Santamarina, 2001). In the case of two contacting soil spheres, the meniscus is typically approximated according to the toroidal approximation (Figure 1).

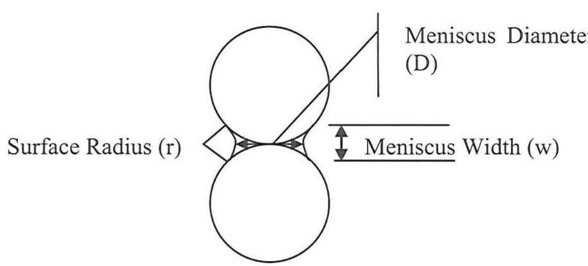

Figure 1. Evaporating water from the menicus between two contacting soil spheres.

Mathematically, the toroidal approximation can be described as follows:

$$\vec{R}(u,v) = [(w \cdot r + \cos(u) \cdot r) \cdot \cos(v), (w \cdot r + \cos(u) \cdot r) \cdot \sin(v), r \cdot \sin(u)]$$

$$\vec{R}_u = (\frac{dR}{du}),\ \vec{R}_v = (\frac{dR}{dv})$$

$$T = cross(\vec{R}_u, \vec{R}_v), \text{ and } Norm = abs(\sqrt{(T_x^2 + T_y^2 + T_z^2)})$$

$$SA = \int_{\pi-0.5\theta}^{\pi+0.5\theta} \int_0^{2\pi} Norm \ \mid du \quad dv$$

$$\theta = arc\cos\left(\frac{2\cdot r^2 - w^2}{2\cdot r^2}\right)$$

Where w = width of meniscus, r = surface radius, θ = angle of curvature, and u and v vary between 0 and 2π.

Subsequently, the fluid volume within the meniscus can be determined as the difference between the volume of liquid in the toroidal approximation and the volume of solid spheres within the meniscus:

$$Volume_{liquid} = \pi \int_{-0.5w}^{0.5w} (r+\frac{D}{2})^2 - (\sqrt{r-x^2})^2 dx$$

$$Volume_{solids} = 2\cdot\left[(\pi\cdot(\frac{w}{2})^2\cdot r_s) - (\frac{\pi(w/2)^3}{3})\right]$$

Where: r_s = radius of contacting solid sphere, D= liquid meniscus diameter. An in-depth study of the rate of evaporation between two contacting silica spheres revealed the controlling parameters that govern the evaporation of water from two contacting silica spheres were the temperature, relative humidity, and the shape of the meniscus (Cutts and Burns, 2009). Soil particle shape will also influence the rate significantly.

In contrast, the rate of evaporation of water from a free surface is not governed by the change in the shape of the meniscus at soil particles, and can be determined relatively simply according to the following equation (Adamson and Gast, 1997):

$$Z = (P - P_v)\left(\frac{1}{2\pi MRT}\right)^{0.5}$$

Where Z = condensation rate (assumed to be equal to the evaporation rate at equilibrium), P = saturated vapor pressure, P_v = ambient partial pressure, M = molecular weight, R = gas constant, and T = temperature. Evaporation of water from a free surface at a temperature of 35 °C and relative humidity of 56%, yields a rate of $1.60x10^{-3}\frac{g}{mm^2\sec}$.

MATERIALS AND METHODS

Six RECPs, all supplied by North American Green (Poseyville, Indiana, USA), were chosen for study: Vmax^3 P550, Vmax^3, SC150, C125BN, S75, and DS150. These six were chosen because they represented a wide range of longevity of projected performance. The tested products were intended for applications that ranged from permanent to short term (60 days), and ranged from construction with relatively stable polymers to bio- or photodegradable polymers and natural fibers

(Table 1 and Figure 2). The products intended for permanent application (Vmax^3 P550 and Vmax^3) were constructed with polypropylene nets designed for stability in the presence of ultraviolet light, while products intended for shorter term applications of two years or less (SC150, DS150, S75) were designed with one or more photodegradable nets. One tested product, C125BN, was designed with both a biodegradable net and matrix.

Table 1. Characteristics of RECPs Tested

Manufacturer	Product	Material	Application
North American Green	Vmax^3 P550	Polypropylene nets and matrix	Permanent
North American Green	Vmax^3	Polypropylene nets, coconut fiber matrix	Permanent
North American Green	SC150	Polypropylene nets, straw/coconut fiber matrix	24 months
North American Green	C125BN	Jute net, coconut fiber matrix	24 months
North American Green	S75	Polypropylene net, straw matrix	12 months
North American Green	DS150	Polypropylene nets, straw matrix	60 days

A medium plasticity silt (MH) with a liquid limit (LL) = 63.9% and plasticity index (PI) = 17.1% was used in the evaporation experiments. The soil is known locally as Piedmont saprolitic soil (Fulton County, Georgia, USA), and has a reddish hue due to the presence of extensive iron oxide coatings on the soil grains; the grain size distribution shows approximately 70% fines content (Figure 3). After thoroughly mixing the soil with City of Atlanta tap water to ensure uniform distribution of moisture, the soil was compacted into waterproof containers at a moisture content of 10.4%. The containers had dimensions of 13.3 cm by 9.5 cm by 6.4 cm and were impermeable on all sides except the top to force a one-dimensional vertical evaporative flux. The mass of the containers was measured as a function of time, and the measured mass difference was attributed to evaporative losses from the test soil. Both air and soil temperatures were measured throughout the duration of the test as well.

Figure 2. Rolled erosion control products tested in the evaporation study.

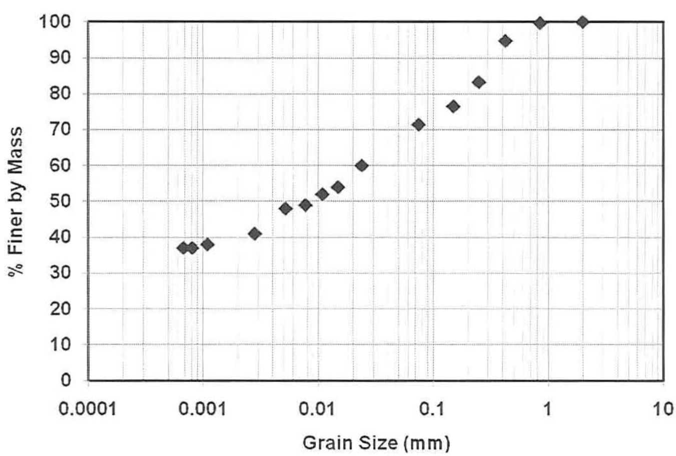

Figure 3. Grain size distribution for the Piedmont soil used in the experiments.

RESULTS

The recorded air and soil temperatures demonstrated that the soil temperature remained relatively stable throughout the duration of the testing program in spite of the significant increase recorded in the prevailing air temperature (Figure 4).

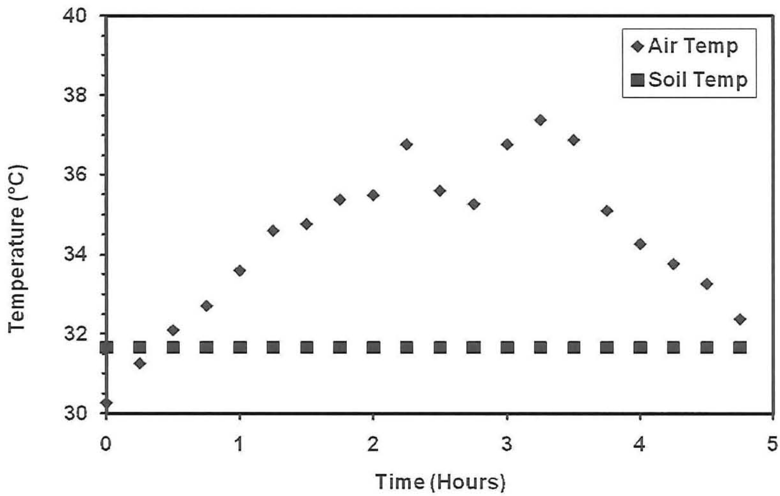

Figure 4. Soil and air temperature throughout the test duration.

For the RECPs that were tested in full shade, the rate of evaporation observed for the samples with RECP covering was less than half the rate that was observed in the control case with no covering (Figure 5). Similar results were seen in the case where the soil containers were placed in full sun (Figure 6).

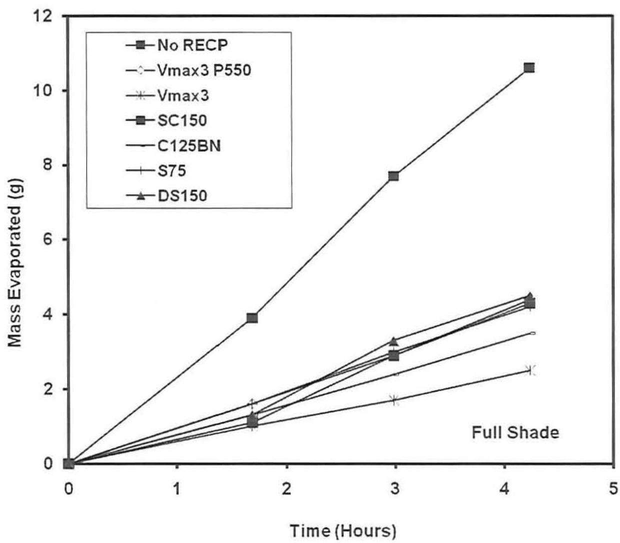

Figure 5. Rate of mass evaporation in full shade throughout the test duration.

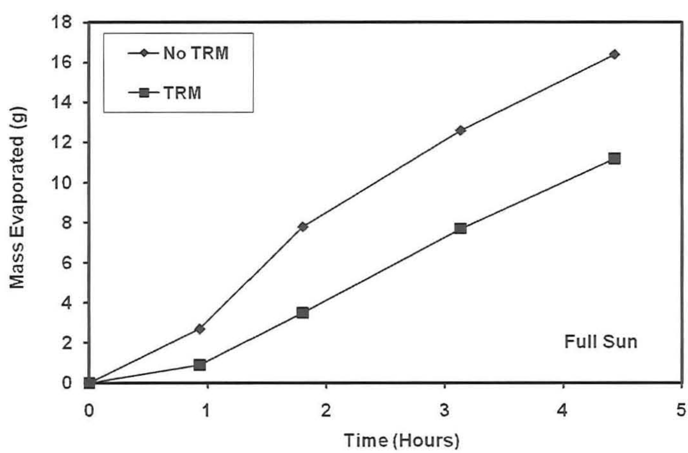

Figure 6. Comparison of the rate of evaporation in full sun, with and without TRM covering.

Examination of the data normalized in terms of flux demonstrated that the differences between the flux from the six different RECPs were relatively small, with $Vmax^3$ demonstrating the lowest flux at apprximately 25% of the flux from the uncovered control case (Figure 7). In general, the evaporative flux was 60-70% lower than the flux recorded in the case where the soil was left uncovered. Interestingly, little correlation was observed between the RECP matrix material and the evaporative flux. The two RECP samples that used straw as the matrix (S75 and DS150) demosntrated similarly high values of flux as were observed in the polypropylene sample ($Vmax^3$ P550) and the straw/coconut sample (SC150). The lowest observed evaporative flux was from the $Vmax^3$ RECP, which occurred in the case of the coconut fiber matrix. Despite the significantly different materials and structure within the RECP matrices, the relative differences in evaporative flux were small, and effectively minor when compared on a product to product basis.

Comparing the rate of evaporation from the soil samples to that previously calculated for evaporation from the free surface of water demonstrated that evaporative losses were much lower in soil systems. As was anticipated, the presence of the soil particles led to formation of menisci, which created tensile forces in the water at the particle surface and greatly decreased the rate of mass transfer away from the particles. Mass transfer was also limited within the tortuous pore space of the soil, further reducing the rate of water movement. The rate of evaporation from a free water surface under the conditions described above is approximately five orders of magnitude greater than that observed in the tested soils, with or without RECP covering.

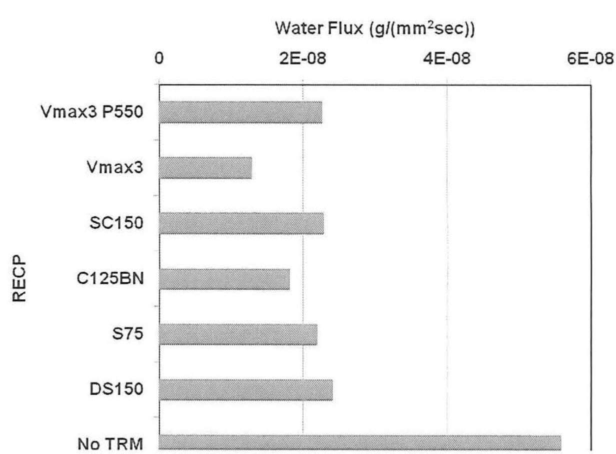

Figure 7. Comparison of water flux from 6 RECPs in shaded conditions.

CONCLUSIONS

Ultimately, the reduction in evaporative flux due to the presence of the RECP had two effects: (1) it allowed the soil to retain additional moisture, thereby increasing the amount of water that will be bio-available; and (2) it increased the amount of time the soil remained in the unsaturated state, which increases the tensile forces between the soil particles and reduces the soil's erodibility. The presence of the RECP is believed to have resulted in a reduced local temperature at the soil and air interface and limited the mass transfer of water from the soil surface, both of which resulted in the reduction of the net evaporative flux from the soil that was covered with an RECP.

ACKNOWLEDGEMENTS

The authors thank North American Green for the donation of the samples that were used in this investigation. Partial funding for this investigation was provided by the Georgia Department of Transportation, and the authors are grateful for the financial support.

REFERENCES

Adamson A.W., Gast A.P. (1997) Physical Chemistry of Surfaces. 6th ed. John Wiley & Sons, Inc.

Cho G.C., Santamarina J.C. (2001) Unsaturated particulate materials-particle-level studies. Journal of Geotechnical and Geoenvironmental Engineering 127:84-96.

Cutts R.E., Burns S.E. (2009) Evolution of Surface Area-to-Volume Ratio for a Water Meniscus Evaporating Between Contacting Silica Spheres. Journal of Colloid and Interface Science 343:58-64.

Shokri N., Lehmann P., Or D. (2009) Characteristics of evaporation from partially wettable porous media. Water Resources Research 45.

Shokri N., Lehmann P., Vontobel P., Or D. (2008) Drying front and water content dynamics during evaporation from sand delineated by neutron radiography. Water Resources Research 44.

International Practices and Guidance: Natural-Fiber Rolled Erosion Control Products

S.K. Bhatia[1], G. Venkatappa Rao[2] and J.L. Smith[3]

[1]Professor, Civil and Environmental Engineering, Syracuse University, 105 Link Hall, Syracuse, NY 13214; PH (315) 443-3352; email: skbhatia@syr.edu
[2]Former Department Chair, Indian Institute of Technology, Delhi, India;
[3]Assistant Professor, Sustainable Construction Management and Engineering, SUNY College of Environmental Science and Forestry, 205 Baker Laboratory, 1 Forestry Drive, Syracuse, NY 13210; PH (315) 470-6866; email: jsmith@esf.edu

ABSTRACT

In recent years, there has been a great deal of interest in the development and use of natural-fiber rolled erosion control products (RECPs) to sustainably manage soil erosion. Natural fibers offer many advantages over synthetic fibers in that they are biodegradable, can absorb water, and can easily conform to underlying soil surfaces. In the US, coir, jute, straw, and wood excelsior fibers are commonly used to manufacture RECPs; however, efforts are being made around the world (e.g. United Kingdom, Canada, and the US) to explore potential uses of other natural fibers, such as hemp, flax, sugarcane, peanut shells, palm leaves, and cotton. Many researchers have characterized the properties of natural-fiber RECPs and documented their successful use in erosion control applications. For example, work has been done in India to evaluate the physical and engineering characteristics of coir and jute fibers for use in erosion control. Research efforts in the US and Europe have focused on the development of standardized test methods for characterizing RECPs and the performance of large- and small-scale tests. Many case histories have been published that document the successful use of natural-fiber RECPs. This paper presents an overview of natural-fiber RECP practices that are being used around the world and emergent fibers that are being evaluated for use as RECPs. International practices and guidance for the selection of natural-fiber RECPs for erosion control are given.

INTRODUCTION

Soil erosion is a significant issue in the sustainable management of land resources. Although agricultural lands are the primary source of soil erosion, with more than 80% being severely to moderately eroded (Pimentel et al. 1995), accelerated erosion rates from unprotected hillslopes and construction sites are of particular concern because of the relatively high rates at which they erode (Ziegler et al. 1997, Viadero 2006). Soil erosion decreases the stability of slopes; reduces soil productivity through the loss of water, nutrients, soil organic matter, and soil biota; and can adversely impact the quality of surface waters entering down-gradient streams.

Rolled erosion control products (RECPs) provide engineers with a low-cost and effective means to meet these challenges. RECPs are temporary degradable or long-term non-degradable products manufactured or fabricated into rolls designed to reduce soil erosion and assist in the growth, establishment, and protection of vegetation (ECTC 2001). Because they are manufactured into rolls, they can be easily installed and anchored along a slope or drainage channel. RECPs provide immediate ground cover to protect against raindrop impact, stabilize seed and soil within their structures, allowing seeds to germinate quickly and vegetation to grow, and reinforce vegetation once it is established.

NATURAL-FIBER RECPs

Many different types of RECPs have emerged since natural-fiber jute mats were first used for erosion control in the 1950s in the US (Lancaster and Myrowich 2005) and in India (C-DOCT 2002). In the US, RECPs made of synthetic fibers, such as polypropylene, polyvinyl chloride, polyester, and nylon initially dominated the market. This could be due in part to their perceived superior performance to natural-fiber RECPs. However, RECPs made of natural fibers, such as coir, jute, straw, and wood excelsior, reemerged in the 1990s. Although it has been shown that natural fibers offer many advantages over synthetic fibers due to their biodegradability, water absorption, and flexibility, it is only in the last 10 years that natural fibers have received attention. This most recent thrust in the development of new natural-fiber products in the US and around the world has stemmed from a renewed focus on sustainability and the use of renewable, locally available, low-cost, and abundant materials.

Shepley et al. (2002) reported that RECPs made of natural fibers were more popular than those made of synthetic fibers in the US, based on a survey of manufacturers of both synthetic and natural fiber RECPs. The most popular erosion control RECPs in the US are currently made of straw and wood excelsior (Shepley et al. 2002), which are native to the US. A review of the 2009 Specifier's Guide (IFAI 2009), which compiles product listings from participating manufacturers, indicates that 53 different natural-fiber RECPs (19 wood, 16 straw, 9 coir, 6 straw/coir blends, and 3 jute) and 28 different non-degradable RECPs (3 with a natural-fiber matrix) are currently available in the US. For these products, coir and jute are predominately exported from Sri Lanka and India.

Work is also being conducted in the US to evaluate other types of natural fibers for use as RECPs. For example, work has been done to evaluate the use of fiber from sugarcane stalks (Thames 1997) and sugarcane bagasse (Dinu and Saska 2006) in RECPs. Sugarcane bagasse erosion control mats were found to be comparable in specific mass, thickness, and swelling, lower in tensile strength, and higher in water absorption to four commercially available straw, coconut, and wood excelsior mats (Dinu and Saska 2006). Fibers from peanut shells have also been evaluated for use in RECPs (Bieak and George 2003.) They found that mats could be made to produce comparable flexibility, strength, and light and moisture transmission requirements to commercially available RECPs. Cotton fiber is also being used in commercially available, hydraulically applied erosion control products (HECPs) (Cotton Inc. 2008). The cotton being used is a byproduct of the cotton-gin process, is non-toxic, adds nutrients to the soil, and requires less water during applications than commonly used HECPs.

In India, RECPs have traditionally been manufactured from coir or jute fibers, which are native to India. India is the largest country that produces coir fiber (Venkatappa Rao and Balan 2000a). Coir has high durability, slow biodegradation, is less sensitive to ultraviolet radiation than other natural fibers, and is reputed to be the strongest of all known natural fibers (C-DOCT 2002). Coir fiber RECPs are also being manufactured in countries such as Canada and South Africa. Jute is also widely available in India; however, degrades quickly in humid conditions and is susceptible to microbial attack (Banerjee and Unni 2000).

Work is also being conducted around the world on other types of natural fibers. For example, extensive work on the use of palm leaves from *Borassus aethiopum*, grown in West Africa, and *Mauritia flexuosa*, grown in Latin America, is being conducted in the United Kingdom (Smets et al. 2007, Bhattacharyya et al. 2009). The palm-leave mats have been found to significantly reduce soil erosion from bare soil slopes. Recently, products made from wheat and barley straw, hemp, and flax have emerged in Canada. Hemp fiber mats are also being manufactured and used in the United Kingdom to protect soil surfaces from wind and rain erosion.

CHARACTERIZATION OF NATURAL FIBERS

Structure type is typically used to broadly define and classify different types of RECPs. In the US, the Erosion Control Technology Council (ECTC) developed classifications for structure type and published standard definitions (ECTC 2001): (1) Erosion control nets (ECNs) are temporary, degradable planar woven natural fiber or extruded geosynthetic meshes used to anchor loose fiber mulches; (2) Open weave textiles (OWTs) are temporary, degradable RECPs composed of processed natural or polymer yarns woven into a matrix, used to provide erosion control and facilitate vegetation establishment; (3) Erosion control blankets (ECBs) are temporary, degradable RECPs composed of natural or polymer fibers that are mechanically, structurally, or chemically bound together to form continuous matrices; and (4) Turf reinforcement mats (TRMs) are long-term, non-degradable RECPs composed of UV-stabilized, non-degradable, synthetic fibers, nettings and/or filaments processed into three-dimensional (3-D) reinforcement matrices. Figure 1 shows several natural-fiber RECPs, characterized as ECBs, OWTs, and TRMs, that are commonly used in the US.

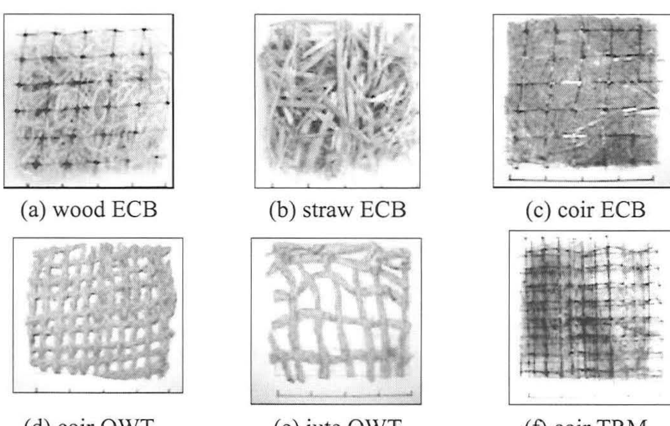

(a) wood ECB (b) straw ECB (c) coir ECB

(d) coir OWT (e) jute OWT (f) coir TRM

Figure 1. Common natural-fiber RECPs used in the US.

Although similar types of RECPs are used around the world, different terminology can be found in some areas. For example, the term "erosion control meshes" (ECMs) is commonly used to refer to OWTs in India (Venkatappa Rao 2000). In the United Kingdom, the term "geotextile" is commonly used to refer to a RECP, and "mats" is broadly used to include OWTs (Bhattacharyya et al. 2009).

Fiber type

Although structure type is important in defining and classifying different RECPs, it is the matrix fiber type that defines the ultimate performance and functional longevity of RECPs. Natural fibers can vary widely in their chemical composition, physical, morphological, and mechanical properties, and longevity. For example, straw RECPs have typical functional longevities in the range of three to twelve months; whereas, coir RECPs have typical functional longevities in the range of three years. The functional longevity and strength of coir fiber is due to its lignin content (C-DOCT 2002). A comparison of lignin and cellulose composition for natural fibers used in RECPs is given in Table 1.

Table 1. Chemical composition of some natural fibers used in RECPs (after Rowell 2001)

Fiber	% Lignin	% Cellulose
Coir	30-45	35-62
Jute	21-26	45-63
Wheat straw	16-23	33-39
Deciduous wood	23-30	38-49
Sugarcane bagasse	18-26	32-37
Cotton	0.7-1.6	85-90
Hemp	9-13	57-77
Flax	21-23	43-47

Natural fibers used in RECPs typically come from vegetable sources due to their enhanced strength, elongation, and durability in comparison to animal and mineral fibers (Rankilor 2000). They can further be categorized based on the part of the plant they come from: (1) bast/stem (i.e. jute); (2) seed/fruit (i.e. coir); (3) stalk (i.e. straw); or (4) hardwood (i.e. wood excelsior). This difference in origin provides the basis for differences in their basic properties. For example, bast/stem fibers generally have higher tensile strengths than other vegetable fibers. Seed/fruit fibers protect the seeds and fruits of plants.

LABORATORY TESTING

Many researchers have characterized the properties of RECPs and documented their successful use in erosion control applications. In India, a significant amount of work has been done to evaluate the physical and engineering characteristics of coir and jute RECPs (i.e. Venkatappa Rao and Balan 2000b, Venkatappa Rao et al. 2000). In other parts of the world, such as in the US and Europe, efforts have focused on the development of standardized test methods for characterizing RECPs (Sprague et al. 2002) and the performance of large-scale and small-scale bench-scale tests (i.e. Rickson 2002 and Smith et al. 2007).

In the US, the Erosion Control Technology Council (ECTC) in conjunction with TRI/Environmental, Inc. (TRI) recently developed index and bench-scale tests for the characterization of RECPs, several of which have become American Society for Testing and Materials (ASTM) standardized test methods. Index tests provide characteristic physical properties of RECPs and allow for the comparison of different RECPs. Performance tests provide information about the erosion control performance of RECPs under conditions similar to the intended application. Although many manufacturers and researchers believe these tests are important, they are not being widely used by manufacturers in the US. In addition, the tests are currently only being performed by one testing laboratory (TRI) and manufacturers' in-house testing laboratories. There have also been few studies that relate basic index properties to laboratory (e.g. Ziegler and Sutherland 1998, Rickson 2002) or field performance (e.g. Fifield 1992, Smith et al. 2005). Selected standardized index and bench-scale tests are summarized below.

Light penetration

Light penetration is measured in accordance with ECTC (2001) and ASTM D6567. In the test, light is projected through frosted glass to dissipate the light, then through a RECP specimen in a closed container. The amount of light that passes through the RECP is measured using a light meter. The percentage light penetration is calculated as the ratio of the amount of light that passes through a RECP specimen to the amount of light that passes without a specimen.

Water absorption

Water absorption testing is performed in accordance with ECTC (2001) and ASTM D1117. In the test, RECP specimens are placed on a screen and submerged in water for 24 hours. The RECP specimens are removed, allowed to drain for 10 minutes, and weighed. The water absorptive capacity is calculated as the ratio of the water held by the RECP to the original dry weight of the specimen.

Rainsplash erosion

Rainsplash erosion testing is performed in accordance with ASTM D7101. In the test, rainfall is produced by a laboratory rainsplash simulator that is capable of creating uniform drops with a median diameter of 3.0 to 3.5mm from a drop height of 2000 mm. An adjustable slope table containing three channels is located beneath the simulator. The base of each channel contains a recessed hole where prepared soil cores are placed and tested.

Tests are performed for durations of 30 minutes. Soil is collected and runoff is measured at 5-minute increments during the test. Tests are conducted for rainfall intensities of 2±0.2 in/hr, 4±0.2 in/hr, and 6±0.2 in/hr. A minimum of five tests is performed for each condition tested. Photographs of the rainfall simulator constructed at Syracuse University are shown on Figure 2.

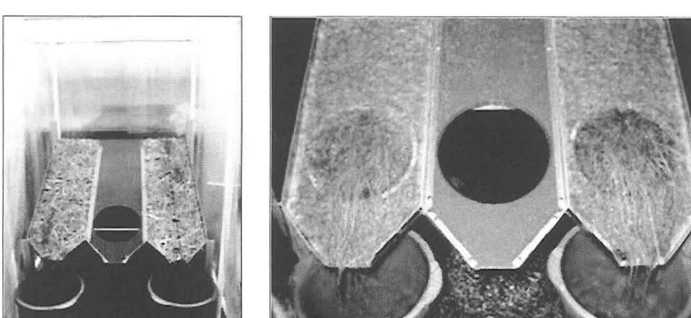

Figure 2. Photographs of the rainsplash simulator at Syracuse University.

Vegetation enhancement

Vegetation enhancement tests are performed in accordance with ASTM D7322. In the test, containers of soil are sown with seeds and watered. RECPs are then placed on the containers, with several containers remaining uncovered to serve as bare soil controls. The containers are then placed in an environmentally controlled chamber. The containers are periodically watered and monitored for vegetative growth. The percentage vegetation improvement is calculated as the ratio of the weight of vegetation in the RECP-covered containers to the non-RECP covered bare soil control containers, measured at 21 days germination. Photographs of the container and environmentally controlled chamber at Syracuse University are shown in Figure 3.

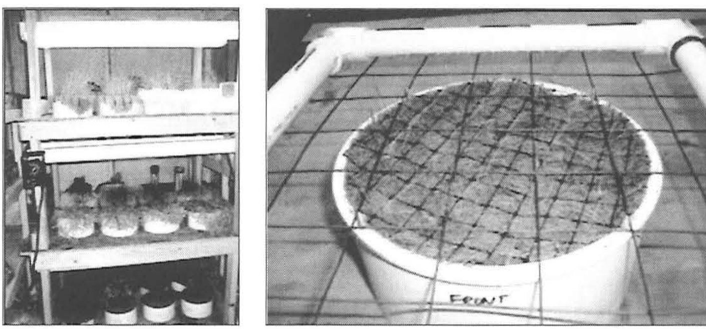

Figure 3. Photographs of the (a) environmentally controlled chamber and (b) container for the vegetation enhancement tests at Syracuse University

Although significant progress has been made in characterizing RECPs and developing test methods, there is a need for universally-accepted RECP test methods and procedures. It is believed that standardization is necessary in countries such as India to be able to compete in international RECP markets. The test methods also need to be thoroughly evaluated to determine their usefulness, repeatability, and reproducibility. There is also a need to establish correlations between measured index properties and bench-scale performance of RECPs and field parameters to aid in the proper design of RECPs. Without this, design will continue to be based on maximum allowable slopes and shear stresses, without consideration for the unique and beneficial properties of natural fibers.

FIELD STUDIES

RECPs are used around the world in a variety of applications and many case studies have been published documenting their successful use. For example, coir erosion control mats are being used to revegetate steep bare slopes in India (Venkatappa Rao and Balan 2000c) and natural jute products are being used for slope protection and quarry restoration in Hong Kong (Lam and Braim 2002). In the US, the largest RECP market is in the highway construction industry, where engineers are faced with erosion from highway drainage ditches and cut and fill slopes (Shepley 2002.) RECPs are also commonly used in landfill, urban and suburban drainage areas, building construction, and landscaping markets (Shepley 2002). In addition to the large number of case studies that have been published, the suitability and performance of RECPs for erosion control applications have been evaluated by many researchers. Some of these are described below.

McCullah and Howard (2000) compared the field performance of 13 different RECPs installed on a 4H:1V slope over a 9-month period. The RECPs were made from straw, rice straw, straw/coconut, coconut, and aspen fibers. Sediment collection troughs were installed at the base of each test section. On average, the RECPs provided an 81% reduction in soil loss than the unprotected bare soil control slope.

Casas et al. (2002) compared the performance of 5 different RECPs for the revegetation of burned slope areas in Spain. The RECPs included a coir grid, a jute grid, a high density polyethylene (HDPE) geogrid, straw mulching, and a straw/coir organic mat. For the study, the RECPs were seeded with 7 different grass species and evaluated for growth every 15 days over a 3-month period. It was found that the straw/coir organic mat, followed by the coir grid, was the most effective RECP for the establishment of vegetation at the site, based on vegetation survival rates.

Bhatia et al. (2002) compared the performance of 7 different RECPs installed in a drainage channel in central New York. The RECPs included wood excelsior and straw/coir ECBs and TRMs made of nylon, PP net with polyolefin matrices, and PP net with coir matrices. The performance of the RECPs was evaluated based on visual observations of vegetative growth and measured deformations of channel cross-sections. With the exception of one TRM, the RECPs were successful in establishing vegetation over the 22-month evaluation period, although to varying degrees. It was also found that the cross-sections, with the exception of two, exhibited soil/sediment deposition. The erosion that did occur was minimal and did not impact the overall performance of the channel.

Smith et al. (2005) considered these RECP properties and related them to the performance of six different RECPs (PP matrix and triple PP net, coir fiber matrix and triple PP net, PP strands reinforced with coir twine, and triple PP mat of bioriented geogrids) installed in a drainage channel in central New York, in terms of both soil erosion and vegetative growth. It was found that percentage area cover and water holding capacity/percentage wet weight play a direct role in initial soil erosion protection and long-term vegetation establishment. It was difficult to assess the importance of RECP induced roughness and depth of water ponded at the site because of the relatively good performance of the RECPs and the limited flow in the channels. However, it is believed that these properties can play an important role in critical applications, such as in highly erosive soils.

Vishnudas et al. (2006) conducted field tests in the Amachal Watershed in Trivandrum, Kerala, India to evaluate the effectiveness of coir RECPs for embankment protection. The fresh coir matting RECP used for the study had a smallest mesh opening of 6 x 6 mm^2, a density of 0.74 kg/m^3, and a tensile strength of 13.8 kN/m^3. The experiment was conducted in three stages, coir RECP with grass *(Axonopus compressus)*, coir RECP alone, and a bare soil control plot. The tensile strength of the RECPs was found to have reduced by about 70% seven months after installation and further reduced by about 81% at the end of nine months. The establishment of vegetation during this period was found to be effective in erosion control.

In summary, a significant amount of work has been done that documents the successful performance of RECPs in erosion control applications. RECPs effectively reduced soil erosion in the majority of the field studies reviewed.

Differences in RECP performance were observed in terms of the growth of vegetation. Several researchers also noted index properties of RECPs that they believe are important to their performance. For example, Smith et al. (2005) found that percentage area cover and water holding capacity/percentage wet weight play a direct role in initial soil erosion protection and long-term vegetation establishment. Although these studies provide important information about the performance of RECPs, the majority of studies are qualitative in nature and only provide information on particular site conditions, such as climate, soil types, vegetation types, and topography.

CONCLUSION

Although significant progress has been made in characterizing RECPs and developing test methods, there is a need for universally-accepted RECP test methods and procedures. RECP test methods need to be thoroughly evaluated to determine their usefulness, repeatability, and reproducibility. There is also a need to establish correlations between measured index properties and bench-scale performance of RECPs and field parameters to aid in the proper design of RECPs.

A significant amount of work has been done that documents the successful performance of RECPs in erosion control applications. RECPs effectively reduced soil erosion in the majority of the field studies reviewed. In general, there was little distinction in the overall performance of the various types of RECPs in terms of minimizing soil erosion, whether they were made of synthetic or natural fibers. Differences in RECP performance were observed in terms of the growth of vegetation. In general, natural fiber RECPs were found to be more effective in establishing vegetation than synthetic fiber RECPs.

Both natural and synthetic RECPs were effective in reducing rainsplash erosion in the laboratory, although to varying degrees, with the exception of buried TRMs. In general, the natural fiber OWTs and ECBs (jute, coir, wood) were more effective in reducing rainsplash erosion than the synthetic fiber TRMs. High surface coverage, thickness, and water absorption capacity were noted as being important RECP properties. In terms of overland flow, there were varying results. RECP properties such as good drapability and thick fibers were noted as being important.

There is a need for: universally-accepted RECP testing methods and procedures; global education on the different types of RECPs available and their effectiveness; and proper design guidelines. These goals will only be realized through international collaboration between manufacturers, designers, engineers, and researchers.

ACKNOWLEDGEMENTS

The authors would like to acknowledge support received from the National Science Foundation (Award #3535848), the Department of Education (Foreign Language and Area Studies Fellowship in South Asia), and the Syracuse University Graduate School (University Fellowship Award).

REFERENCES

Banerjee, P.K., and Unni, E.B. (2000) "Growth prospects of natural geotextiles," Coir Geotextiles, Emerging Trends, Edited by G.V. Rao and K. Balan, The Kerala State Coir Corporation Ltd. (KSCC), Alappuzha, Kerala, India, November 2000, 15-30.

Bhatia, S.K., Smith, J.L., Lake, D., and Walowsky, D. (2002) "A technical and economic evaluation of geosynthetic rolled erosion control products in highway drainage channels," Geosynthetics International, 9 (2), 125-148.

Bhattacharyya, R., Davies, K., Fullen, M.A., and Booth, C.A. (2009). "Utilization of Palm-mat Geotextiles to Conserve Agricultural Soils," Proceedings of the International Erosion Control Association (IECA) Conference (Environmental Connection 09). Reno, NV, February 2009,

Bieak, N., and George, B.R. (2003). "Utilization of peanut shell fibers in nonwoven erosion control materials," *International Nonwovens Journal*, Winter 2003, 60-65.

Casas, B., Montavez, I., Bertran, M., Sanchis, E., and Fos, M. (2002) "Evaluation of different erosion control covers in the revegetation of slope areas," Proceedings of 33rd Annual Conference, International Erosion Control Association (IECA), Orlando, Florida, February 2002, 31-36.

Centre for Development of Coir Technology (C-DOCT) (2002) "Comprehensive reference book on coir geotextiles," edited by Ayyar, T.S.R., Nair, C.G.R., and Nair, S.N.B., Kerala, India, May 2002, 339 pp.

Cotton Incorporated. (2008). "New Cotton –Based Erosion Control Product Honored by Better Roads Magazine," American's Cotton Producers and Importers, Press Release, January 22, 2008.

Dinu, I., and Saska, M. (2006). "Production and properties of soil erosion control mats made from sugarcane bagasse," *Journal of American Society of Sugarcance Technologies*, 36-46.

ECTC (2001) "Standard terminology for RECPs," http://www.ectc.org/guide/chap3.htm> (July 24, 2004).

Fifield, J.S. (1992) "How effective are erosion control products in assisting with dry land grass establishment with no irrigation?," The Environment is our Future: Proceedings of Conference. XXIII, IECA, Reno, NV, Feb., 321-333.

Industrial Fabrics Association International (IFAI). (2009). *Geosynthetics 2010 Specifier's Guide*. 27:6, 117-122.

Lancaster, T and Myrowich, M, (2005) "14 years of guidance and growing the RECP industry," http://www.ectc.org/source-docs/2005site/SCTCHistory.pdf (July 15, 2006).

Lam, C.L. and Braim, M. (2002) "Slope protection and quarry restoration in Hong Kong using natural geotextiles," Proceedings of Conference 33, IECA, Orlando, Florida, February 25-March 1, 2002, 73-80.

McCullah, J., and Howard, V. (2000) "Shasta College erosion control blanket study, research quantifies erosion from slopes," Land and Water, Sept/Oct, 2000, 44:5.

Pimentel, D., Harvey, C., Resosudarmo, P., Sinclair, K., Kurz, D., McNair, M., Crist, S., Shpritz, L. Fitton, L., Saffouri, R., and Blair, R. (1995) "Environmental and economic costs of soil erosion and conservation benefits," Science 267:5201, February 24, 1995.

Rankilor, P.R. (2000) "Textiles in civil engineering. Part 1-geotextiles," Handbook of Technical Textiles, edited by Horrocks, A.R. and Anand, S.C., Woodhead Publishing.

Rickson, R.J. (2002) "Salient properties of erosion control geotextiles," Proceedings 33rd Annual Conference, IECA, Orlando, 499-506.

Rowell, R.M. (2001) "Performance driven composites from lignocellulosic resources," Proceedings of the International Conference on Science and Technology of Composite Materials, Argentina, Dec. 10-12, 29-32.

Shepley, B., Smith, R., and Jackson, G.L. (2002) "Market analysis of erosion control Mats," United States Department of Agriculture Forest Service, Forest Products Laboratory, Research Note FPL-RN-0284.

Smets, T., Poesen, J., Fullen, M.A., and Booth, C.A. (2007). "Effectiveness of palm and simulated geotextiles in reducing run-off and inter-rill erosion on medium and steep slopes," *Soil Use and Management*, September 2007, 23, 306-316.

Smith, J.L., Bryz-Gornia, C.J., Bhatia, S.K., and Walowsky, D. (2005) "A comparative study of RECPs: lab testing and field performance," GeoFrontiers 2005, TX, Jan.

Smith, J.L., Davieau, M.R., and Bhatia, S.K. (2007) "Evaluation of soil erosion using the rainsplash technique," ASCE Geo-Denver 2007 Conference, February 18-21, 2007 Denver, CO, accepted for publication.

Sprague, C.J., Carver, C.A., and Allen, S. (2002) "Development of RECP performance test methods," Journal of Geotechnical Testing, December 2002, 25:4.

Thames, J. L. (1997). Sugar cane fiber geotextiles. Ph.D. Diss., Louisiana State University, Baton Rouge, LA (Diss. Abstr. AAT9736044).

Venkatappa Rao, G. (2000). "Classification of erosion control products." Coir Geotextiles, Emerging Trends, Edited by G.V. Rao and K. Balan, KSCC, Alappuzha, Kerala, India, November 2000, 107-111.

Venkatappa Rao, G., and Balan, K. (2000a). "Coir geotextiles – a perspective." Coir Geotextiles, Emerging Trends, Edited by G.V. Rao and K. Balan, KSCC, Alappuzha, Kerala, India, November 2000, 5-14.

Venkatappa Rao, G., and Balan, K. (2000b). "Test procedures for coir geotextiles." Coir Geotextiles, Emerging Trends, Edited by G.V. Rao and K. Balan, KSCC, Alappuzha, Kerala, India, November 2000, 43-65.

Venkatappa Rao, G., and Balan, K. (2000c). "Improving the environment by vegetation growth." Coir Geotextiles, Emerging Trends, Edited by G.V. Rao and K. Balan, KSCC, Alappuzha, Kerala, India, November 2000, 81-106.

Venkatappa Rao, G., Dutta, R.K., and Sivaramakrishnan, R. (2000). "Evaluation of Indian made erosion control products." Coir Geotextiles, Emerging Trends, edited by G.V. Rao and K. Balan, KSCC, Alappuzha, Kerala, India, November 2000, 113-129.

Viadero, R.C. (2006) "Managing soil erosion and runoff from construction sites," Government Engineering, Jan-Feb, 40-41.

Vishnudas, S., Savenije, H.H.G., Van der Zaag., Anil., K.R and Balan., K. (2006). "The protective and attractive covering of a vegetated embankment using coir geotextiles." Hydrology and Earth System Sciences, 10:565-574.

Ziegler, A.D. and Sutherland, R. A. (1998). "Reduction in interrill sediment transport by rolled erosion control systems." Soil and Tillage Research, 45 (3-4): 265-278.

On the Stress Dependent Contact Erosion in Vibro Stone Columns

Y. Zou[1], C. Boley[2] and J. Wehr[3]

[1] Institute for Soil Mechanics and Foundation Engineering, University of the Federal Armed Forces Munich, Werner-Heisenberg-Weg 39, 85577 Neubiberg, Germany; yazhou.zou@unibw.de
[2] Institute for Soil Mechanics and Foundation Engineering, University of the Federal Armed Forces Munich, Werner-Heisenberg-Weg 39, 85577 Neubiberg, Germany; conrad.boley@unibw.de
[3] Keller Holding GmbH, 63067 Offenbach Germany; j.wehr@kellerholding.com

ABSTRACT

In order to investigate the hydraulic contact erosion during and after the installation of a stone column, model tests were carried out in the laboratory. Under a critical hydraulic gradient, some fine soil particles in the subsoil around the stone column may be brought into the pore space of the stone column under certain conditions. The critical hydraulic gradient not only depends on the type of stone columns and the fine grained soils around the stone columns, but also on the stress state in the subsoil. Terzaghi's filter criteria (Terzaghi 1948) do not apply to determine the critical hydraulic gradient. For the stone columns with a suitable grain size distribution the hydraulic contact erosion will not occur, and a geotextile cover around the stone column hardly influences the critical hydraulic gradient. The critical hydraulic gradient can be estimated by using present theoretical models.

INTRODUCTION

Vibro replacement stone columns are commonly used to improve saturated soft subsoil which consists mainly of fine grained soils (Kirsch 1979). A cylindrical vibrator penetrates the subsoil to a designed depth at first (Fig. 1a). During the penetration the subsoil consisting of fine grained soils around the vibrator is displaced laterally. Then, a coarse grained material exerting gradually the bottom of the vibrator is compacted by means of lateral vibration of the vibrator from the designed depth to the top of the ground surface (Fig. 1b). Subsequently a stone column made of coarse grained material is constructed in the subsoil (Fig. 1c). The coarse grained material is usually gravel, stone and sand. Through vibration the subsoil made of fine grained soils around the stone column is furthermore displaced laterally. Through the lateral compression a filter zone can be developed and at the same time an excess pore water pressure u_e occurs in the subsoil around the stone column (Fig, 1d). The measured results in situ have shown that the excess pore water pressure can be up to 35kN/m^2 (Weber 2006). Under the excess pore water pressure u_e the displaced subsoil begins to drain radially into the stone column (Fig. 1d). The hydraulic gradient and the radial seepage force next to the boundary between the fine grained soil and the stone column can be relatively high at the beginning of the drainage. If the pore size of the stone column is relatively large and the excess pore water pressure is very high, the high seepage force may bring the particles of fine grained soil into the pore space of the stone column. That means that hydraulic contact erosion may occur at the boundary between the fine grained soil and the stone column under the condition of a very high excess pore water pressure. The hydraulic contact erosion may lead then to loosening or softening of the subsoil near the contact boundary and thus may reduce the bearing capacity of the stone column (Weber 2006).

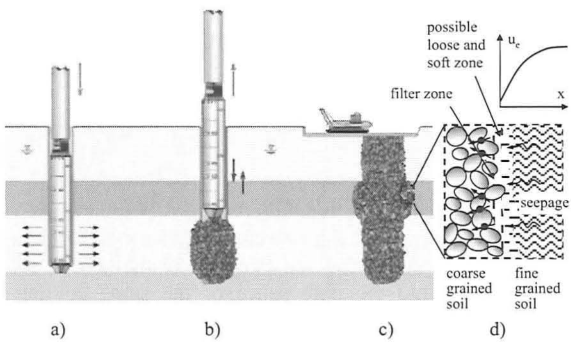

Figure 1. Constructing a stone column and excess pore water pressure u_e

In order to avoid damage due to hydraulic contact erosion to the subsoil, columns can be surrounded by a geotextile (Raithel et al. 2005). The stone columns surrounded by a geotextile can also be used to improve the soft subsoil which consists of peat or mucky clay (Raithel 2006). The investigations of hydraulic contact erosion have shown that the critical hydraulic gradient of hydraulic contact erosion is dependent not only on the type of soils but also on the stress state at the contact boundary (Zou 1999 and Schmitz 2006).

In order to investigate the failure mechanisms and the critical hydraulic gradient of the hydraulic contact erosion during and after constructing stone columns in different soils with and without surrounding geotextile, model tests were carried out in laboratory. The experimental apparatus and results are reported in this paper. The mechanisms of the hydraulic failure in different soils and the effects of soil types and stress states on the critical hydraulic gradient are analyzed. The critical hydraulic gradients for different soils and under different stress states were estimated with different theoretical models. Some conclusions are made for practical applications.

EXPERIMENTS

Materials

Three coarse grained soils G-1 to G-3 were used as the material of the model stone columns for the tests. Their grain size distributions are shown in Figure 2. The grain size of G-1 and G-2 are very uniform. G-3 is a mixture of sand and gravel. Their material parameters, i.e. grain size d_{17} for mass percentage 17%, uniformity coefficient C_u, the minimum and maximum void ratio e_{min} and e_{max} are listed in Table 1. The void ratio e_{min} and e_{max} are measured under dry conditions.

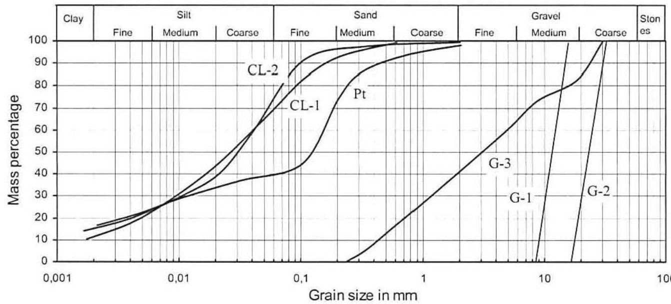

Figure 2. Grain size distribution

Table 1. Material parameters of coarse grained soils

Material	d_{17} (mm)	C_u (-)	e_{max} (-)	e_{min} (-)	I_D (-)	e (-)
G-1	9	1.4	0.39	0.27	0,50	0.33
G-2	18	1.4	0.46	0.33	0,62	0.38
G-3	0.6	12.5	0.40	0.25	0,53	0.32

Three fine grained soils CL-1, Pt and CL-2 are used as fine grained soils around the model stone columns for the tests. Their grain size distributions are also shown in Figure 2. According to USCS classification they are called inorganic clays of low plasticity (CL-1), peat (Pt) and inorganic clays of low plasticity (CL-2). The organic content in the peat (Pt) is very high. Their material parameters, i.e. liquid limit w_L, plastic limit w_P, organic content V_{org}, effective cohesion c′ and effective angle of friction φ′ base on direct shear tests are listed in Table 2. The liquid limit w_L and plastic limit w_P of the peat are very high. After the early research results (Zou 1999 and Schmitz 2006) the critical hydraulic gradient of hydraulic contact erosion depends primarily on the strength of the fine grained soil, on the size of the coarse grained soil and on the stress state in the fine grained soil. Therefore, the details on fine grained fabric are not reported in this paper as important content.

Table 2. Material parameters of fine grained soils

Material	w_L (%)	w_P (%)	V_{org} (%)	c′ (kN/m^2)	φ′ (°)
CL-1	27	16	< 1	7.2	31
Pt	156	78	25	12	20
CL-2	41	15	3	7.5	31

The geotextile Type 100/200 from the company HUESKER was used as cover surrounding the model stone columns. The effective opening size of the geotextile is $O_{90} = 0.2$ mm. The water flow velocity through the geotextile under the water pressure head $H_w = 50$ m is $v_{H50} = 5 \cdot 10^{-3}$ m/s.

Experimental apparatus and procedures

All tests were carried out in a specially designed model box (Figure 3). The front wall of the model box consists of Plexiglas. The coarse grained soil 1 to model a stone column was constructed in the middle of the saturated fine grained soil 2 which models the soils around stone columns in situ. The model stone column can be surrounded by geotextile (GT) or without geotextile. Above and below the saturated fine grained soil two clay layers 3 were laid as a sealing. Both the coarse and saturated fine grained soils can be loaded by a pressurized air cushion 4 under the pressure σ_v vertically. Under the pressure p the water in the tank 5 can flow through the entrance tube 6, porous plate 7 and the pore space of the saturated fine grained soil 2 and the stone column 1, and then through the perforated plate 8 into the sedimentation tank 9. Afterwards it flows out through the output tube 10. The fine soil particles washed out are deposited in the sedimentation tank 9. The vertical pressure (stress) σ_v in air cushion 4 and the pressure p in the water tank 5 can be regulated. The length L of flow lines in the fine grained soil 2 is known. With the pressure p, the length L und the unit weight γ_w of water the hydraulic gradient $i = p/(L \cdot \gamma_w)$ in the fine grained soil 2 can be calculated. Prior to testing the fine grained soil 2 was saturated.

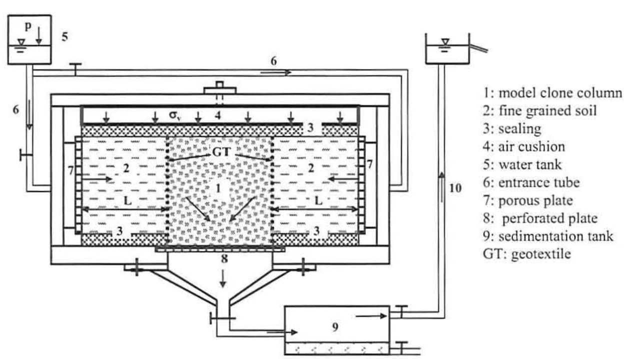

Figure 3. Experimental apparatus

Under a constant vertical stress σ_v the pressure p in the water tank 5, and the hydraulic gradient i can be increased stepwise. The interval of a pressure increase is approx. 10 hours. The dry mass m_d of the fine soil particles deposited in the tank 9 can be determined depending hydraulic gradient i. The discharge q depends on hydraulic gradient i and can be determined by measuring the water volume ΔV_w flowing through the saturated fine grained soil. If under the pressure $p = p_{cr}$ for a constant pressure σ_v a hydraulic fracture occurs, i.e. a continuous flow canal has been formed in the fine grained soil, the discharge q (or the water volume ΔV_w)

increases evidently and a large amount of fine soil particles are brought into the void space of the model stone column, and the corresponding hydraulic gradient is defined as critical hydraulic gradient i_{cr}.

Under different pressures σ_v and with different soil materials as model stone columns and as fine grained soils around the model stone columns, 19 model tests were carried out in laboratory. The vertical stress σ_v, the length L of flow lines in the fine grained soil, the coarse grained materials and the fine grained soils for the 19 model tests are listed in table 3. The relative density I_D and the void ratio e of the model stone columns for the tests are shown in table 1.

Table 3. Test program and critical hydraulic gradient

Test-No.	Stone column	Fine grained soils	Vertical stress σ_v (kN/m^2)	With Geotextile	L (cm)	Critical hydraulic gradient i_{cr}
1 / 2	G-1/G-2	CL-1	30	No	16	15 / 15
3 / 4			60		16	35 / 35
5 / 6			90		16	53 / 53
7 / 8			120		16	70 / 60
9 / 10			150		16	90 / 80
11	G-1		180		16	110
12 / 13	G-3	CL-2	60	No / Yes	10	55 / 45
14 / 15			90	No / Yes	10	75 / 75
16 / 17			120	No / Yes	10	85 / 85
18 / 19		Pt	60	No / Yes	10	55 / > 55

OBSERVATIONS AND EXPERIMENTAL RESULTS

Observations

When the pressure p in the water tank 5 which corresponds to the hydraulic gradient, was relatively low, seepage occurred in the fine grained soil, but none or only a few of fine soil particles have been brought into the pore space of the stone column. With the increase of hydraulic gradient more and more fine soil particles were seen in the pore space of the stone column (Figure 4). When the pressure p in the water tank 5 was relatively high or near the vertical stress σ_v, a continuous flow canal was formed in the fine grained soil, and a large amount of fine soil particles have been brought into the pore space of the stone column. Figure 4 shows the proof of an eroded flow canal. The corresponding hydraulic gradient is the critical hydraulic gradient i_{cr} named above.

Experimental results

The increase of the dry mass m_d of the fine soil particles deposited in the tank 9 with increasing hydraulic gradient i for tests 5 and 6 is shown in Figure 5, for example. Because the dry mass m_d deposited in the tank 9 is very low in relation to the total original mass which depends also on the height and width of the fine grained soil, a normalized dry mass by the total original mass is not important. At first the dry mass m_d increases linearly with the hydraulic gradient. Just below the hydraulic gradient i_{cr} the dry mass m_d increases very evidently. This means that a large amount of fine grained soil has been washed away at the hydraulic gradient i_{cr}. The variations of discharge q with increasing hydraulic gradient i for tests 5 and 6 are also shown in Figure 5. The discharge q also increases linearly with the hydraulic gradient. At the same hydraulic gradient i_{cr} the discharge q suddenly becomes very high. This means that a continuous flow canal has been formed in the fine grained soil. This hydraulic gradient i_{cr} is the critical hydraulic gradient. It is very clear that just below the critical hydraulic gradient i_{cr} a continuous flow canal (no flow path) has been formed.

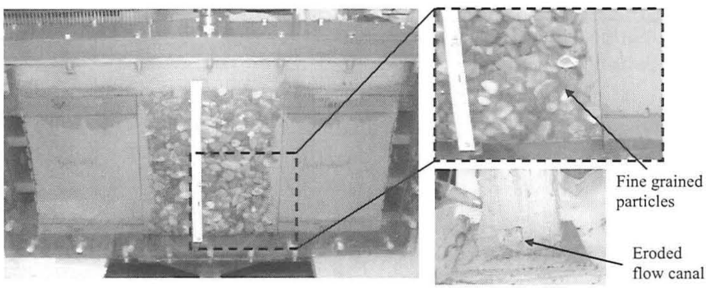

Figure 4. Fine soil particles in the stone column and eroded flow canal

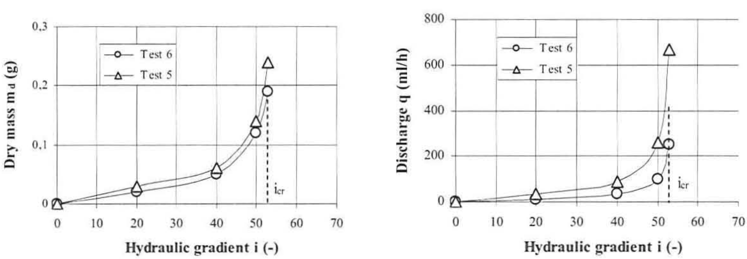

Figure 5. Dry mass m_d and discharge q depending on the hydraulic gradient i

The critical hydraulic gradients i_{cr} of the tests are listed in tables 3 and 4. The dependence of the critical hydraulic gradient i_{cr} on the vertical stress σ_v for different stone column materials (coarse grained soils) and for different fine grained soils, with and without geotextile, are shown in Figures 6. Below a low vertical stress σ_{vc}, e.g. $\sigma_v < \sigma_{vc} = 80\ kN/m^2$, the critical hydraulic gradient i_{cr} increases linearly with the vertical stress σ_v, and for the same fine grained soil the critical hydraulic gradient i_{cr} is independent of the material of stone columns. In this case, the pressure p in the water tank 5, corresponding to i_{cr} has always been near to the vertical stress σ_v. The vertical effective stress in the fine grained soil was equal to zero approximately. That means that a continuous flow canal will occur if the pore water pressure is equal to the vertical stress σ_v. Therefore, the hydraulic gradient corresponding to the vertical stress σ_v is an upper boundary of the critical hydraulic gradient.

Table 4. Critical hydraulic gradient

Test-No.	1/2	3/4	5/6	7/8	9/10	11	12/13	14/15	16/17	18/19
i_{cr} (-)	15/15	35/35	53/53	70/60	90/80	110	55/45	75/75	85/85	55 / > 55

Above a relatively high vertical stress σ_{vc}, e.g. $\sigma_v > \sigma_{vc} = 80$ kN/m^2, the dependence of the critical hydraulic gradient i_{cr} on the vertical stress σ_v deviates from the linear relation (Figure 6). In this case, the critical hydraulic gradient i_{cr} is lower than the upper boundary. Under the same vertical stress $\sigma_v > \sigma_{vc}$ the critical hydraulic gradient i_{cr} is different for different coarse grained soils (Figure 6 a). The finer the materials of stone columns are for the same fine grained soil, the higher is the critical hydraulic gradient i_{cr}. After the early research results (Rehfeld 1967, Zou 1999 and Schmitz 2006) the critical hydraulic gradient i_{cr} depends on the pore size of coarse grained soils. The larger the pore size, the lower is the critical hydraulic gradient i_{cr}. The grain size of G2 is larger than the grain size of G1. The pore size of the G2 is larger than the pore size of G1. Therefore, the critical hydraulic gradient i_{cr} of the stone columns G2 is lower than that of the stone columns G1. Particularly, the larger the pore size of coarse grained soils, the lower is the critical vertical stress σ_{vc}. More details on the influence of the pore size on the critical hydraulic gradient i_{cr} and its physical mechanisms were reported by Rehfeld 1967, Zou 1999 and Schmitz 2006.

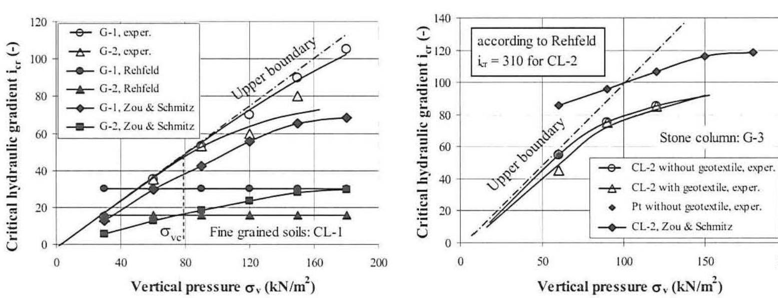

a) b)

Figure 6. Dependence of critical hydraulic gradient i_{cr} on vertical stress σ_v

Using G-3 (a mixture of sand and gravel) as the material of the model stone column, the critical hydraulic gradient i_{cr} with and without geotextile is almost identical (Figure 6 b). This means that, in this case, the geotextile surrounding the column does not influence the critical hydraulic gradient i_{cr}. If the critical hydraulic gradient i_{cr} is near the upper boundary, the critical hydraulic gradient is also independent on the type of fine grained soils by using G-3 as the material of the model stone column.

The experimental results have indicated that the critical hydraulic gradient i_{cr} also depends on the length L of the flow lines. More research in that area will be necessary to clarify the details.

THEORETICAL ESTIMATION

In order to estimate critical hydraulic gradients i_{cr}, Rehfeld 1967 proposed the theoretical equation (1):

$$i_{cr} = \frac{c'}{4.4 \cdot d_p \cdot \gamma_w \cdot \tan\varphi'} \tag{1}$$

Where d_p is the so-called equivalent pore diameter of the coarse grained soil (stone column) and can be calculated with equation (2):

$$d_p = 0.535 \cdot \sqrt[6]{C_u} \cdot e \cdot d_{17} \tag{2}$$

By using the theoretical equations (1) and (2) after Rehfeld 1967 as well as the parameters listed in tables 1 and 2 the critical hydraulic gradients i_{cr} are calculated and shown in Figures 6, in comparison with the experimental results. Because in the theoretical equation (1) the influence of stress state was not considered, the calculated critical hydraulic gradient is independent of the vertical stress σ_v. For stone columns G-1 and G-2 and for the fine grained soil CL-1 the calculated critical gradient i_{cr} is lower than the experimental results for $\sigma_v > 30$ and 50 kN/m^2 respectively (Figure 6 a). For stone column G-3 and for the fine grained soil CL-2 the calculated critical gradient is much higher than the experimental results (Figure 6 b). The discrepancy between the experimental data and theoretical results may be primarily due to neglecting the influence of stress state. The strength parameters c′ and φ′, the model parameter d_p and the model assumption of Rehfeld 1967 may influence the theoretical results.

In order to estimate the critical hydraulic gradient i_{cr} depending on the vertical stress σ_v, Zou 1999 proposed the equation (3):

$$i_{cr} = \frac{2c' - (\zeta - \xi \cdot \tan\varphi') \cdot \sigma_v}{0.5 \cdot d_p \cdot \gamma_w \cdot (1 + \xi_0 \cdot \tan\varphi')} \tag{3}$$

Schmitz 2006 has determined the dependence of the parameters ξ_0 and ζ in equation (3) on the vertical stress σ_v by means of numerical calculations and proposed that the value of the parameter ξ in equation (3) should be between 0.2 and 0.6. Using equations (3) and (2), with the parameters in tables 1 and 2 as well as with $\xi = 0.46$ the critical hydraulic gradients i_{cr} depending on the vertical stress σ_v are calculated, where the parameters ξ_0 and ζ depending on the vertical stress σ_v are determined according to Schmitz 2006 and are shown in Figure 7.

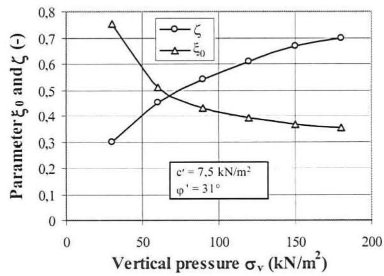

Figure 7. Parameters ξ_0 and ζ in dependence on vertical stress σ_v

The calculated critical hydraulic gradients i_{cr} are shown in Figures 6, in comparison with the experimental results. The calculated critical hydraulic gradient i_{cr} according to Zou and Schmitz depends on the vertical stress σ_v. For stone column G-1 and G-2 and for the fine grained soil CL-1 the calculated critical gradient i_{cr} is lower than the experimental results (Figure 6 a). For stone column G-3 and for the fine grained soil CL-2 the calculated critical gradient is higher than the experimental results (Figure 6 b). The discrepancy between the experimental data and theoretical results may be primarily due to material and model parameters.

To estimate the critical hydraulic gradient accurately, the parameter in tables 1 and 2 as well as the parameters ξ_0 and ζ in equation (3) must be determined reasonably.

CONCLUSIONS

Terzaghi's filter criteria (Terzaghi 1948) are geometric criteria. Therefore they do not apply to determine the critical hydraulic gradient.

If the excess pore water pressure occurring during the installation of a stone column is very high, the dissipation of the excess pore water pressure may theoretically cause a process of fine grained soil around the stone column moving into the pore space of the stone column. The higher the excess pore water pressure is, the more fine soil particles are brought into the pore space of stone columns. Under a very high excess pore water pressure, a continuous flow canal may occur. Thus, hydraulic contact erosion may occur at the boundary between the fine grained soil and the stone column. Within our investigations it is checked whether the above mentioned processes can occur under conditions of practical relevance.

The critical hydraulic gradient of the hydraulic contact erosion not only depends on the materials of stone columns and the fine grained soil around the stone columns, but also on the stress state in the subsoil. The larger the pore size of the stone column, the lower is the critical hydraulic gradient. The higher the shear strength and the stress of the fine grained soil, the higher is the critical hydraulic gradient. For a relatively low stress in the subsoil the critical hydraulic gradient is corresponding to the vertical stress σ_v in the subsoil. If the excess pore water pressure in the subsoil is near the vertical stress σ_v, the hydraulic contact erosion may occur. For relatively high stresses in the subsoil, the water pressure corresponding to the critical hydraulic gradient is lower than the vertical stress σ_v in the subsoil.

The measured results in situ have shown that the excess pore water pressure is not very high (Weber 2006). If the grain size distribution of stone columns is well graded, the strength of the fine grained soils is relatively high and thus hydraulic contact erosion will not occur in the subsoil surrounding the stone column.

If the material of stone columns has a suitable grain size distribution, e.g. well graded, a geotextile surrounding the stone column hardly influences the critical hydraulic gradient i_{cr}.

The critical hydraulic gradient for the hydraulic contact erosion can be estimated using the theoretical equation (1) or (3) approximately. For an accurate estimate of the critical hydraulic gradient, reasonable determination of the model and soil parameters in equation (1) and (3) is necessary.

So far our investigations have shown that contact erosion of soil surrounding vibro stone columns has no significant influence for a wide variety of conditions in situ.

REFFERENCES

Kirsch, K. (1979). "Erfahrungen mit der Baugrundverbesserung durch Tiefenrüttler. " *Geotechnik* 2, 1979, 21-32.

Raithel, M., Kempfert, H.G. and Kirchner, A. (2005). "Berechnungsverfahren und Bemessung von ummantelten Säulen – Entwicklung und aktueller Stand." Geotechnik 1, 2005, 20-31.

Raithel, M. (2006), "Ummantelte Säulen zur Gründung von Bauwerken auf weichen Böden." *Ummantelte Säulen der* EBGEO.

Rehfeld, E. (1967). "Die Erosionsbeständigkeit bindiger Lockergesteine – die wichtige Grundlage zur Dimensionierung von Dichtungsschichten aus natürlichen Erdstoffen." Wissenschaftliche Zeitschrift der Technischen Universität Dresden, Heft 5, 16.

Schmitz, S., Boley, C. and Zou, Y. (2006). "Stress dependent erosion in layered soil." First Mediterranean Symposium on Advances in Geomaterials and Structures in Hammamet, Tunesien, S. 147 – 152.

Schmitz, S. (2007). "Zur hydraulischen Kontakterosion bei bindigen Basiserdstoffen." Mitteilungen des Institutes für Bodenmechanik und Grundbau, Universität der Bundeswehr München, Heft 19.

Terzaghi, K. & Peck, R. (1948). „Soil mechanics in engineering practice. John Wiley and Sons Inc. New York.

Weber, T.M. (2006). " Centrifuge modeling and testing of stone columns." *Professorship for Geotechnical Engineering,* 2nd AMGISS School & Workshop, ETH Zurich, 11-14 Sep. 2006.

Zou, Y. (1999). "Der vom Spannungszustand und Bodengefüge abhängige Erosionsdurchbruch bindiger Böden." *Wasserwirtschaft*, Nr. 11, S. 554 – 559.